KU-11-3

Improving Infrastructure Sustainability I: Extending Useable Lives of Steel Bridges by Halting Distortion-Induced Fatigue Crack Propagation Using Pretensioned Bolts and Plate Washers

By

Hao Liu

Caroline Bennett

Adolfo Matamoros

Jian Li

Ron Barrett-Gonzalez

Stan Rolfe

A Report on Research Sponsored by
The Kansas Department of Transportation

Structural Engineering and Engineering Materials
SM Report No. 109
September 2015

THE UNIVERSITY OF KANSAS CENTER FOR RESEARCH, INC.

2385 Irving Hill Road – Campus West, Lawrence, Kansas 66045

Executive Summary

Drilling crack-arrest holes to halt fatigue crack propagation is a simple technique that is commonly used by bridge owners controlling and/or repairing fatigue cracking in steel bridges. Well-established relationships exist for sizing the diameter of the crack-arrest holes for in-plane fatigue loading; however, the effectiveness of crack-arrest holes under out-of-plane (distortion-induced) fatigue is not well-understood.

Distortion-induced fatigue cracking is much more common in steel bridge infrastructure than in-plane fatigue cracking, and bridge owners often utilize drilled crack-arrest holes in these cases as a "first response" against fatigue cracks discovered during inspections. The purpose of the crack-arrest hole is to smooth out the sharp crack tip, reducing the stress concentration and halting/delaying crack propagation. Common knowledge has been that large diameter crack-arrest holes are more effective at halting crack propagation under distortion-induced fatigue than small diameter crack-arrest holes. However, drilling large diameter crack-arrest holes can have strength implications for a structure, and may not be desirable. Additionally, there is little evidence in the literature that large diameter crack-arrest holes perform better than small diameter crack-arrest holes under distortion-induced fatigue.

A study examining the effectiveness of crack-arrest holes of varying diameters under distortion-induced fatigue loading was performed. The investigation was comprised of both experimental and analytical components. The experimental study was performed on segments of plate girder loaded under distortion-induced fatigue. Crack-arrest holes of various diameters were drilled at the tips of the cracks of different lengths, and their effectiveness were evaluated. A suite of three-dimensional, solid-element finite element analyses was also used to parametrically vary crack-arrest hole diameter, placement, and crack length. The study also included an analytical examination of using pretensioned bolts and plate washers in a crack-arrest hole. Limited effectiveness was noted for this technique, so the majority of the research focused on appropriate crack-arrest hole sizing and placement.

The findings from the experimental and analytical components of this study were compared against common industry practices. The results show that crack-arrest hole placement,

rather than hole diameter, has a much greater effect on the effectiveness of the crack-arrest hole in bridge girders susceptible to distortion-induced fatigue.

Acknowledgements

The authors of this report would like to gratefully acknowledge funding from the Kansas DOT and express thanks for their support of the work performed under this project, and for knowledgeable guidance and input provided by Mr. John Jones throughout the project activities.

Finally, the authors are grateful to the many graduate and undergraduate students who have contributed their talents to this project, especially: Ms. Amanda Hartman, Mr. Fatih Alemdar, Mr. Gary Simmons, Ms. Temple Overman, and Mar. Say Hak Bun.

Table of Contents

List of Tables

List of Figures

1. Introduction & Background

Fatigue cracking is a common problem afflicting thousands of steel bridges in the U.S. highway bridge inventory, and the scale of the problem is poised to increase over the next decade due to deferred maintenance and utilization beyond original design lives. As the mean age of steel bridges increases, fatigue damage caused by cumulative vehicular loading cycles also increases.

Maintaining and repairing these bridges is an expensive and time-consuming endeavor, often requiring engineering of tailored retrofit solutions. However, a nearly universally-accepted first line of defense against fatigue crack propagation is the common practice of drilling a crack-arrest hole at the tip of a crack.

Crack-arrest holes are a time-honored, simple solution for stopping fatigue crack propagation. They stop fatigue crack propagation by blunting the crack tip and reducing the stress concentration at the crack tip. The radius of a crack tip is very small, approaching zero, and the curvature (*1/radius*) approaches infinite. Correspondingly, the stress concentration factor (Eqn 1.1) at the crack tip approaches infinite. The crack-arrest hole changes the radius and curvature to that of the crack-arrest hole and reduces the stress concentration factor substantially. From Barsom and Rolfe (1997):

$$k_t = \frac{\sigma_{\max}}{\sigma_{nom}} \qquad \textbf{Equation 1.1}$$

Where k_t is the stress concentration factor, σ_{max} is the maximum stress at the edge of the crack, and σ_{nom} is the stress sufficiently far away from the crack that it is not influenced by the crack.

For example, the stress concentration factor at the edge of an ellipse is represented in Equation 1.2 (Barsom and Rolfe 1997):

$$k_t = \left(1 + 2\frac{a}{b}\right)$$ **Equation 1.2**

Where k_t is the stress concentration factor, *2a* is the length of the major axis of the ellipse and *2b* is the length of the minor axis of the ellipse.

For sharp cracks *b* approaches *0* and *a/b* becomes very large; then k_t also becomes very large. By placing a crack-arrest hole of radius *r* at the tip of the crack, *r* replaces *b* and the stress concentration factor reduces from infinite to a relatively small finite number.

The formula for determining the diameter of the crack-arrest hole to stop fatigue crack propagation was first presented in Rolfe and Barsom (1977) and is in the latest edition of Barsom and Rolfe (1999). Fisher et al. (1980; 1990) used the same formula but developed a different constant from different experimental testing. The formula (Eqn. 1.3) relates the required radius of the crack-arrest hole to the yield strength of the steel, the range of the stress intensity factor, and the half-length of the crack along with a constant from experimentation.

The formula was presented in the following form (Rolfe and Barsom 1977):

$$\frac{\Delta K}{\sqrt{\rho}} = C\sqrt{\sigma_{ys}}$$ **Equation 1.3**

Where *C* is a constant derived from experimental testing, *r* is required radius of the crack-arrest-hole, s_{ys} is the yield strength of the steel and ΔK is the range of the stress intensity factor.

Equation 1.3 was based on a series of experiments on various steel plates with edge notches; all the notches were the same length, *a*, and all had the same constant radius at the tip. Yield strengths of the steel plates varied between 248 MPa (36 ksi) to 758 MPa (110 ksi). The loading, which consisted of uniaxial, cyclical loads, was varied to provide stress ratios ($R = s_{max}/s_{min}$) of –1.0 (full stress reversal), 0.1, and 0.5. This plate geometry with the uniaxial, tension-compression loading resulted in Mode I type fracture, where Mode I fracture is a tension-opening crack. For this edge notch configuration, the range of the stress intensity factor can be determined by:

$$\Delta K = \Delta\sigma\sqrt{\pi a}$$ **Equation 1.4**

Where *ΔK is* range of the stress intensity factor, *Δσ* is cyclic stress range (σ_{max} - σ_{min}) for the fluctuating stresses, and *a* is the length of the edge crack ($^1/_2$ the length of the crack for an interior crack).

When Eqn. 1.4 is substituted into Eqn. 1.3, Eqn. 1.5 results:

$$\frac{\Delta\sigma\sqrt{\pi a}}{\sqrt{\rho}} = C\sqrt{\sigma_{ys}}$$ **Equation 1.5**

This can be rearranged in terms of *r* and *a*, and becomes:

$$\rho = \left(\frac{\pi(\Delta\sigma)}{C^2\sigma_{ys}}\right)a$$ **Equation 1.6**

The crack-arrest formula is also found in Fisher et al. (1980; 1990). Fisher et al. conducted a series of experiments on rolled, wide-flange shapes (Fisher et al. 1980) and welded-plate girders (Fisher et al. 1990) where the full-scale members were configured and loaded in such a manner that they were subjected to both in-plane bending stresses and out-of plane distortion stresses (Figure 3.6). This combination resulted in distortion-induced fatigue cracking at locations where cross-bracing attached to the connection plates, which were in turn welded to the girder webs. The steel used in the studies by Fisher (1980; 1990) was limited to Gr. A370 steel, which had measured yield strength of 248 MPa (36 ksi).

The fatigue cracking was caused by a complex, triaxial stress field and resulted in a Mode III failure (shear in a plane perpendicular to direction of crack growth) or in a complex mode with both Mode III and bending stress components. When fatigue cracks developed in the members, holes were drilled at the ends of the crack tips; these holes typically had diameters of 19mm (¾ in), 25.4mm (1in), or 31.75mm (1¼ in). The tests were restarted and continued until the cracks reinitiated or the tests were stopped. For the tests performed on the rolled shapes, the control stress variable was the stress range in the normal flexural bending stresses as measured in

the beam web at the bottom of the gusset at mid-span (Figure 3.1). The stress ranges were 41.4, 62.0, 82.7, or 103.4 MPa (6, 9, 12, or 15 ksi). For tests on the plate girders, testing was controlled by limiting the in-plane bending stress to either 41.4 or 82.7 MPa (6 or 12 ksi) and inducing out-of-plane distortion stress of either low, medium, or high values. The out-of-plane distortion stress was calculated from strains measured in the web gap with strain gages and then extrapolated back to the edge of the transverse stiffener.

Despite the differences in the testing methodology, Fisher et al. (1980) used Eqns. 1.3 & 1.4 for determining the required radius of the crack-arrest hole but developed a different constant, *C*. Using Eqns. 1.3 and 1.4 resulted in Eqn. 1.5 for both Rolfe and Barsom (1977) and Fisher et al. (1980, 1990). Since *C* was derived from different testing methodologies, the values for *C* depend on using consistent units. Table 1.1 provides the consistent units and the corresponding values for *C* from Rolfe and Barsom (1977) and from Fisher et al. (1980, 1990) in both SI and US Customary units.

Table 1.1: Values for *C* and Units for Crack -Arrest Hole Equations

Units	*C* – Rolfe and Barsom (1977)	*C* – Fisher et al. (1980)	$\Delta\sigma$	σ_{ys}	*a*	*r*
SI	26.3	10.5	MPa	MPa	mm	mm
US	10	4	ksi	ksi	in.	in.

Fisher et al. (1990) states that, if the out-of-plane bending stress at the transverse stiffener is greater than 103 MPa (15 ksi) or if the in-plane bending stress in the web at the web to flange weld is greater than 41 MPa (6 ksi), the crack-arrest hole with a radius as calculated from the Eqn. 1.6 using the constant $C = 4$ will not prevent the crack from reinitiating on the other side of the hole. Rolfe and Barsom (1977) did not specify a restriction on in-plane load in their discussion of the formula.

In practice, crack-arrest holes have exhibited a wide range of performance. Typically, crack-arrest holes sized according to Eqn. 1.6 for in-plane fatigue have performed satisfactorily. Crack-arrest holes have not exhibited the same propagation-halting performance under distortion-induced fatigue loading, and the reason for this is not entirely clear.

One reasonable hypothesis is that crack-arrest holes are not commonly drilled to the diameter required when using Eqn. 1.6 with C=4, as this often results in very large hole diameter requirements. Commonly-encountered crack lengths and grades of steel often necessitate crack-arrest hole diameters greater than 4 in., which at best removes a significant amount of steel section, and more often than not is simply geometrically impossible. When faced with this situation, bridge engineers usually specify the largest crack-arrest hole that they consider feasible and reasonable, which is often on the order of 1 in. diameter. Therefore, it is reasonable to consider whether the fact that such crack-arrest holes are "undersized" contributes to crack re-initiation.

Subscribing to this hypothesis, McGormley and Koob (2001) suggested the use of a large-hole retrofit to retrofit for distortion-induced fatigue. This procedure involves fabricating two large-diameter holes (3-4 in.) in the web gap region – one on both sides of the connection stiffener. No literature was found assessing the performance of this repair technique, but it has been implemented on numerous bridge structures across the U.S.

Another reasonable hypothesis as to why crack-arrest holes have not exhibited good crack-arresting capabilities under distortion-induced fatigue is that crack-arrest holes cannot be expected to perform similarly in distortion-induced fatigue as they do under in-plane fatigue. If this hypothesis is true, then the crack-arrest hole relationship introduced in Eqn. 1.3 may not be applicable for distortion-induced fatigue cracking.

Information is needed to determine the effects of crack-arrest hole diameter, placement, and crack type on propensity for crack re-initiation under distortion-induced fatigue loading for the purpose of providing guidance to bridge engineers faced with making decisions when faced with active cracking in steel bridges. Decades of implementation with mixed results have shown that the level of information available to bridge engineers with respect to crack-arrest hole sizing for distortion-induced fatigue is inadequate.

2. Objective and Scope

The overall objective of this research was to examine the effectiveness of crack-arrest holes of varying diameters, placement, and crack length for steel bridge girders subjected to distortion-induced fatigue. The scope of the study included both physical experimentation and computer simulations.

3. Research Approach

The approach taken in this research utilized a suite of finite element models in which crack length, crack placement, and crack-arrest hole diameter were varied. In addition, a model of the hole retrofit described in McGormley and Koob (2001) was created and compared to the results from the broader suite of FE models. A physical test was conducted on a girder segment loaded in distortion-induced fatigue to provide context to the finite element analyses.

3.1. Modeling Methodology

The effects of out-of-plane bending and cross-frame loading were studied through use of computational simulations performed using the commercially-available finite element software, Abaqus. The baseline geometry for each model included a single 3.0 m [10 ft] long by 1.52 m [5.0 ft] deep simply-supported steel girder section, dimensioned in Figure 3.1 and Figure 3.2. In this simplified girder model, no bridge deck was included. The depth of this section was chosen to represent a reasonable girder depth for a multi-girder highway overpass. The length of the girder section was chosen to be twice the girder depth. The connection stiffener welded at mid-span was truncated 6.0 mm [1.4 in.] from the face of each adjacent flange. A 25 mm [1.0 in.] clip produced a web gap region of 35 mm [1.38 in.]. The end stiffeners were attached to both the top and bottom flange and welded to the entire depth of the web on sides. The flanges were connected to the web by welds on both the interior and fascia side along the width of the web.

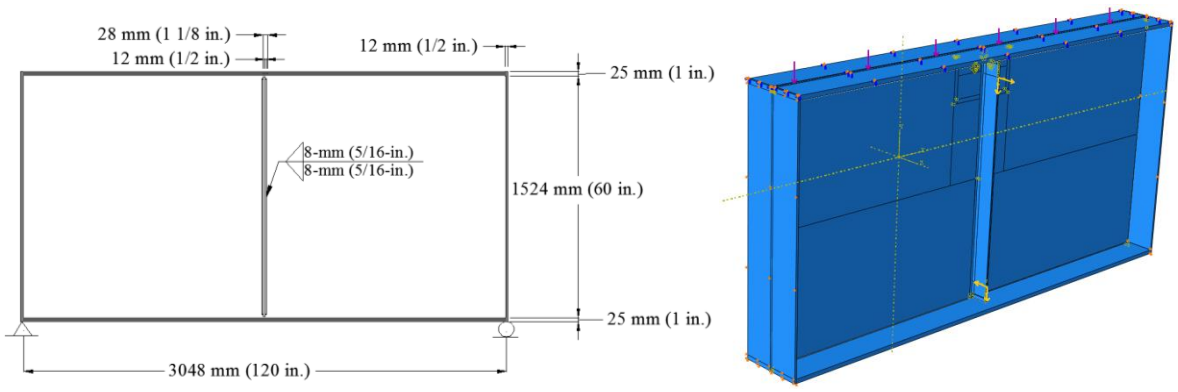

Figure 3.1: Elevation view of girder section and model geometry

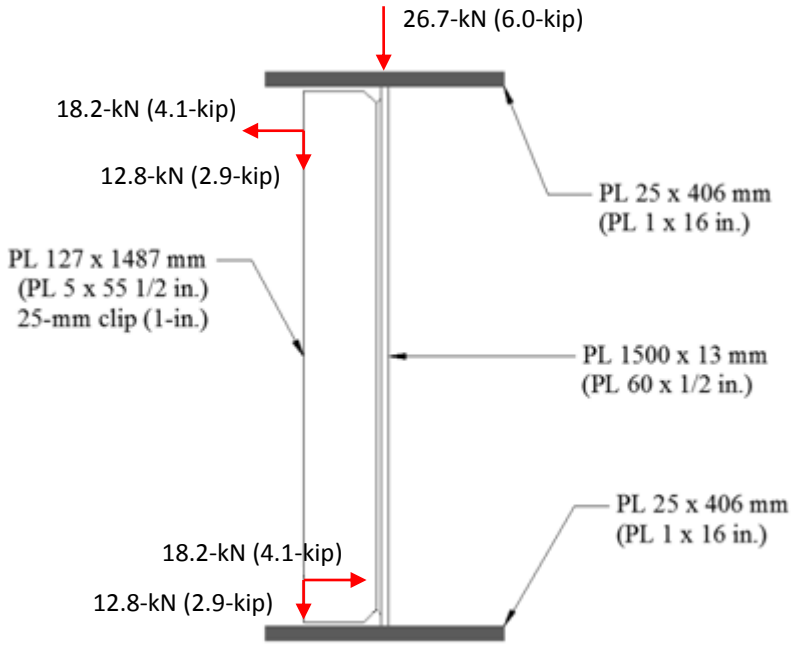

Figure 3.2: Girder cross-section

A 26.7 kN [6.0 kip] pressure load was placed over a 12 mm [1/2 in.] width at the center of the top flange, to simulate the maximum design truck load over this girder section. An 18.2 kN [4.1 kip] point load was placed 105 mm [4.1 in.] from the top of stiffener at the center of the exterior face of the stiffener, 127 mm [5.0 in.] from the interior surface of the web. The load was directed perpendicular to the surface and pointed away from the girder. A 12.8 kN [2.87 kip] point load was load was placed at the same location as the 18.2 kN [4.1 kip] point load. This load

was directed parallel to the surface and pointed toward the bottom flange. A corresponding 18.2 kN [4.1 kip] point load and a 12.8 kN [2.87 kip] point load was placed 105 mm [4.1 in.] from the bottom of stiffener at the center of the exterior face of the stiffener, 127 mm [5.0 in.] from the interior surface of the web. These force couples, shown in Figure 3.2, model the out-of-plane forces induced by cross-frame connections during bending deformation.

Eight-node, cubic elements with 24 degrees of freedom were used in the meshes for the flanges, web, and stiffeners. Four-node tetrahedral elements with 12 degrees of freedom each were utilized to conform to the special geometrical aspects of the weld. All the fillet welds were modeled as right triangle cross-sections. All steel sections and welds were modeled as isotropic, linear elastic materials with an elastic modulus of 200,000 MPa [29,000 ksi] and a Poisson's ratio of 0.3. Tie constraints were used to connect the fillet welds to the surfaces they bring together.

3.2.Modeling of Cracks, Crack-Arrest Holes, and Computing Stresses

Cracks were modeled as a rectangular cut extruded through the thickness of the web and with a 0.25 mm [0.01 in.] width; length of the cracks was varied through the study. Crack-arrest holes were modeled as a circular cut extruded through the web thickness. Four different crack patterns were considered within the modeling effort, as diagrammed in Figure 3 and described here:

- Diagonal crack: a crack that occurs at the toe of the connection plate-to-web weld and extends diagonally into the web (Figure 3.3a);
- Horseshoe-shaped crack: a crack that follows the toe of the connection plate-to-web weld (Figure 3.3b);
- Horseshoe-shaped crack and web-to-flange crack: two cracks occurring simultaneously – a crack around the toe of the connection plate-to-web weld and a crack along the toe of the web-to-flange weld (Figure 3.3c); and
- Web-to-flange crack: a crack along the toe of the web-to-flange weld (Figure 3.3d).

For diagonal cracks, except the 102 mm [4.0 in.] crack-arrest hole, the total crack length was measured as the crack-arrest hole diameter combined with the existing, undrilled crack

length. For horseshoe-shaped and web-to-flange cracks, except the 102 mm [4.0 in.] crack-arrest hole, the total crack length was measured as the radius of the crack-arrest hole combined with the existing crack length. The total crack length was kept constant for all three crack types. For the 102 mm [4.0 in.] crack-arrest hole, the placement was such that the hole was drilled 3.18 mm [1/8 in.] into both the flange weld and stiffener weld.

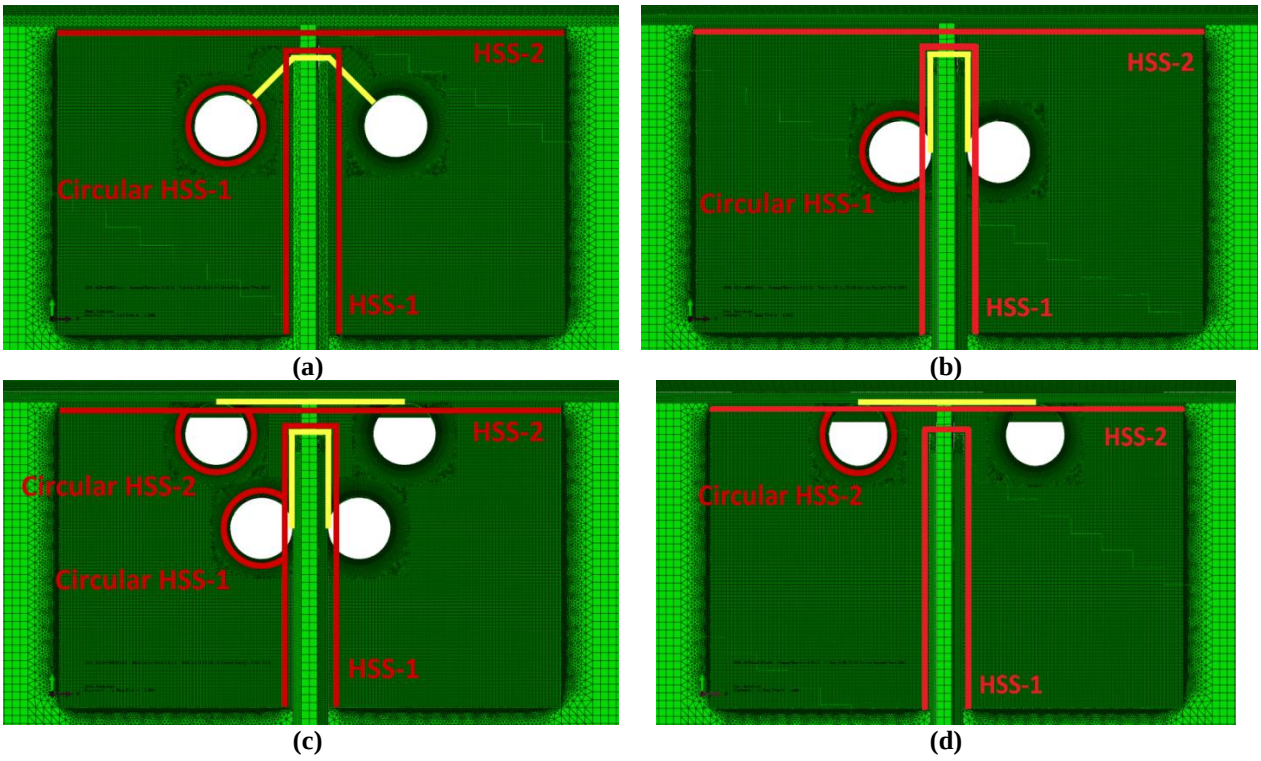

Figure 3.3: Crack placement and Hot Spot Stress paths for FE models: (a) Diagonal-type crack pattern; (b) Horseshoe-shaped crack; (c) Horseshoe-shaped crack and web-to-flange weld crack; (d) Web-to-flange weld crack

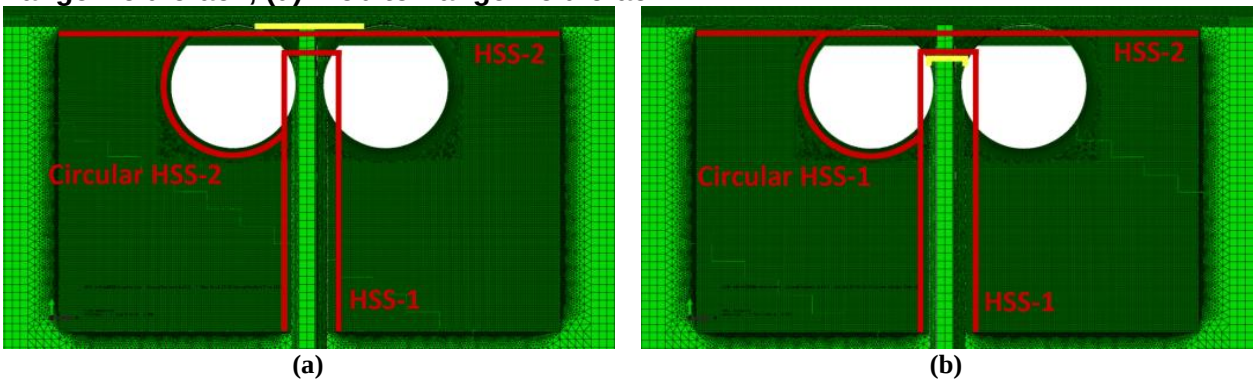

Figure 3.4: Crack placement and Hot Spot Stress paths for: (a) 101.6 mm [4.0 in] hole for web-to-flange weld crack (b) 101.6 mm [4.0 in] hole for horseshoe-shaped crack

3.3.Mesh Convergence Study

Stresses computed in the models near the locations of crack-arrest holes were found to be sensitive to mesh density; therefore, a mesh convergence study was performed. The mesh convergence study was conducted for a model that included diagonal crack. A large enough area was partitioned such that all crack types with different lengths and varying hole diameters would fit within the partitioned region. The most coarse and most dense mesh configurations for the region near the crack-arrest hole in the girder web are shown in Figure 3.5 (a) and (b), and consisted of three concentric circular regions around the holes which allowed gradually increasing element size away from the crack-arrest hole. Rectangular partitions were also created around the crack. The mesh was configured using several regions with increasing mesh density near the crack-arrest hole. The results for convergence study are illustrated in Figure 3.5 (c). A minimum element size of 0.71 mm [0.028 in] at the path half the thickness of the web away from the edge of crack-arrest hole was selected in this study, which is the configuration shown in Figure 3.5b.

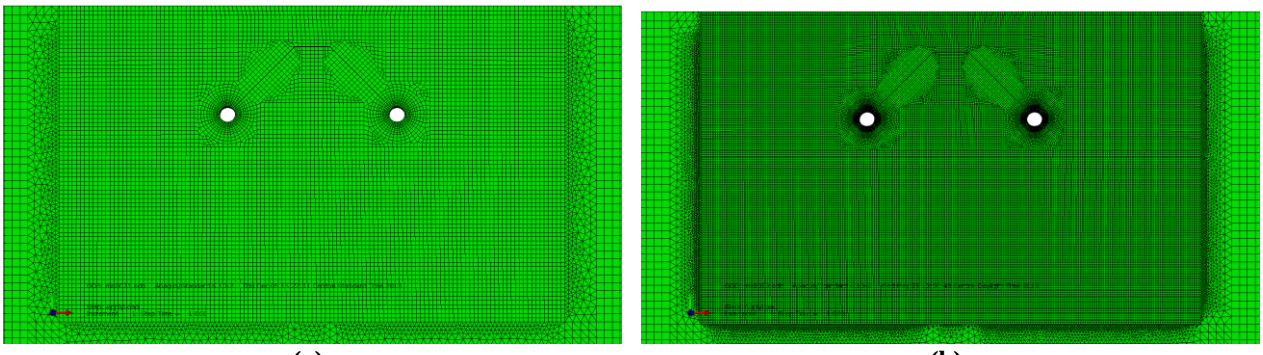

(a) **(b)**

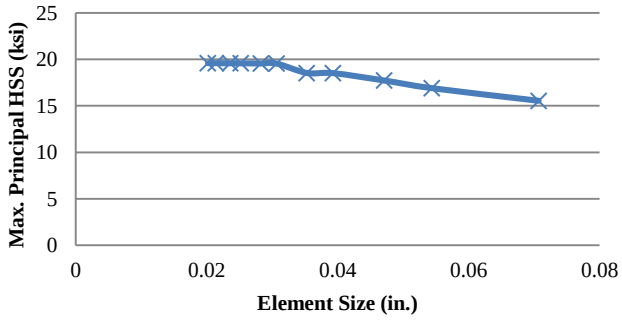

(c)

Figure 3.5: (a) Mesh in the vicinity of the crack-arrest holes for an element size of 1.80 mm [0.071 in]; (b) Mesh in the vicinity of the crack-arrest holes for an element size of 0.71 mm [0.02 in]; c) Effect of element size around the crack-arrest hole path on maximum principal HSS.

3.4.Model Validation

As described, the primary investigative technique used in this study was based upon a suite of refined, three-dimensional finite element simulations. To provide context to the simulations and to validate the finite element modeling approach, a physical test was performed on a built-up steel girder loaded in distortion-induced fatigue. A description of the physical test and findings pertinent to validating the FE simulations are presented in the following sections.

The physical test setup was comprised of a built-up steel girder that was connected to the concrete laboratory floor such that the girder was tested upside-down. The bottom flange of the girder in the laboratory was restrained to the laboratory floor over its entire length. One end of a cross-frame was attached to a connection plate located at mid-length of the girder. The opposite end of the cross-frame was attached to an actuator, which pulled upwards on the cross-frame, simulating the effect of distorsion-induced fatigue.

The web, bottom flange, and top flange of the test girder all had 345 MPa [50 ksi] yield strength. A connection plate 873 mm [34.4 in] tall and 127 mm [5.0 in.] wide was welded to the web at the middle of the girder. All stiffeners had a 32 mm [1 ¼ in.] cropped end and a thickness of 10 mm [3/8 in.]. A cross-frame was used to connect the connection plate and a WT section. The cross-frame was made up of three L76x76x10 mm [L3x3x3/8 in.] angles of which two were in a X-configuration, and one was as a horizontal member.

The girder of the subassembly was instrumented with three linear variable differential transformers (LVDTs) along the height of the girder and nine strain gages. Two strain gages were placed at the top and bottom web-gaps where the cracks were expected to initiate. Three LVDTs were used to capture the out-of-plane deflection at three different locations.

The subassembly was tested with cyclic tensile load that ranged from 2.2 kN [0.5 kip] to 25.3 kN [5.7 kip] applied by an MTS actuator connected to a WT section that was connected to the cross-frame. The test progressed as described in the following and in Figure 3.6:

Stage 1. Cyclic loading was applied to the girder, and a horseshoe-shaped crack initiated and propagated to 38-mm (1½-in) long around the connection plate-to-web weld. The girder was inspected often using UV light and dye

penetrant to determine crack growth rate, and the data was collected continuously while the girder was being cycled.

Stage 2. Next, a pair of crack-arrest holes were drilled at the tips of the cracks, one on each side of the connection plate. The diameter of the holes was 50.8 mm (2 in.). Since the cracking followed the connection plate weld, there was not enough room to drill the holes such that the tips of the cracks were located at the center of the holes; this is a common problem for cracking in this type of fatigue detail. Therefore, the holes were drilled about 3-mm ($^1/_8$-in) over the weld instead of placing the holes' circumference right at the edge of the weld. Around the holes, strain gages were installed to capture the deformation.

Stage 3. The specimen was cycled at the same load range as in Stage 1 of the test. The inspection procedures were carried out the same ways as mentioned in Stage 1. The specimen was tested until new cracks appeared and propagated to 76-mm (3-in.) long. The two new cracks did not originate from the crack-arrest holes, but originated at the weld.

Stage 4. Another pair of 50.8 mm (2 in.) diameter holes was drilled at the tips of the cracks. The location of the hole placement and the testing procedures were carried in the same way as in Segment 2.

Stage 5. Small cracks were noted to appear at the toe of the web-to-flange weld.

Stage 6. Additional cracking occurred at the connection plate-to-web weld; this crack did not originate from the crack-arrest hole, but originated from the weld, a short distance from the crack-arrest hole.

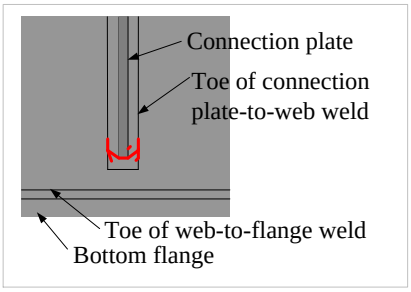

Stage 1- Initial crack formation

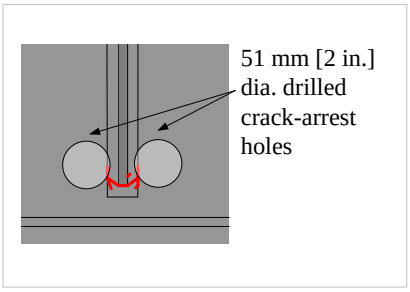

Stage 2 – Drilled crack-arrest holes at tips of cracks

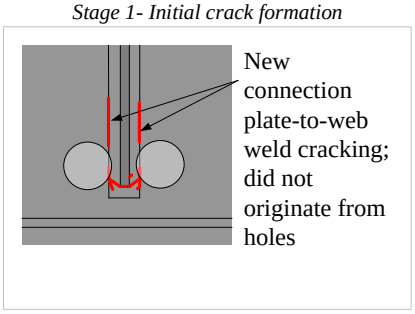

Stage 3 – New cracks initiate at the connection plate-to-web weld, above the drilled crack-arrest holes (but not out from the holes)

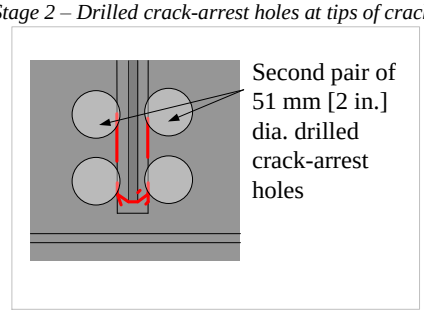

Stage 4 – New crack-arrest holes were drilled

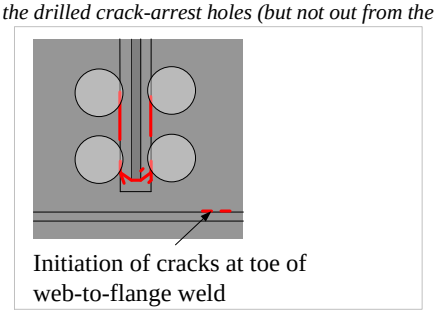

Stage 5 – Crack initiation was noted at web-to-flange weld

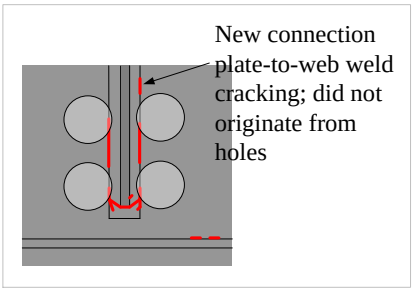

Stage 6 – New crack initiated at the connection plate-to-web weld, above the drilled crack-arrest hole (but not out from the hole)

Figure 3.6: Progression of cracking in physical test girder; red lines indicate crack locations

Drilling a pair of 51 mm (2.0 in) crack-arrest holes at the tips of the horseshoe-shaped crack eliminated the high stress demand at the tips of the crack. However, the stress concentrated at new locations along the stiffener-to-web weld at a small distance from the edge of the holes. The magnitude of stress was above the yield stress which resulted in cracking at those locations (Figure 3.7). Since the highest stress demand did not start at the edge of the holes, the existing cracks were assumed to have not yet propagated. New cracks did not initiate until the cycle count reached approximately 420,000. The cracks were located along the stiffener-to-web weld at 12.7 mm [0.5 in] away from the edge of the holes. There were no signs of cracks coming from the edge of the holes. The deformation data collected from strain gages on the top of the holes, shown in Figure 3.7, indicated that magnitude of strain was close to the strain at yield, shown in Figure 3.8. The strain on the left crack-arrest hole was higher than the strain value obtained on

the right crack-arrest hole as well. The lateral deflection along the height of the girder clearly indicated that the deflection of the girder was reduced significantly, resulting from the web becoming more flexible due to the presence of the holes, shown in Figure 3.9.

(a) (b) (c)

Figure 3.7: a) Crack-arrest hole and strain gage (circled) on the left of the connection plate; b) Crack-arrest hole and strain gage (circled) on the right of the connection plate; c) A new crack on the left of connection plate

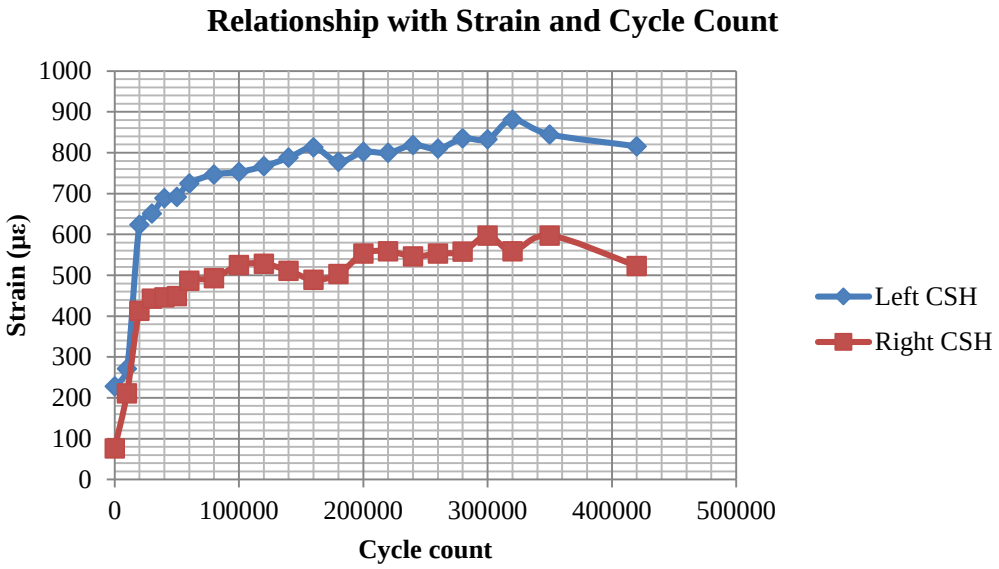

Figure 3.8: Relationship between strain and cycle count for one pair crack-arrest holes

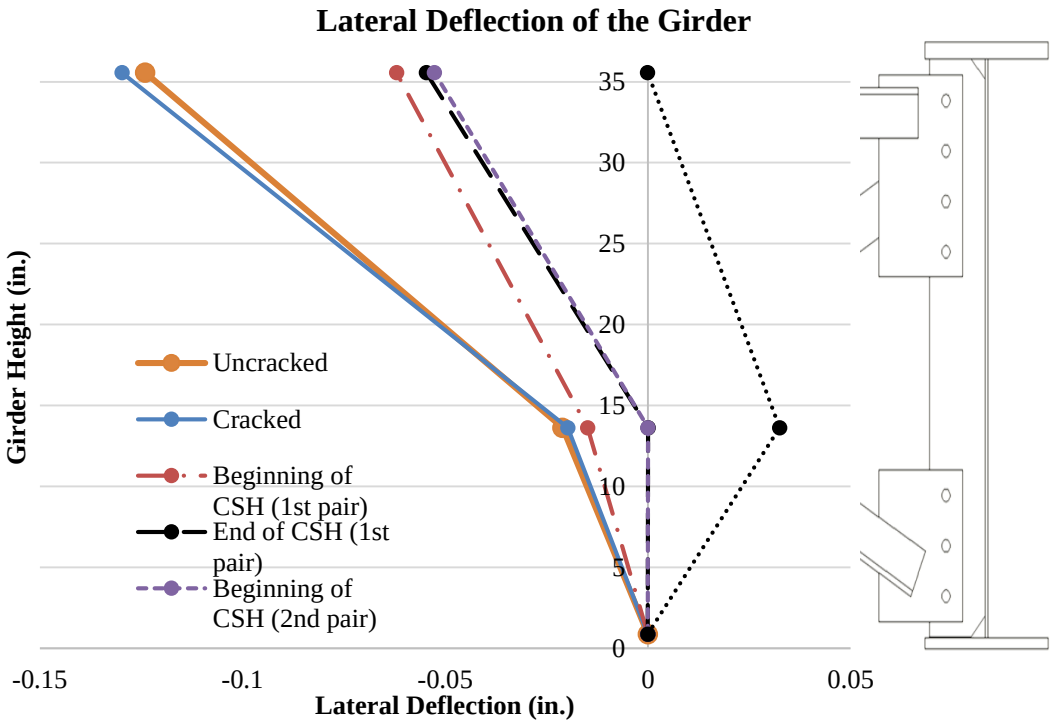

Figure 3.9 : Lateral deflection along the height of the girder

The FE model results with a second pair of crack-arrest holes induced new high stress locations along the stiffener-to-web weld at approximately about 38.1 mm [1.5 in.] from the edge of the holes as shown in Figure 3.10. Those results were also comparable to the results from the physical testing. New cracks first initiated at about 19 mm [0.75 in.] away from the edge of the holes at approximately 980,000 cycles, and then propagated towards the edge of the holes. The deformation indicated that the highest strain was located on the right of the connection plate. The lateral deflection along the height of the girder was once again greatly reduced, as shown in Figure 3.9, and the web became more flexible.

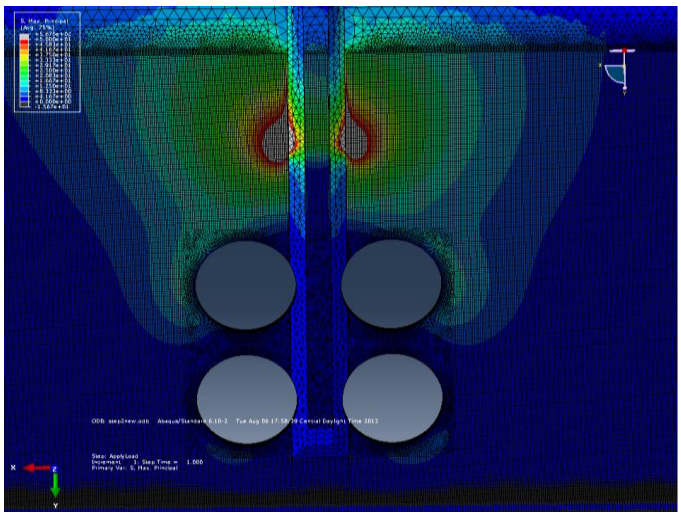

Figure 3.10: Finite Element model of two pairs of crack-arrest holes

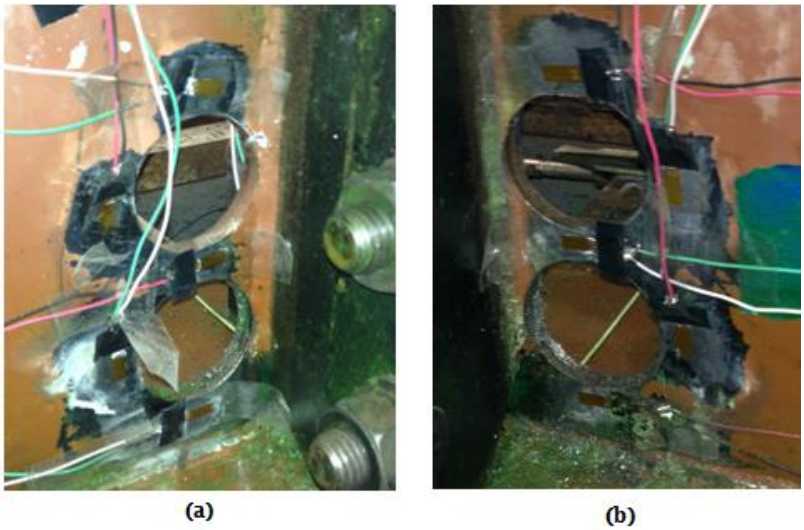

Figure 3.11: Strain gage placement around two pairs of crack-arrest holes in the physical testing: (a) Left side of the connection plate (b) Right side of the connection plate

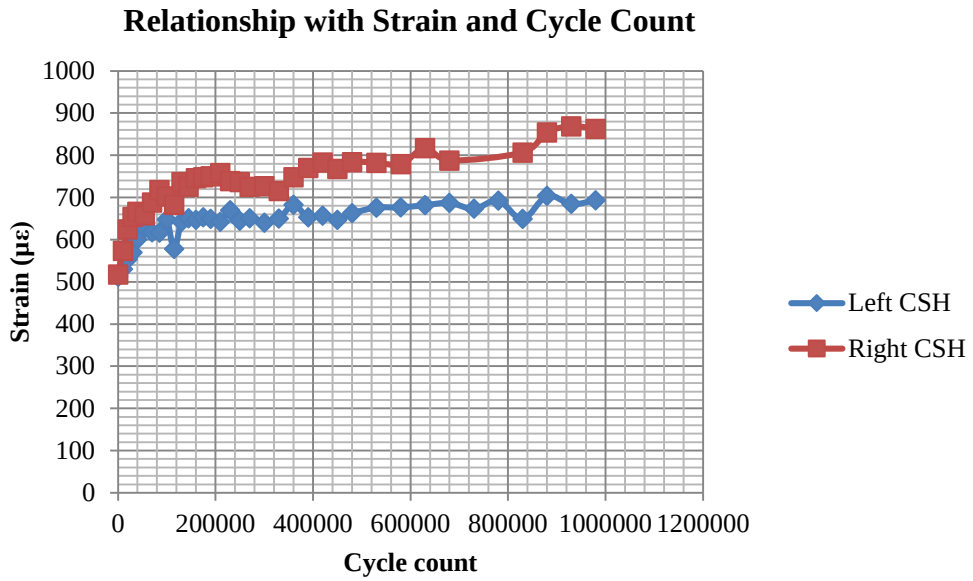

Figure 3.12: Relationship between strain and cycle count at the top of the second pair crack-arrest holes

3.5.Model Including Plate Washer & Tensioned Bolt

The effect of a plate washer with a pretensioned bolt installed in a crack-arrest hole was also examined. In the diagonal crack-arrest hole model with 152 mm [6 in.] crack length and 25 mm [1 in.] hole diameter, two 76 mm × 76 mm × 6 mm [3 in. × 3 in. × 1/4 in.] plate washers were attached to the frontal side of the web covered on the crack-arrest holes through two pretensioned bolts, as shown in Figure 3.13. A 124.5 kN [28 kip] pretensioning load was applied on the bolt. The material used for the plate washer and bolt was steel.

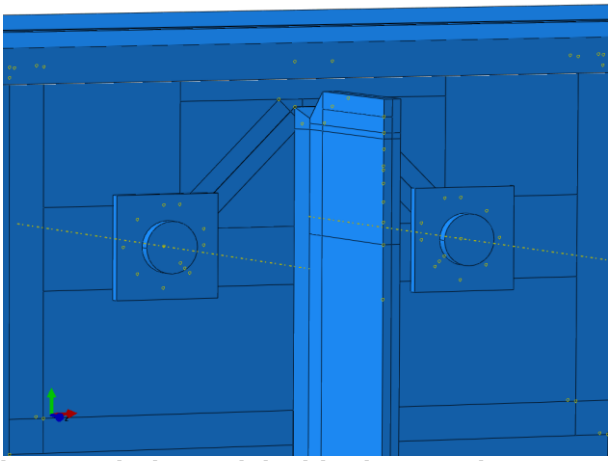

Figure 3.13: Diagonal crack-arrest hole model with plate washer & tensioned bolt

4. Results and Discussion

For each diagonal crack, horseshoe crack, horizontal crack, and horseshoe & horizontal crack, the effect of crack-arrest holes was evaluated by changing the diameter of the holes using values of 12.7 mm [0.5 in.], 25.4 mm [1.0 in.], 50.8 mm [2.0 in.], 63.5 mm [2.5 in.], and 76.2 mm [3.0 in.] drilled at crack tips. The length of diagonal and horseshoe crack was altered using values of 69.9 mm [2.75 in.], 101.6 mm [4.0 in.], and 152.4 mm [6.0 in.]. The length of horizontal crack was varied by 139.7 mm [5.5 in.], 203.2 mm [8.0 in.], and 304.8 mm [12.0 in.]. Results for varying stress paths have been compiled in Figure 4.2 through Figure 4.5 for each crack type. Table 4.1 through Table 4.5 presents maximum principal stress as a function of hole diameter for each stress path. Representative plots for maximum principal stress for all crack placement types are shown in Figure 4.1. These stress contours are presented with limits from 0 to 345 MPa [50 ksi].

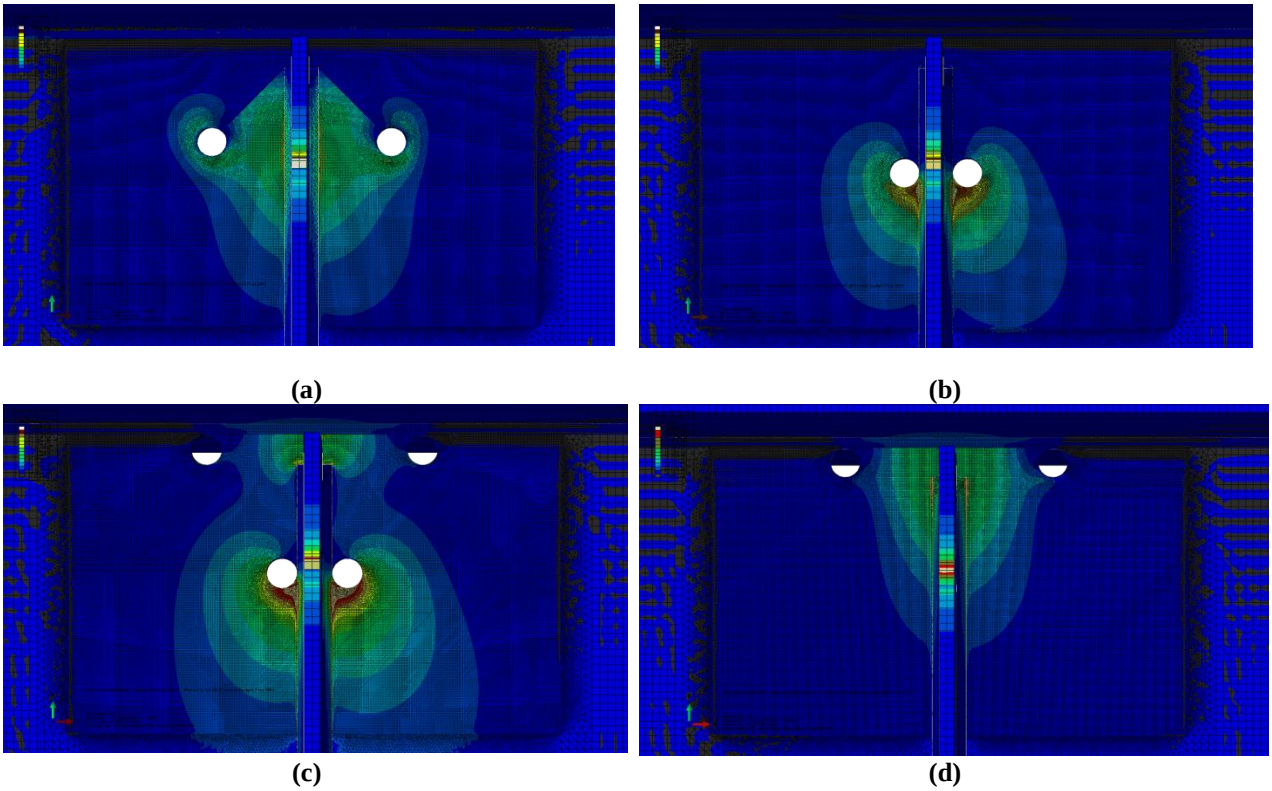

(a) **(b)**

(c) **(d)**

Figure 4.1: (a) Maximum principal stress for diagonal shaped crack-arrest hole models; (b) Maximum principal stress for horseshoe shaped crack-arrest hole models; (c) Maximum principal stress for horizontal & horseshoe shaped crack-arrest hole models; (d) Maximum principal stress for horizontal shaped crack-arrest hole models

Table 4.1: Diagonal crack stresses

Maximum Principal Stresses for 69.9 mm [2.75 in.] Crack

	Circular HSS-1	HSS-1	HSS-2
Diameter, mm [in.]	Peak Stress, MPa [ksi]	Peak Stress, MPa [ksi]	Peak Stress, MPa [ksi]
12.7 [0.5]	127 [18.4]	157 [22.7]	-0.41 [-0.059]
25.4 [1.0]	161 [23.4]	168 [24.3]	-0.22 [-0.032]
50.8 [2.0]	222 [32.2]	234 [33.9]	-0.25 [-0.036]

Maximum Principal Stresses for 101.6 mm [4.0 in.] Crack

	Circular HSS-1	HSS-1	HSS-2
Diameter, mm [in.]	Peak Stress, MPa [ksi]	Peak Stress, MPa [ksi]	Peak Stress, MPa [ksi]
12.7 [0.5]	150 [21.7]	170 [24.7]	-0.52 [-0.076]
25.4 [1.0]	150 [21.7]	172 [24.9]	-0.25 [-0.036]
50.8 [2.0]	197 [28.6]	196 [28.4]	-0.29 [-0.042]
76.2 [3.0]	237 [34.4]	247 [35.8]	8.19 [1.19]

Maximum Principal Stresses for 152.4 mm [6.0 in.] Crack

	Circular HSS-1	HSS-1	HSS-2
Diameter, mm [in..]	Peak Stress, MPa [ksi]	Peak Stress, MPa [ksi]	Peak Stress, MPa [ksi]
12.7 [0.5]	187 [27.1]	184 [26.7]	-0.42 [-0.061]
25.4 [1.0]	154 [22.3]	188 [27.2]	-0.22 [-0.032]
50.8 [2.0]	184 [26.7]	206 [29.9]	0.99 [0.143]
76.2 [3.0]	208 [30.2]	212 [30.8]	10.9 [1.579]

Table 4.2: Horseshoe-shaped crack stresses

Maximum Principal Stresses for 69.9 mm [2.75 in.] Crack

	Circular HSS-1	HSS-1	HSS-2
Diameter, mm [in.]	Peak Stress, MPa [ksi]	Peak Stress, MPa [ksi]	Peak Stress, MPa [ksi]
12.7 [0.5]	252 [36.6]	364 [52.8]	-0.46 [-0.067]
25.4 [1.0]	263 [38.2]	286 [41.5]	-0.23 [-0.034]
50.8 [2.0]	250 [36.3]	263 [38.1]	-0.26 [-0.037]
76.2 [3.0]	241 [35.0]	252 [36.5]	16.7 [2.42]

Maximum Principal Stresses for 101.6 mm [4.0 in.] Crack

	Circular HSS-1	HSS-1	HSS-2
Diameter, mm [in.]	Peak Stress, MPa [ksi]	Peak Stress, MPa [ksi]	Peak Stress, MPa [ksi]

12.7 [0.5]	314 [45.6]	449 [65.1]	-0.48 [-0.070]
25.4 [1.0]	312 [45.2]	335 [48.6]	-0.21 [-0.030]
50.8 [2.0]	283 [41.0]	296 [42.9]	-.21 [-0.030]
76.2 [3.0]	268 [38.8]	277 [40.2]	-0.27 [-0.039]

Maximum Principal Stresses for 152.4 mm [6.0 in.] Crack

	Circular HSS-1	HSS-1	HSS-2
Diameter, mm [in.]	Peak Stress, MPa [ksi]	Peak Stress, MPa [ksi]	Peak Stress, MPa [ksi]
12.7 [0.5]	408 [59.2]	583 [84.5]	-0.53 [-0.077]
25.4 [1.0]	389 [56.4]	414 [60.1]	-0.23 [-0.033]
50.8 [2.0]	338 [49.0]	350 [50.8]	-0.20 [-0.029]
76.2 [3.0]	312 [45.2]	320 [46.4]	-0.24 [-0.035]

Table 4.3: Horizontal & horseshoe crack stresses

Maximum Principal Stresses for 69.9 mm [2.75 in.] Crack

	Circular HSS-1	Circular HSS-2	HSS-1	HSS-2
Diameter, mm [in.]	Peak Stress, MPa [ksi]	Peak Stress, MPa [ksi]	Peak Stress, MPa [ksi]	Peak Stress, MPa [ksi]
12.7 [0.5]	298 [43.2]	22.8 [3.30]	431 [62.5]	122 [17.7]
25.4 [1.0]	290 [42.1]	56.5 [8.20]	314 [45.6]	98.6 [14.3]

Maximum Principal Stresses for 101.6 mm [4.0 in.] Crack

	Circular HSS-1	Circular HSS-2	HSS-1	HSS-2
Diameter, mm [in.]	Peak Stress, MPa [ksi]	Peak Stress, MPa [ksi]	Peak Stress, MPa [ksi]	Peak Stress, MPa [ksi]
12.7 [0.5]	379 [54.9]	20.7 [3.0]	554 [80.4]	178 [25.8]
25.4 [1.0]	356 [51.7]	32.4 [4.7]	382 [55.4]	172 [25.0]
50.8 [2.0]	307 [44.5]	77.2 [11.2]	319 [46.2]	100 [14.5]

Maximum Principal Stresses for 152.4 mm [6.0 in.] Crack

	Circular HSS-1	Circular HSS-2	HSS-1	HSS-2
Diameter, mm [in.]	Peak Stress, MPa [ksi]	Peak Stress, MPa [ksi]	Peak Stress, MPa [ksi]	Peak Stress, MPa [ksi]
12.7 [0.5]	501 [72.6]	29.6 [4.3]	748 [109]	259 [37.5]
25.4 [1.0]	461 [66.8]	22.1 [3.2]	488 [70.8]	267 [38.7]
50.8 [2.0]	385 [55.9]	52.4 [7.6]	394 [57.1]	244 [35.4]
76.2 [3.0]	346 [50.2]	100 [14.5]	349 [50.6]	161 [23.3]

Table 4.4: Horizontal crack stresses

Maximum Principal Stresses for 139.7 mm [5.5 in.] Crack

	Circular HSS-1	HSS-1	HSS-2
Diameter, mm [in.]	Peak Stress, MPa[ksi]	Peak Stress, MPa[ksi]	Peak Stress, MPa[ksi]
12.7 [0.5]	16.2 [2.35]	141 [20.4]	154 [22.3]
25.4 [1.0]	88.1 [12.78]	147 [21.3]	129 [18.7]
50.8 [2.0]	192 [27.86]	203 [29.5]	7.58 [1.10]

Maximum Principal Stresses for 203.2 mm [8.0 in.] Crack

	Circular HSS-1	HSS-1	HSS-2
Diameter, mm[in.]	Peak Stress, MPa[ksi]	Peak Stress, MPa[ksi]	Peak Stress, MPa[ksi]
12.7 [0.5]	1.72 [0.25]	179 [26.0]	179 [25.9]
25.4 [1.0]	41.4 [6.00]	180 [26.1]	168 [24.4]
50.8 [2.0]	141 [20.48]	169 [24.5]	93.1 [13.5]
76.2 [3.0]	205 [29.67]	212 [30.8]	4.48 [0.65]

Maximum Principal Stresses for 304.8 mm [12 in.] Crack

	Circular HSS-1	HSS-1	HSS-2
Diameter, mm [in.]	Peak Stress, MPa[ksi]	Peak Stress, MPa[ksi]	Peak Stress, MPa[ksi]
12.7 [0.5]	2.21 [0.32]	219 [31.8]	201 [29.13]
25.4 [1.0]	4.34 [0.63]	220 [31.9]	199 [28.83]
50.8 [2.0]	88.0 [12.76]	205 [29.7]	167 [24.16]
76.2 [3.0]	151 [21.91]	188 [27.3]	102 [14.79]

Table 4.5: 101.6 mm [4.0 in.] diameter hole stresses

Maximum Principal Stresses for 101.6 mm [4.0 in.] Diameter Hole

	Circular HSS	HSS-1	HSS-2
	Peak Stress, MPa [ksi]	Peak Stress, MPa [ksi]	Peak Stress, MPa [ksi]
Horizontal 101.6 mm [4.0 in.]	245 [35.6]	256 [37.1]	0.717 [0.10]
Horseshoe 101.6 mm [4.0 in.]	245 [35.6]	255 [37.0]	50.7 [7.35]

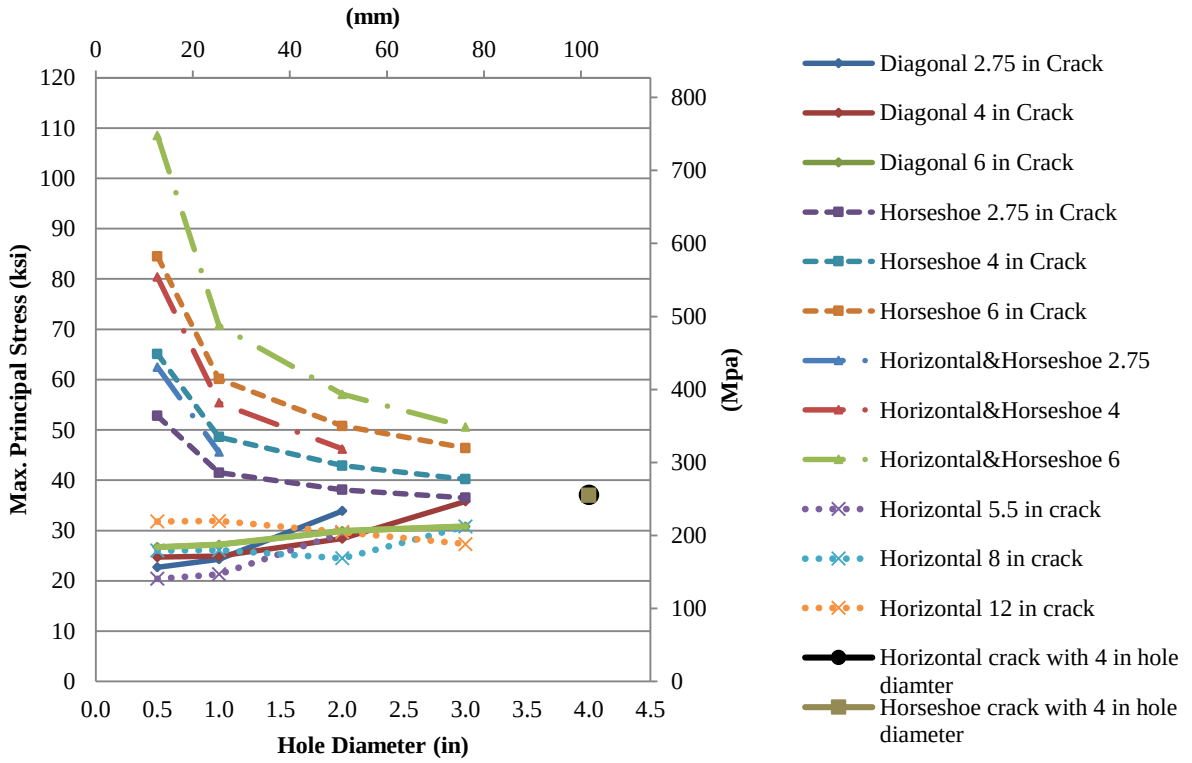

Figure 4.2: HSS-1 for various crack placements, lengths, and hole diameters

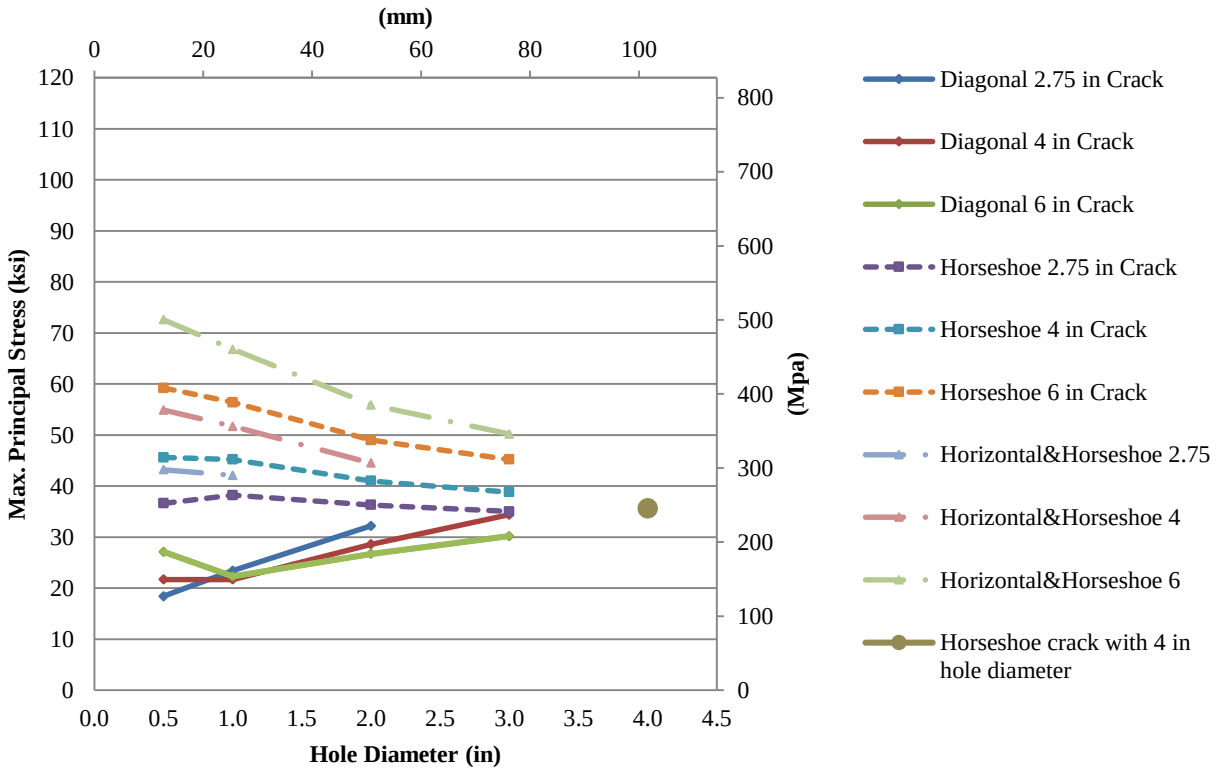

Figure 4.3: CHSS-1 for various crack placements, lengths, and hole diameters

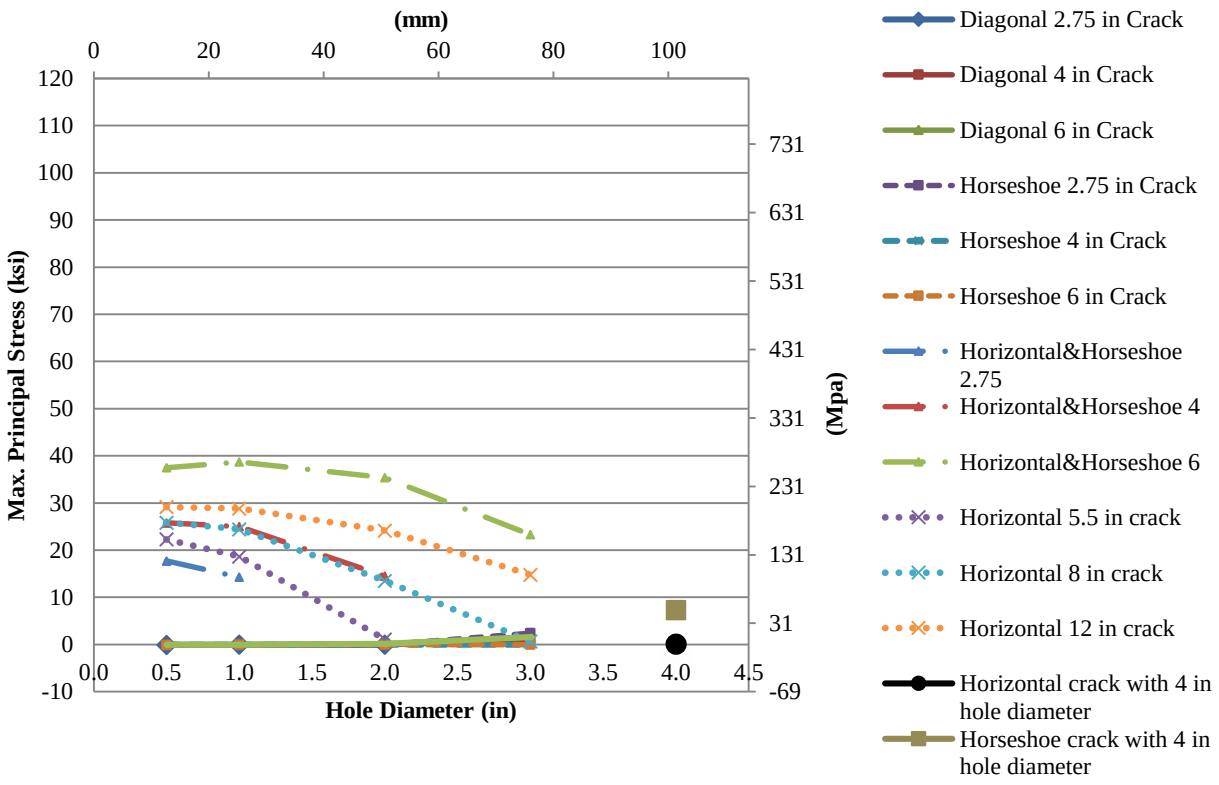

Figure 4.4: HSS-2 for various crack placements, lengths, and hole diameters

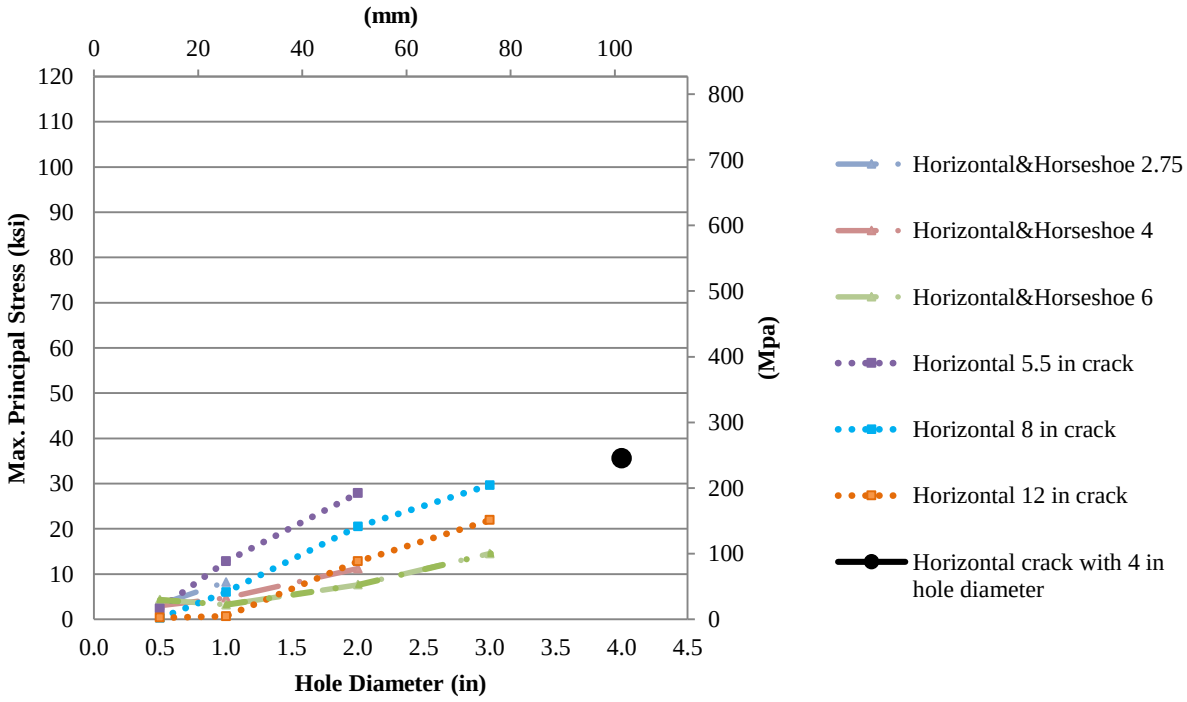

Figure 4.5: CHSS-2 for various crack placements, lengths, and hole diameters

4.1.Effect of crack-arrest holes for diagonal crack

As shown in Figure 3.3, the crack was modeled to occur as a diagonal crack and the paths from which stresses were measured are referred to as HSS-1, HSS-2 and circular HSS-1 (CHSS-1) respectively. The effect of crack-arrest holes on HSS in the steel girder section is shown in Table 4.1 and Figure 3.6. In Figure 3.6a, HSS-1 increased with increasing hole diameter for 69.9 mm [2.75 in.], 101.6 mm [4.0 in.], and 152.4 mm [6.0 in.] arrest hole sizes. By increasing the hole diameter, the edge of the hole translated closer to the stiffener and flange, causing a stress concentration to form at the welds. Under distortion-induced fatigue, large diameter crack-arrest holes do not perform better than small diameter crack-arrest holes. The data showed that for diagonal crack occurring on the steel girder section, drilling smaller crack-arrest holes for shorter crack lengths was most effective for 152.4 mm [6.0 in.] crack lengths. The rate of stress change decreased with increasing crack length. The rate of stress change varied the most for the shortest crack length, which was 69.9 mm [2.75 in.]. The trend for the magnitude of HSS-2 generally decreased before increasing with increasing crack-arrest hole diameter.

4.2.Effect of crack-arrest holes for horseshoe crack

Figure 3.3 shows the crack modeled as a horseshoe crack. The paths will be referred to as HSS-1, HSS-2 and CHSS-1 respectively. The results for these variations are compiled in Table 4.2 and presented graphically in Figure 3.6. In general, increasing the diameter of holes resulted in a reduction of HSS-1 and CHSS-1. Similar to the relationship for diagonal models, the magnitude of HSS-2 decreased then increased with increasing hole size for 69.9 mm [2.75 in.], 101.6 mm [4.0 in.], and 152.4 mm [6.0 in.] crack length models. At the same hole diameter, increasing the crack length led to an increase in HSS-1 and CHSS-1. The smaller diameter holes for shorter length cracks decreased the HSS more than larger diameter holes for longer length cracks.

4.3.Effect of crack-arrest holes for horizontal & horseshoe crack

Another crack pattern is a horizontal and horseshoe crack occurring simultaneously. As shown in Figure 3.3, these paths will be referred to as HSS-1, HSS-2, CHSS-1 and CHSS-2 respectively. The results are shown in Table 4.3. Similar to the relationship for horseshoe crack

models, increasing the diameter of crack-arrest holes resulted in a reduction of HSS-1, HSS-2 and CHSS-1 for each length combination of cracks. The CHSS-2 increased when the crack-arrest holes diameter increased for different crack lengths. Due to the crack edge translating closer to the stiffener, the stress concentrated near the stiffener weld.

4.4.Effect of crack-arrest holes for horizontal crack

For the horizontal crack shown in Figure 3.3, the paths will be referred to as HSS-1, HSS-2 and CHSS-2 respectively. The results presented in Table 4.4 and Figure 3.6 show that the HSS-1 for a 139.7 mm [5.5 in.] crack increased with an increase in hole diameter. However, the HSS-1 for the 203.2 mm [8.0 in.] crack decreased then increased for increasing hole diameters. The HSS-1 for a 304.8 mm [12.0 in.] crack always decreased with increasing holes diameters. The HSS-2 decreases when the diameter increased while the CHSS-2 increased with increasing holes size.

4.5.Large-hole retrofit

McGormley and Koob studied the behavior of large-hole retrofits to address distortion-induced cracking. Their results showed that the large hole provided a cost-effective and practical solution to addressing distortion-induced cracking. In this study, a horizontal crack model and a horseshoe crack model with 101.6 mm [4.0 in.] diameter holes were developed, as shown in Figure 3.4. The results are presented in Table 4.5, as well as in Figure 4.2 through Figure 4.5. For the horizontal crack model, the HSS-2 for the 101.6 mm [4.0 in.] diameter hole model was less than the stresses in the smaller diameter hole models. However, the HSS-1 and circular HSS for the 101.6 mm [4.0 in.] diameter hole model was larger than the stresses analyzed in smaller diameter hole models. For the horseshoe crack model, the HSS-1 and circular HSS for a 101.6 mm [4.0 in.] diameter hole were nearly the same as the stresses found in the 69.9 mm [2.75 in.] crack model with 76.2 mm [3.0 in.] diameter hole. The HSS-2 for the horseshoe crack model with a 101.6 mm [4.0 in.] diameter hole model was higher than the stresses measured in the smaller diameter hole models. This showed that large diameter crack-arrest holes did not perform better than small diameter crack-arrest holes for certain crack configurations.

4.6.Effect of including pretensioned bolt with plate washer

The effect of a plate washer with pretensioned bolt for the diagonal crack-arrest hole model with 152 mm [6 in.] crack length and 25 mm [1 in.] hole diameter was also evaluated. The screenshots showing the stresses around the crack for the diagonal crack-arrest hole model with plate washer and the diagonal crack-arrest hole model without plate washer are shown in Figure 4.6. The results compared with the diagonal crack-arrest hole model without plate washer are presented in Figure 4.7. The peak circular HSS for the model with plate washer was slightly higher than the stress for the model without plate washer. The peak HSS-1 for the model without plate washer was slightly higher than the stress for the model with plate washer. The HSS-2 value for the model with plate washer and the model without plate washer waalmost the same. Therefore, it was found that the effect of plate washer and pretensioned bolt on reducing the hot spot stress caused by the distortion-induced fatigue was almost the same with the effect of drilling crack-arrest holes. Additionally, stresses along the connection-plate-to-web-weld remained approximately unchanged, indicating that the retrofit application should not be expected to be effective in this application.

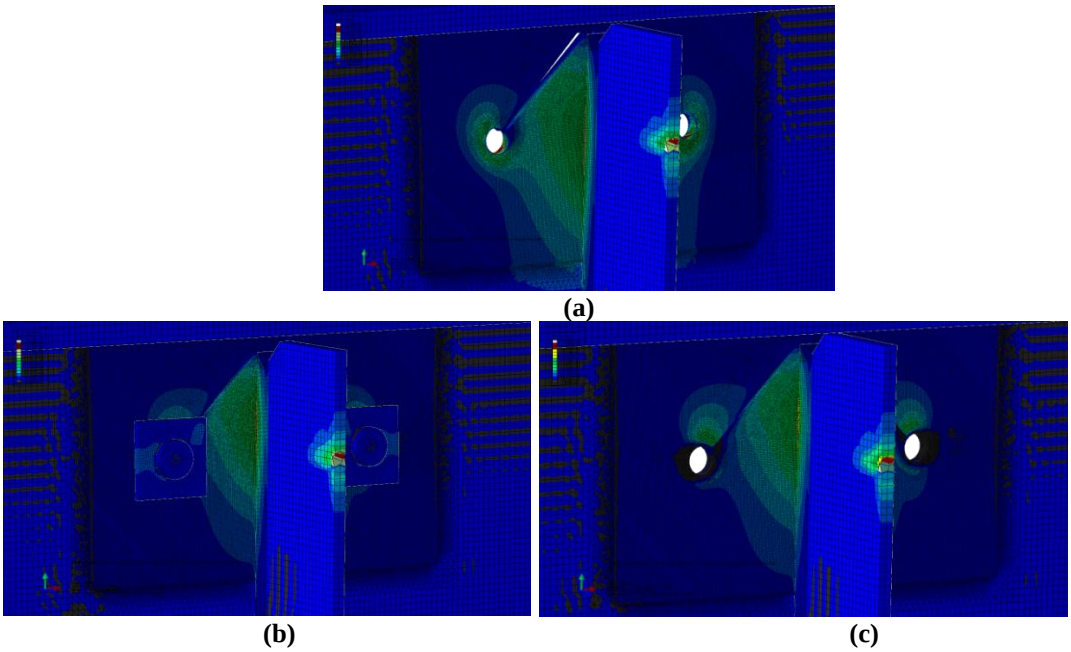

(a)

(b) **(c)**

Figure 4.6: (a) Maximum principal stress for diagonal shaped crack-arrest hole model without plate washer; (b) Maximum principal stress for diagonal shaped crack-arrest hole model with plate washer; (c) Maximum principal stress for diagonal shaped crack-arrest hole model with plate washer (plate washer is not shown)

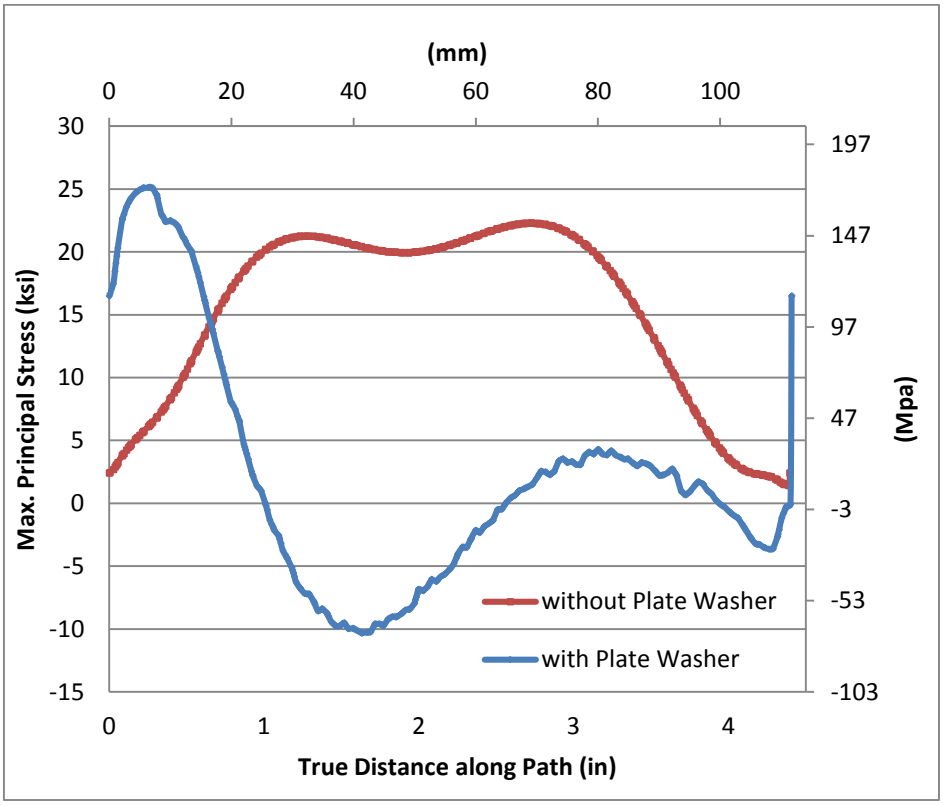
(mm)
0
20
40
60
80
100
30
25
20
15
10
5
0
-5
-10
-15
197
147
97
47
-3
-53
-103
(Mpa)
Max. Principal Stress (ksi)
without Plate Washer
with Plate Washer
0
1
2
3
4
True Distance along Path (in)

(a)

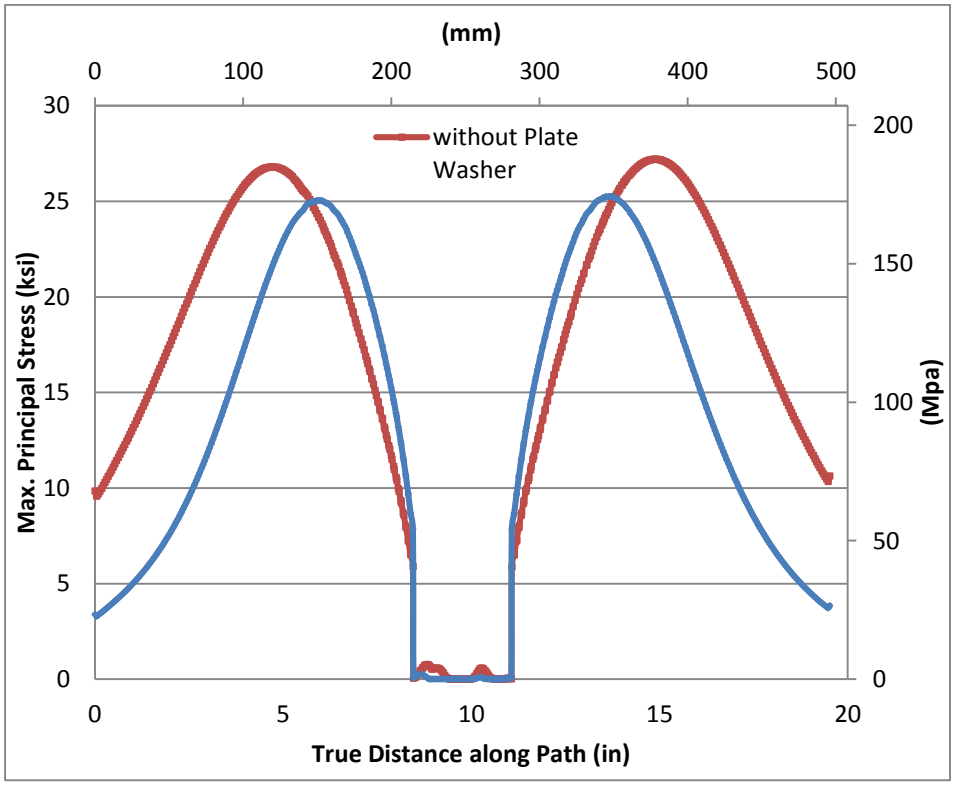
(mm)
0
100
200
300
400
500
30
25
20
15
10
5
0
200
150
100
50
0
(Mpa)
Max. Principal Stress (ksi)
without Plate Washer
0
5
10
15
20
True Distance along Path (in)

(b)

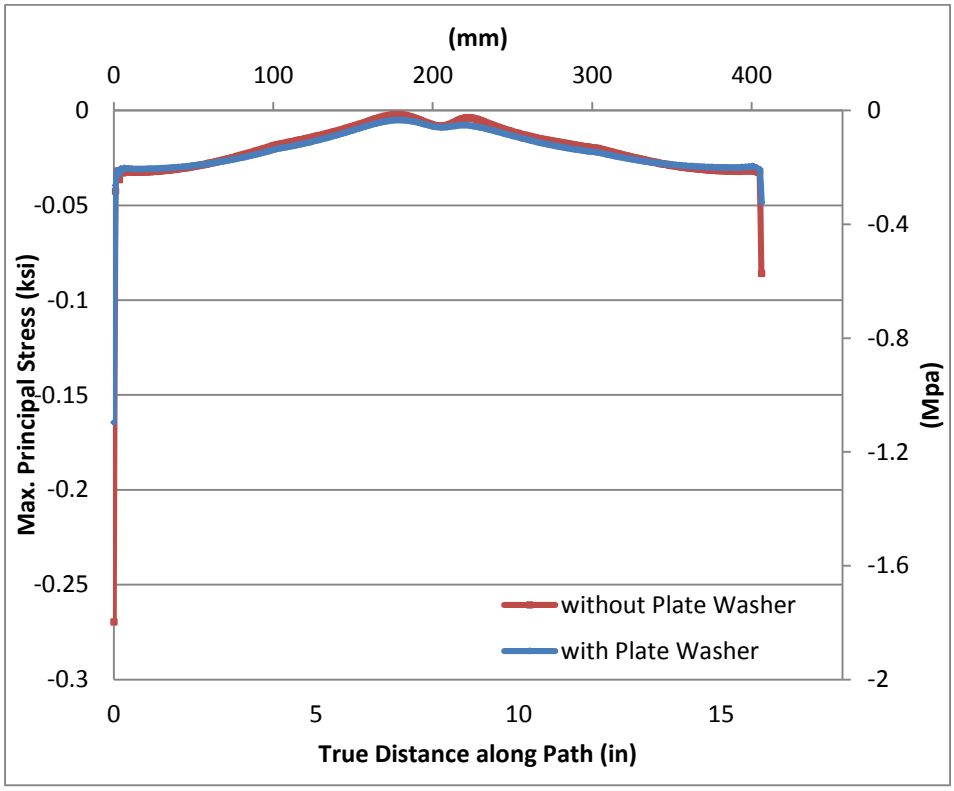

(c)

Figure 4.7: (a) Circular HSS comparison between diagonal shaped crack-arrest hole model without plate washer and model with plate washer; (b) HSS-1 comparison between diagonal shaped crack-arrest hole model without plate washer and model with plate washer; (c) HSS-2 comparison between diagonal shaped crack-arrest hole model without plate washer and model with plate washer along the path

5. Conclusions

Common knowledge has been that large diameter crack-arrest holes are more effective at halting crack propagation under distortion-induced fatigue than small diameter crack-arrest holes. However, because the cracks often occur in the girder webs at stiffener-to-web or flange-to-web welds, drilling large diameter crack-arrest holes cause stress concentrations near the weld, which do not perform better than small diameter crack-arrest holes under distortion-induced fatigue. Additional, we found drilling crack-arrest holes for shorter crack length cracks was more effective than drilling crack-arrest holes for longer length cracks. This implies that crack-arrest hole placement, rather than hole diameter, has a much greater effect on the effectiveness of the crack-arrest hole in bridge girders susceptible to distortion-induced fatigue. Also, we found installing plate washer does not perform better than drilling crack-arrest holes on reducing the hot spot stress caused by distortion-induced fatigue.

Experimental results showed that by drilling crack-arrest holes at the tips of the crack, the web became more flexible. This resulted in a decrease in lateral deflection of the girder and an improvement in the fatigue category detail to at least category B' as well as increasing overall fatigue life of the girder. From the results of inspection, the existing cracks never reinitiated from the holes. New cracks tended to form along the stiffener-to-web weld at a distance from the holes. The holes provided a wider area in the web for stresses to be distributed away from the stiffener. These studies concluded that a 50.8-mm [2.0-in.] crack-arrest holes was effective in stopping horseshoe cracks from propagating. However, since the stress demand at the connection-plate-to-web weld were high, new cracks initiated along the stiffener-to-web weld at a small distance away from the drilled holes.

6. References

Alemdar, F. (2011) “Repair of bridge steel girders damage by distortion-induced fatigue”.

Castiglioni, C., et. al. (1988). “Evaluation of fatigue cracking at cross diaphragms of a multigirder steel bridge”. Journal of Constructional Steel Research, vol. 9, no. 2, pp. 95-110.

Jajich, D., and Schultz, A. E. (2003). “Measurement and Analysis of Distortion-Induced Fatigue in Mutligirder Steel Bridges”. Journal of Bridge Engineering, vol. 8, no. 2, pp. 84-91.

Keating, P. B. (1994). “Focusing on fatigue”. Civil Engineering—ASCE, vol. 64, no. 11, pp. 54-57.

Marquis, G., and Kahonen, A. (1995). "Fatigue testing and analysis using the hot spot method". Technical Research Centre of Finland.

McGormley, J. C., and Koob, M. J. (2001). “Large Hole Retrofits to Address Distortion-Induced Cracking”.

Roddis, W. M. Kim, and Zhao, Yuan (2001). “Out-of-Plane Fatigue Cracking in Welded Steel Bridges: Why It Happened and How It Can Be Repaired”. Welding Innovation, vol. 27, no. 2, pp. 2-7.

Tedesco, J. W., et. al. (1995). “Finite Element Method Analysis of Bridge Girder-Diaphragm Interaction”. Computers and Structures, vol. 56, no. 2-3, pp. 461-473.

Appendix A: Maximum Principal Stress around Crack-arrest Holes for Diagonal Crack Type

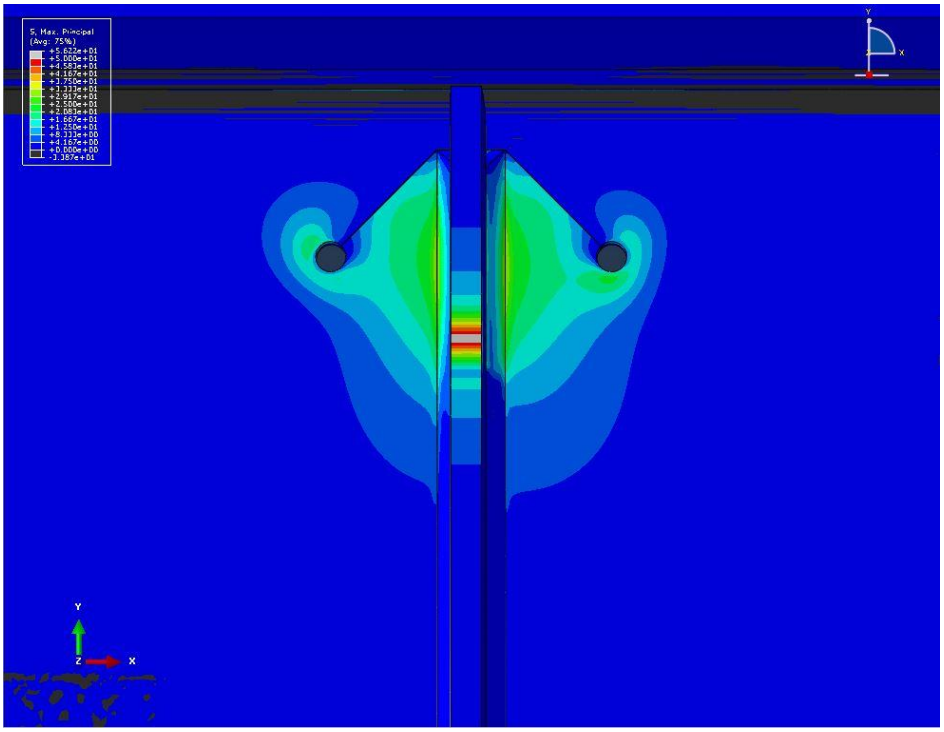

CHSS-1 = 127 Mpa [18.4 ksi]

HSS-1 = 157 Mpa [22.7 ksi]

HSS-2 = -0.41 Mpa [-0.059 ksi]

69.9 mm [2.75 in.] Crack Length & 12.7 mm [0.5 in.] Hole Diameter

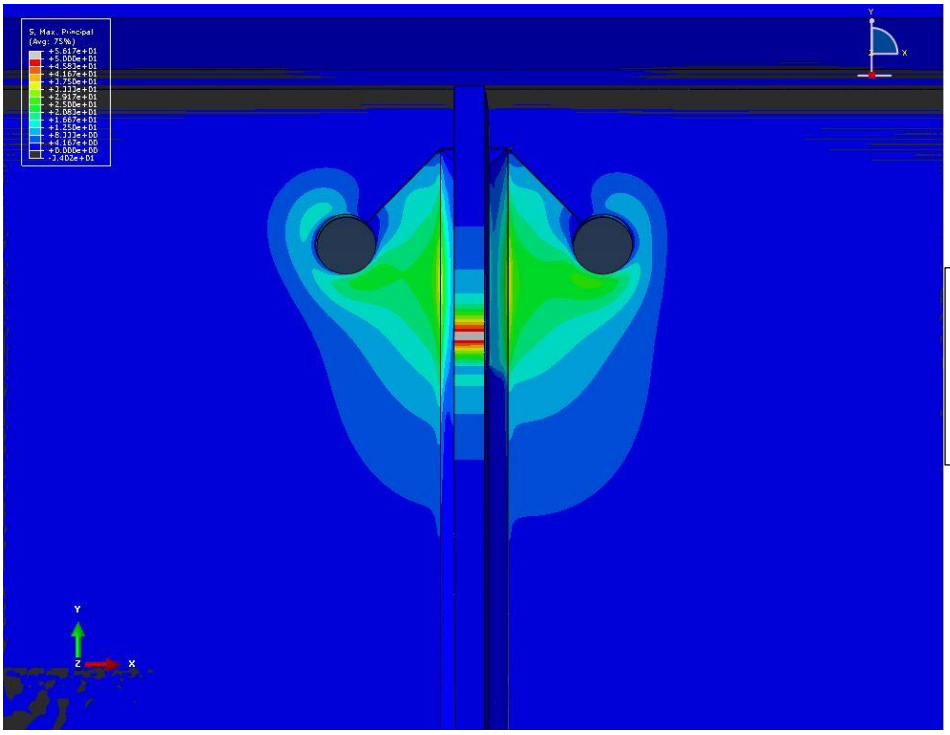

CHSS-1 = 161 Mpa [23.4 ksi]

HSS-1 = 168 Mpa [24.3 ksi]

HSS-2 = -0.22 Mpa [-0.032 ksi]

69.9 mm [2.75 in.] Crack Length & 25.4 mm [1.0 in.] Hole Diameter

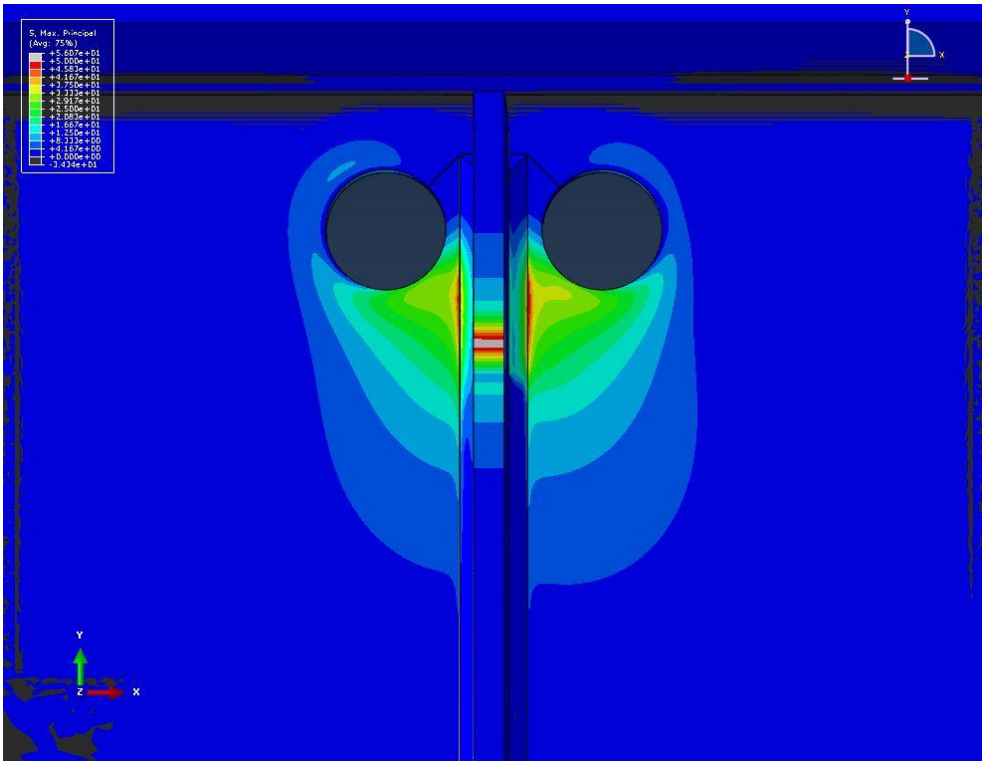

CHSS-1 = 222 Mpa [32.2 ksi]

HSS-1 = 234 Mpa [33.9 ksi]

HSS-2 = -0.25 Mpa [-0.036 ksi]

69.9 mm [2.75 in.] Crack Length & 50.8 mm [2.0 in.] Hole Diameter

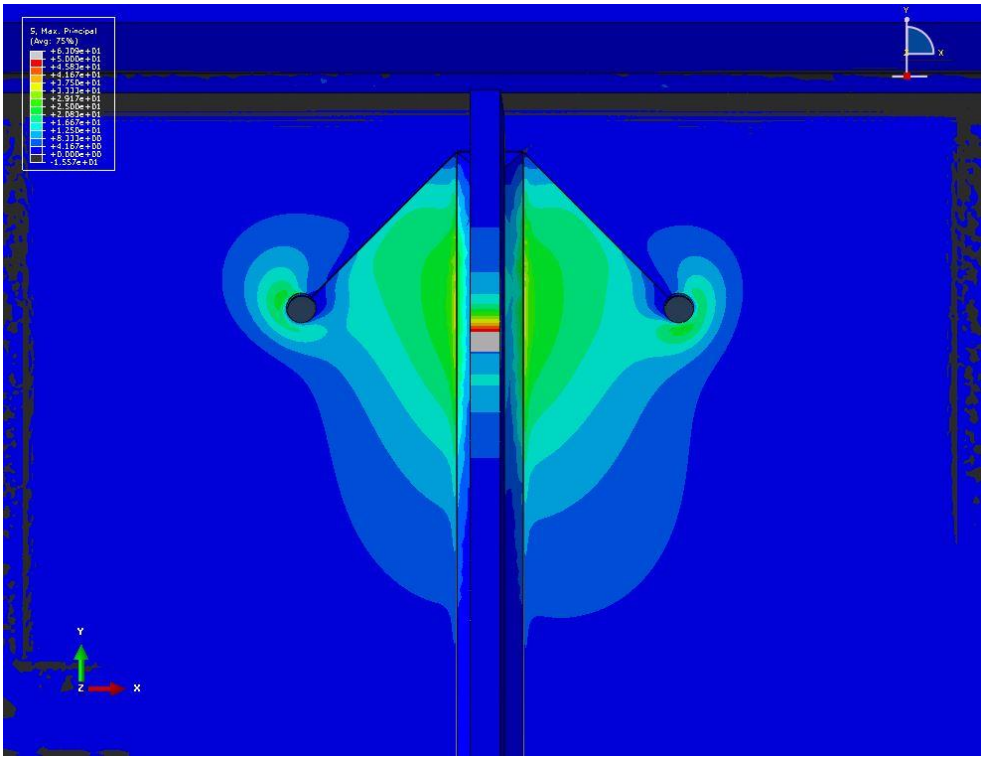

CHSS-1 = 150 Mpa [21.7 ksi]

HSS-1 = 170 Mpa [24.7 ksi]

HSS-2 = -0.52 Mpa [-0.076 ksi]

101.6 mm [4.0 in.] Crack Length & 12.7 mm [0.5 in.] Hole Diameter

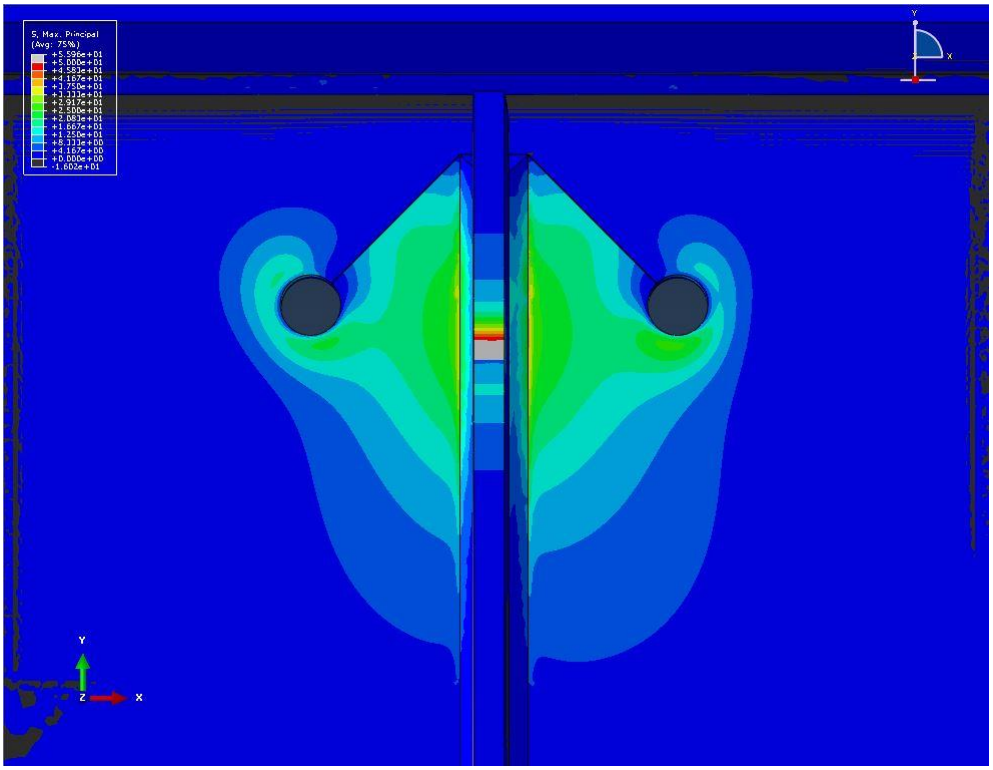

CHSS-1 = 150 Mpa [21.7 ksi]

HSS-1 = 172 Mpa [24.9 ksi]

HSS-2 = -0.25 Mpa [-0.036 ksi]

101.6 mm [4.0 in.] Crack Length & 25.4 mm [1.0 in.] Hole Diameter

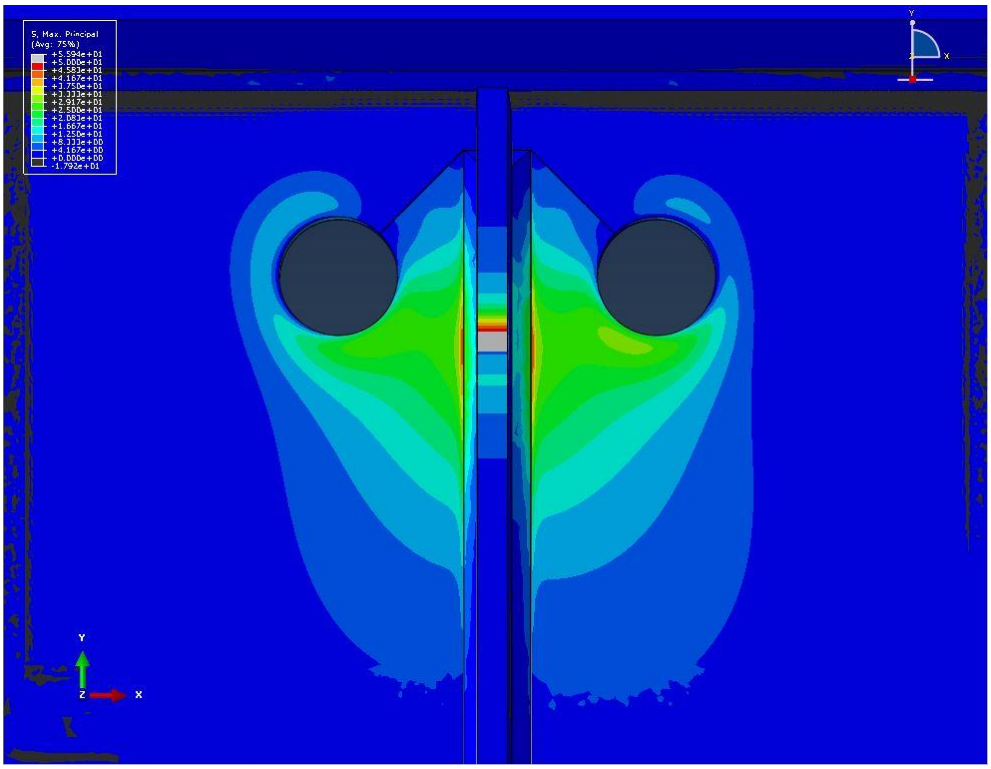

CHSS-1 = 197 Mpa [28.6 ksi]

HSS-1 = 196 Mpa [28.4 ksi]

HSS-2 = -0.29 Mpa [-0.042 ksi]

101.6 mm [4.0 in.] Crack Length & 50.8 mm [2.0 in.] Hole Diameter

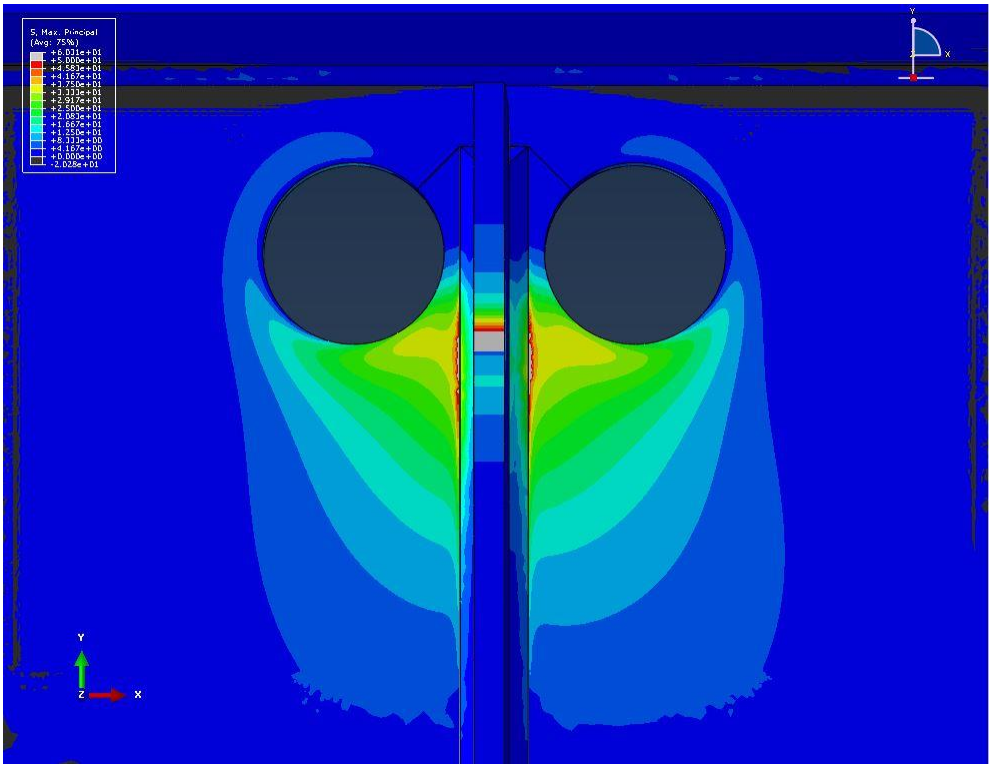

CHSS-1 = 237 Mpa [34.4 ksi]

HSS-1 = 247 Mpa [35.8 ksi]

HSS-2 = 8.19 Mpa [1.19 ksi]

101.6 mm [4.0 in.] Crack Length & 76.2 mm [3.0 in.] Hole Diameter

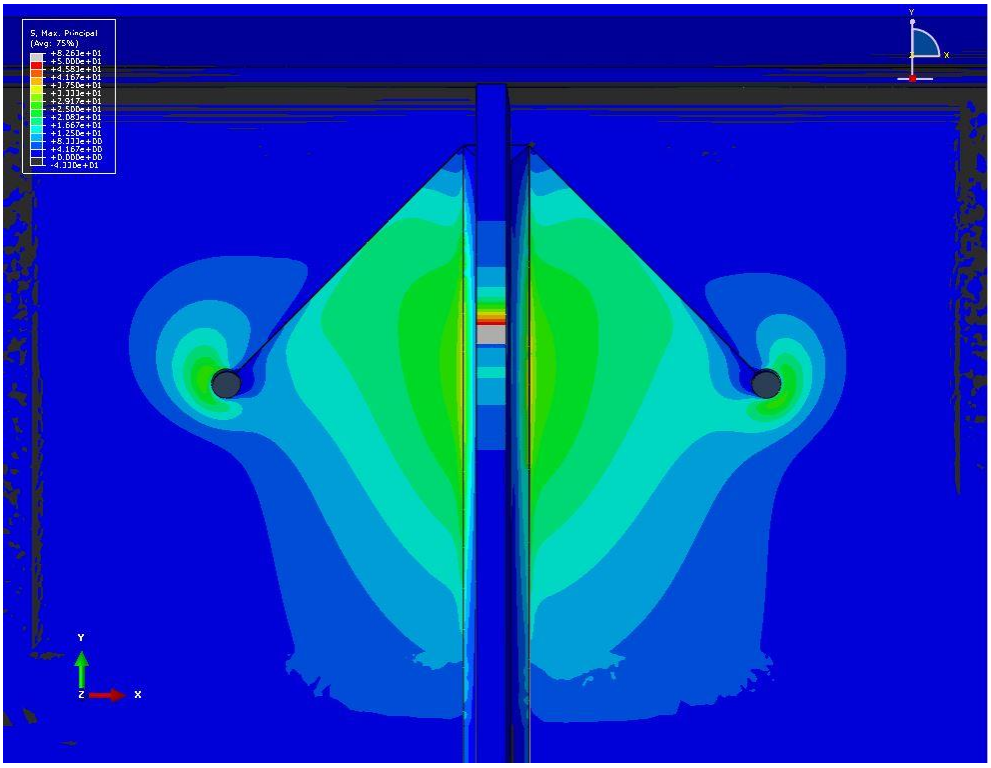

CHSS-1 = 187 Mpa [27.1 ksi]

HSS-1 = 184 Mpa [26.7 ksi]

HSS-2 = -0.42 Mpa [-0.061 ksi]

152.4 mm [6 in.] Crack Length & 12.7 mm [0.5 in.] Hole Diameter

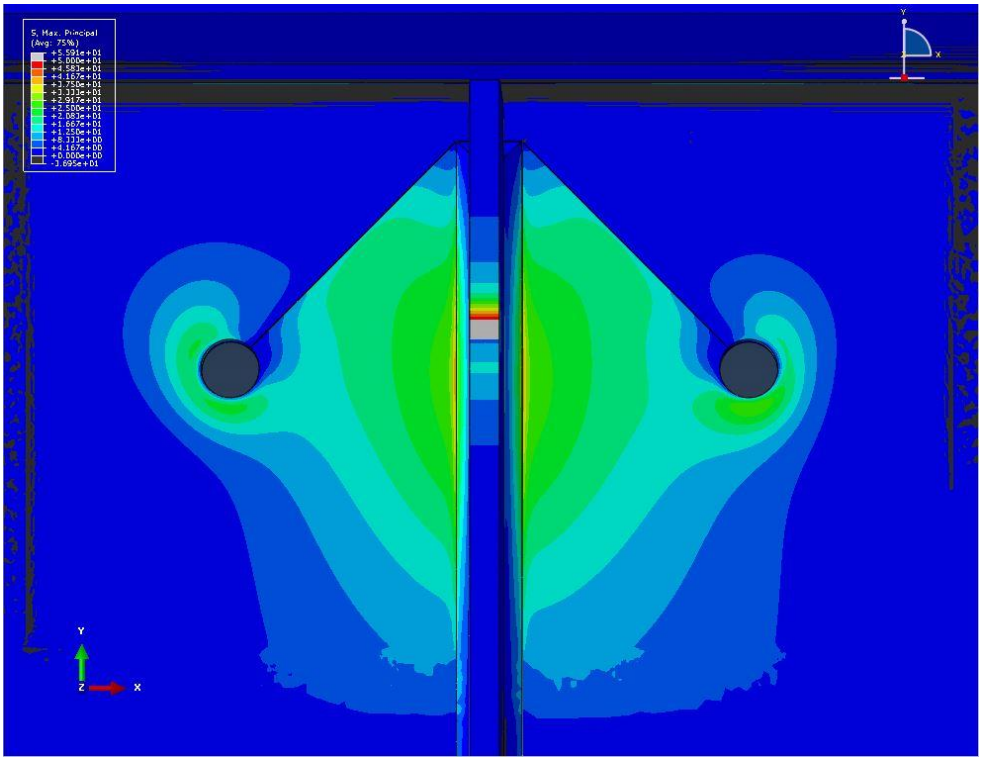

CHSS-1 = 154 Mpa [22.3 ksi]

HSS-1 = 188 Mpa [27.2 ksi]

HSS-2 = -0.22 Mpa [-0.032 ksi]

152.4 mm [6 in.] Crack Length & 25.4 mm [1.0 in.] Hole Diameter

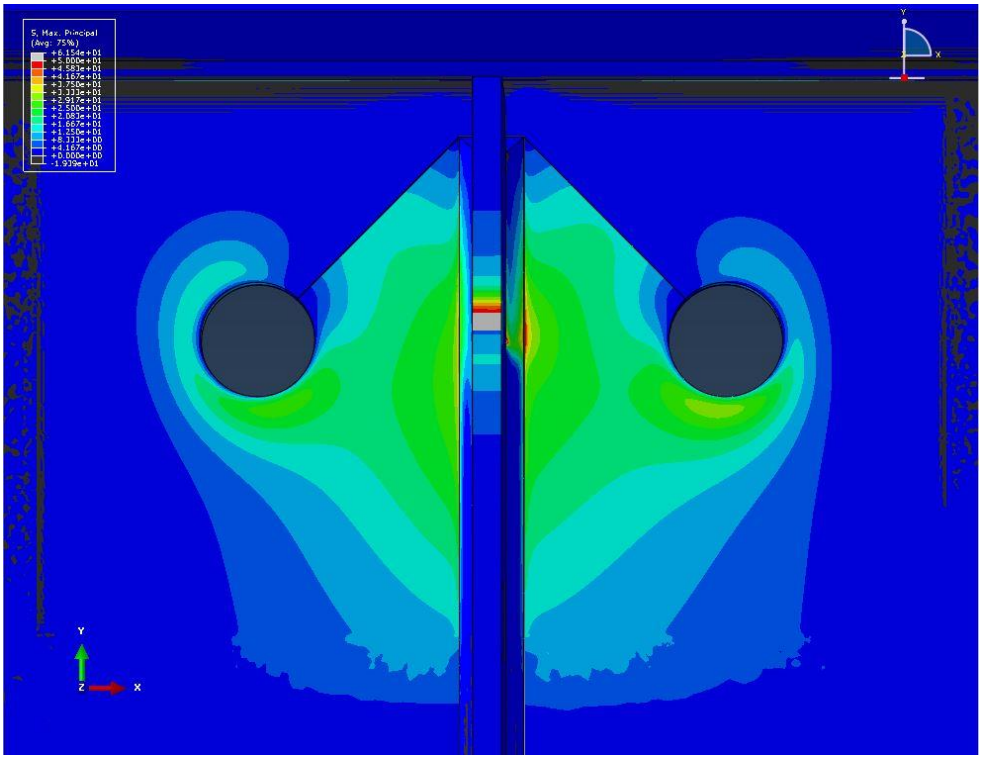

CHSS-1 = 184 Mpa [26.7 ksi]

HSS-1 = 206 Mpa [29.9 ksi]

HSS-2 = 0.99 Mpa [0.143 ksi]

152.4 mm [6 in.] Crack Length & 50.8 mm [2.0 in.] Hole Diameter

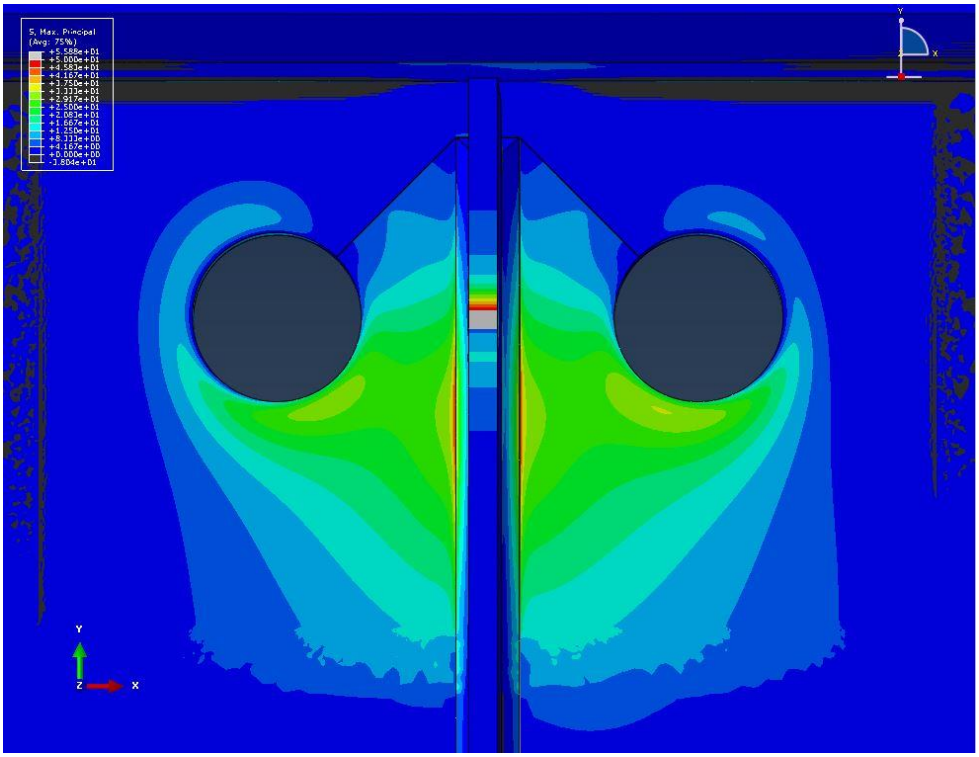

CHSS-1 = 208 Mpa [30.2 ksi]

HSS-1 = 212 Mpa [30.8 ksi]

HSS-2 = 10.9 Mpa [1.579 ksi]

152.4 mm [6 in.] Crack Length & 76.2 mm [3.0 in.] Hole Diameter

Appendix B: Maximum Principal Stress around Crack-arrest Holes for Horseshoe Crack Type

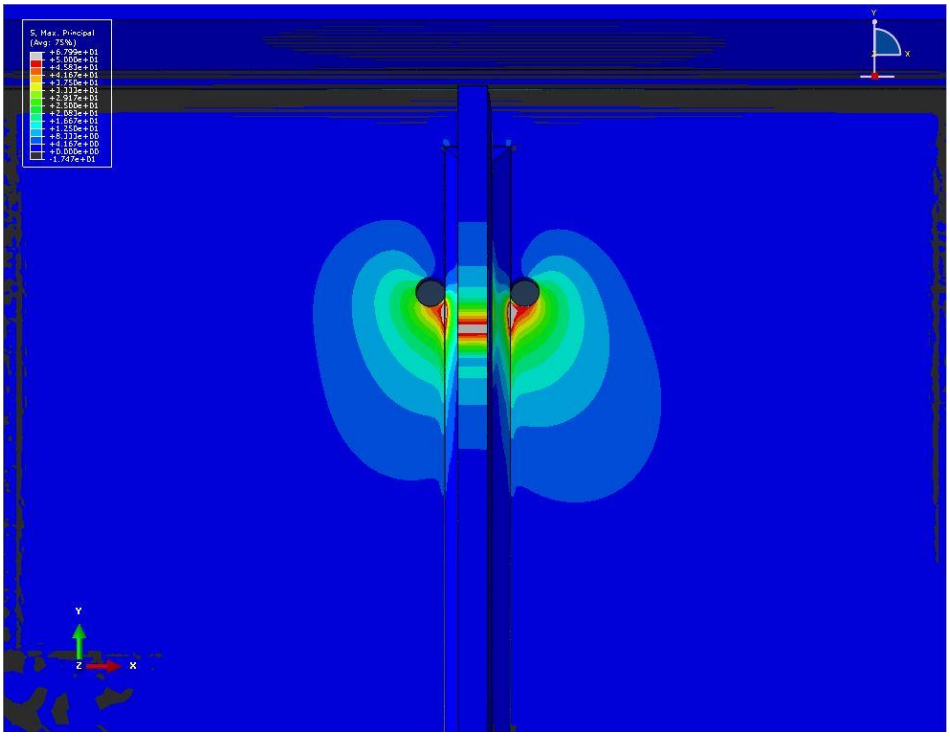

CHSS-1 = 252 Mpa [36.6 ksi]

HSS-1 = 364 Mpa [52.8 ksi]

HSS-2 = -0.46 Mpa [-0.067 ksi]

69.9 mm [2.75 in.] Crack Length & 12.7 mm [0.5 in.] Hole Diameter

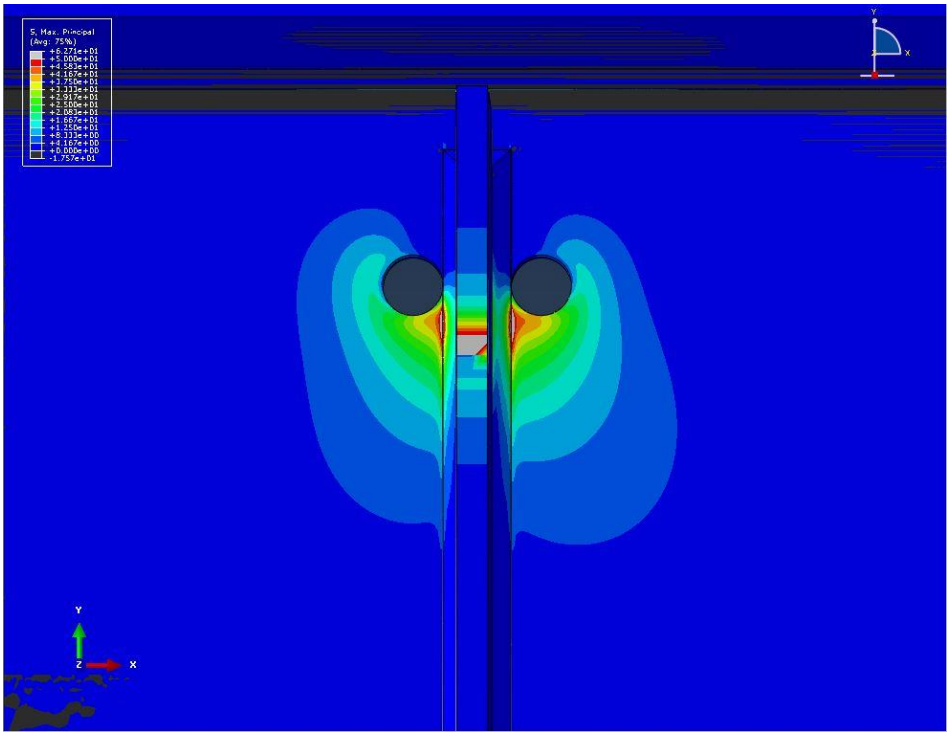

CHSS-1 = 263 Mpa [38.2 ksi]

HSS-1 = 286 Mpa [41.5 ksi]

HSS-2 = -0.23 Mpa [-0.034 ksi]

69.9 mm [2.75 in.] Crack Length & 25.4 mm [1.0 in.] Hole Diameter

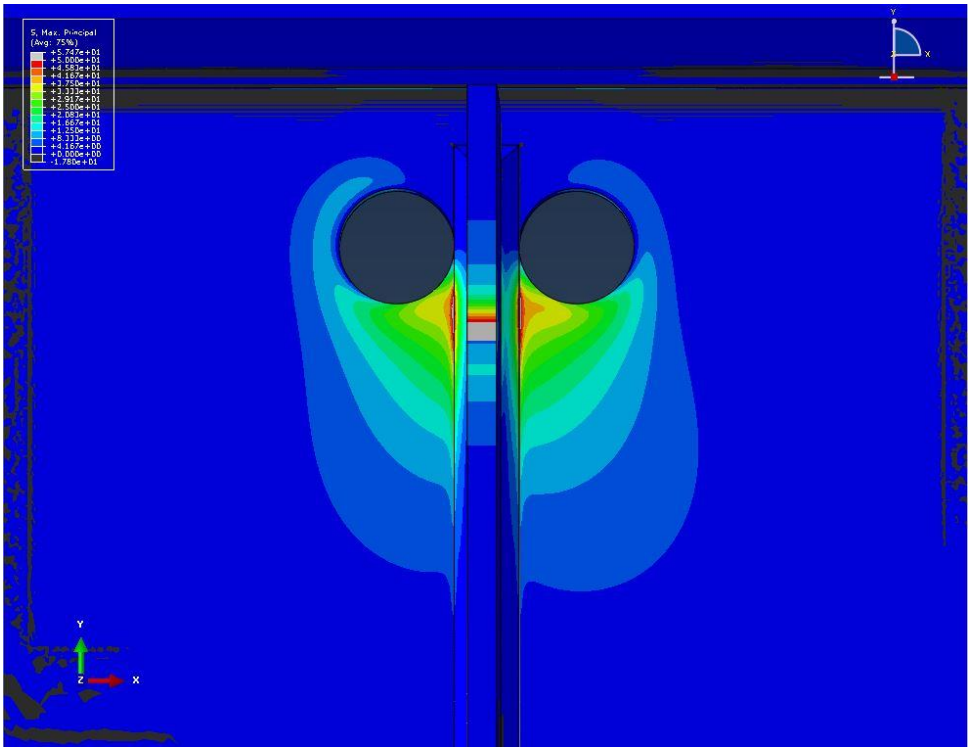

CHSS-1 = 250 Mpa [36.3 ksi]

HSS-1 = 263 Mpa [38.1 ksi]

HSS-2 = -0.26 Mpa [-0.037 ksi]

69.9 mm [2.75 in.] Crack Length & 50.8 mm [2.0 in.] Hole Diameter

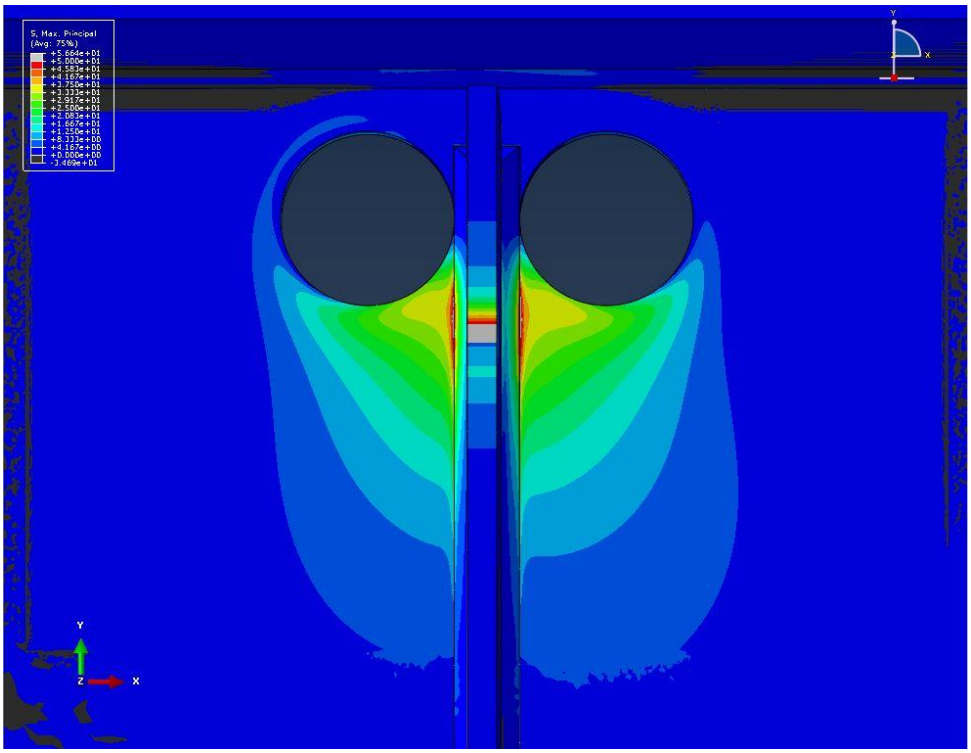

CHSS-1 = 241 Mpa [35.0 ksi]

HSS-1 = 252 Mpa [36.5 ksi]

HSS-2 = 16.7 Mpa [2.42 ksi]

69.9 mm [2.75 in.] Crack Length & 76.2 mm [3.0 in.] Hole Diameter

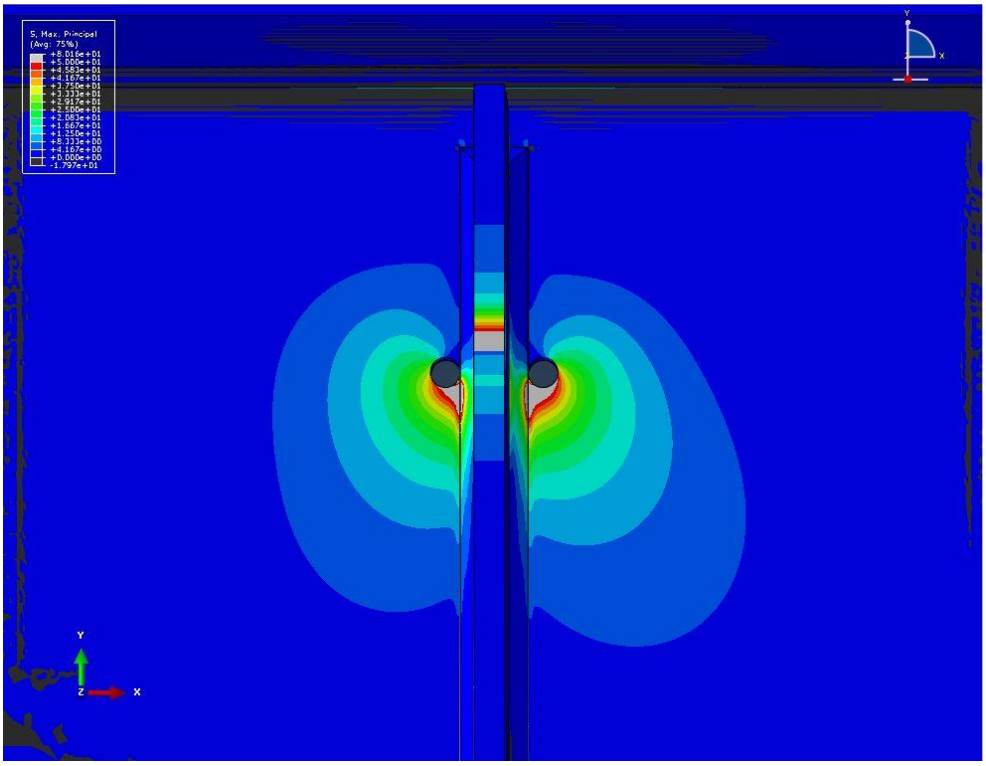

CHSS-1 = 314 Mpa [45.6 ksi]

HSS-1 = 449 Mpa [65.1 ksi]

HSS-2 = -0.48 Mpa [-0.070 ksi]

101.6 mm [4.0 in.] Crack Length & 12.7 mm [0.5 in.] Hole Diameter

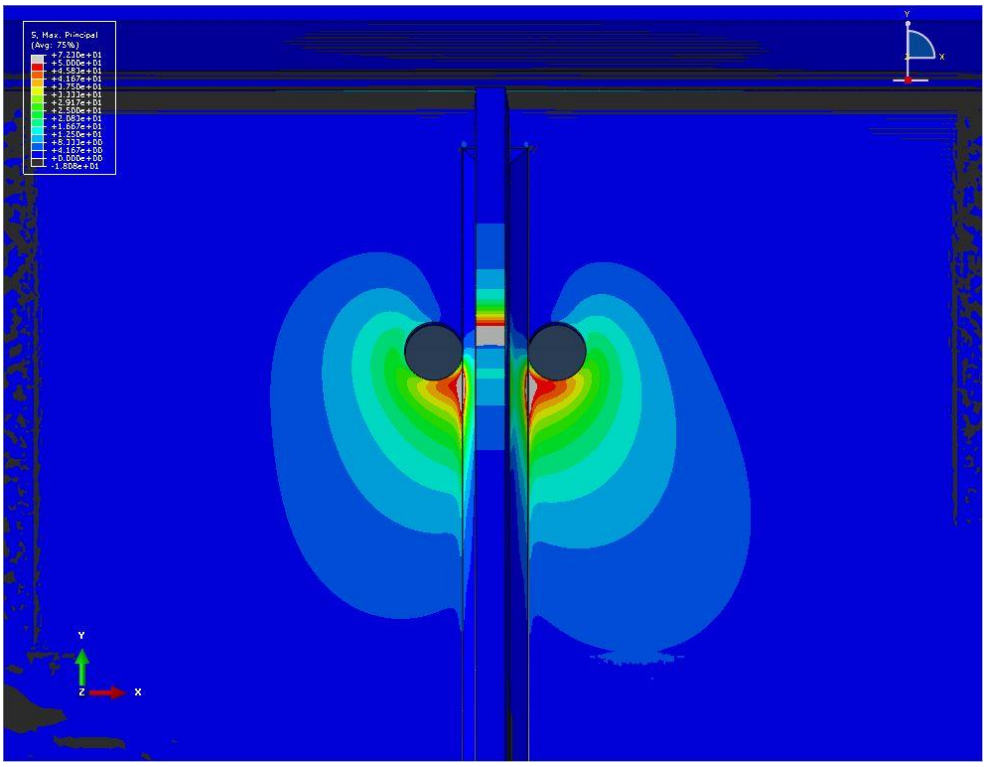

CHSS-1 = 312 Mpa [45.2 ksi]

HSS-1 = 335 Mpa [48.6 ksi]

HSS-2 = -0.21 Mpa [-0.030 ksi]

101.6 mm [4.0 in.] Crack Length & 25.4 mm [1.0 in.] Hole Diameter

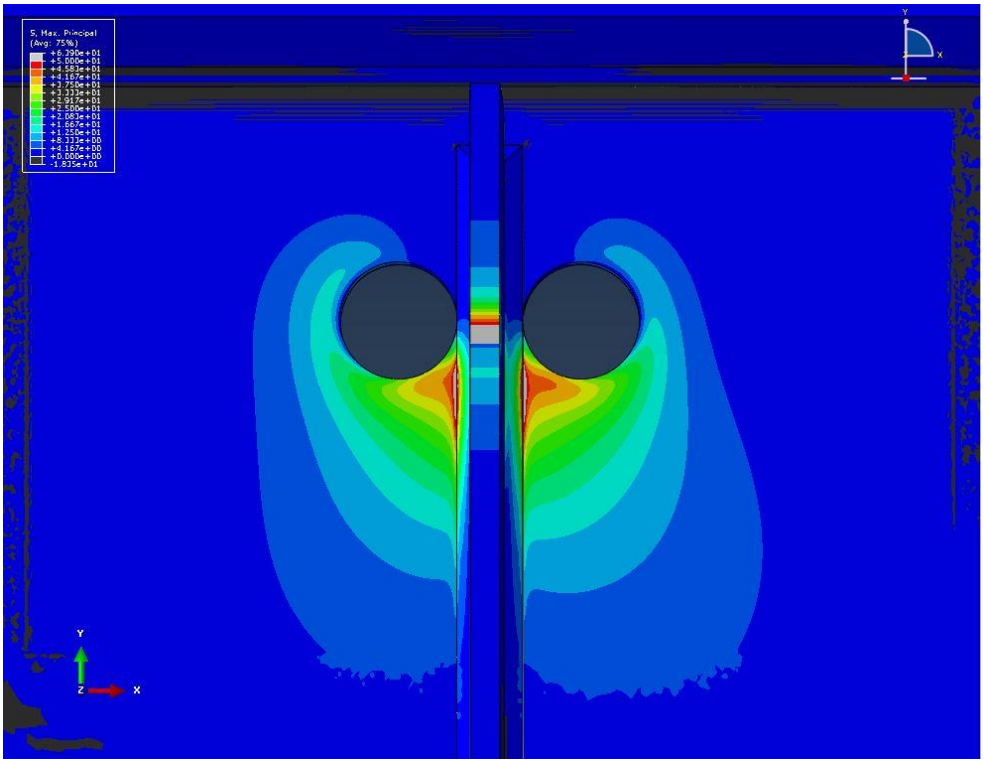

CHSS-1 = 283 Mpa [41.0 ksi]

HSS-1 = 296 Mpa [42.9 ksi]

HSS-2 = -0.21 Mpa [-0.030 ksi]

101.6 mm [4.0 in.] Crack Length & 50.8 mm [2.0 in.] Hole Diameter

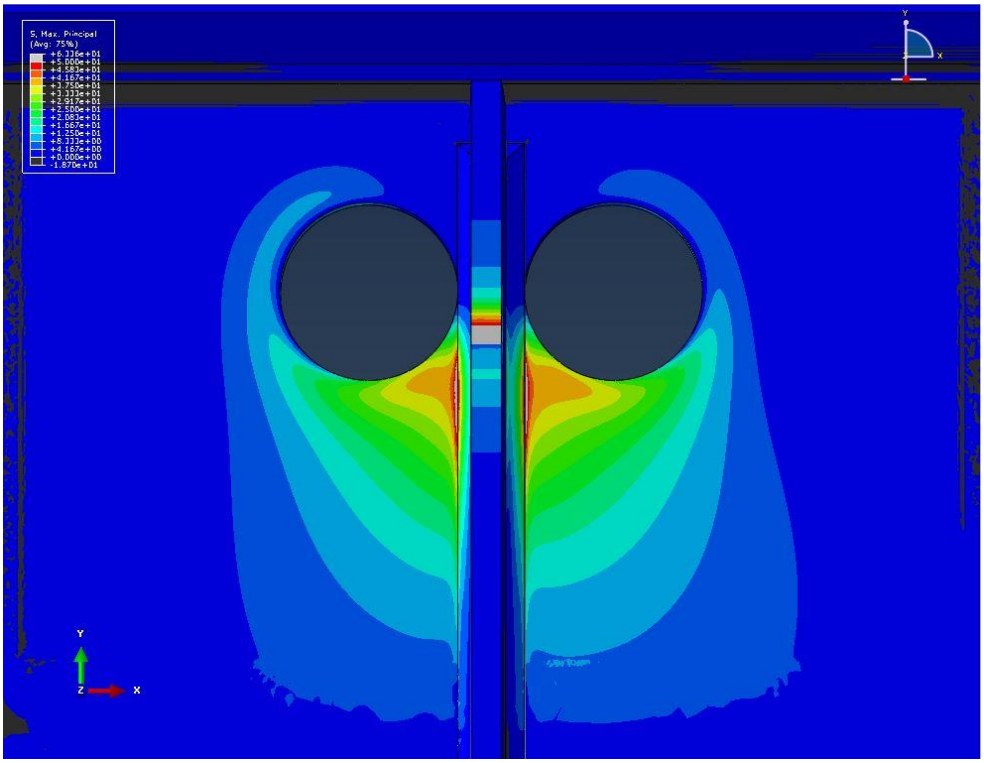

CHSS-1 = 268 Mpa [38.8 ksi]

HSS-1 = 277 Mpa [40.2 ksi]

HSS-2 = -0.27 Mpa [-0.039 ksi]

101.6 mm [4.0 in.] Crack Length & 76.2 mm [3.0 in.] Hole Diameter

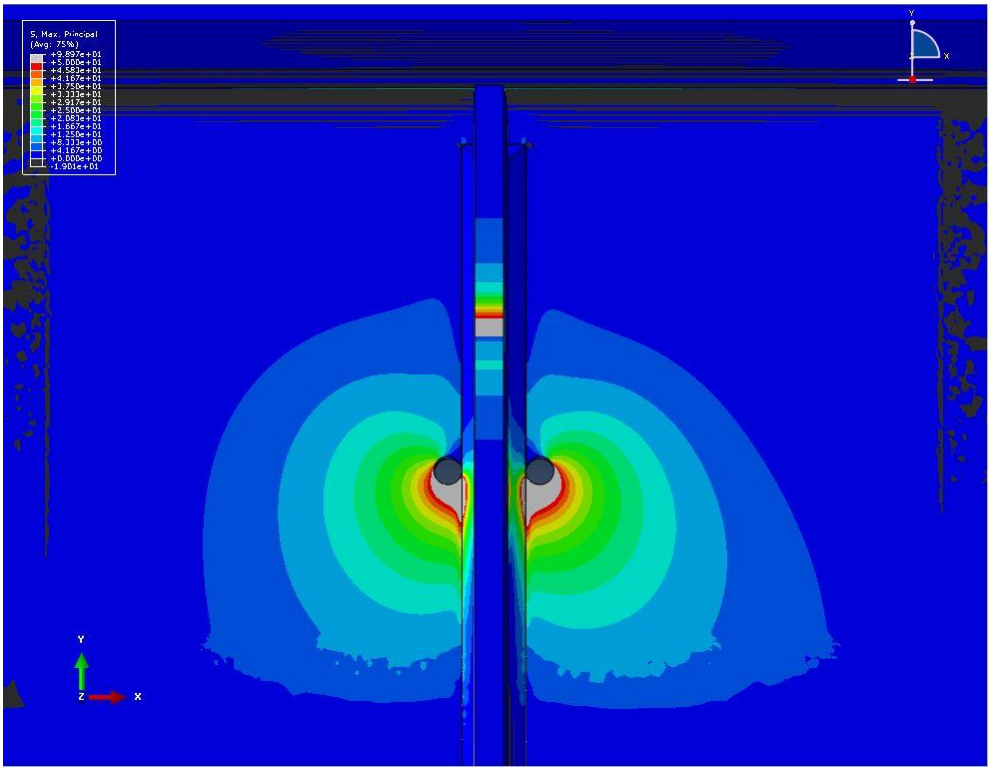

CHSS-1 = 408 Mpa [59.2 ksi]

HSS-1 = 583 Mpa [84.5 ksi]

HSS-2 = -0.53 Mpa [-0.077 ksi]

152.4 mm [6 in.] Crack Length & 12.7 mm [0.5 in.] Hole Diameter

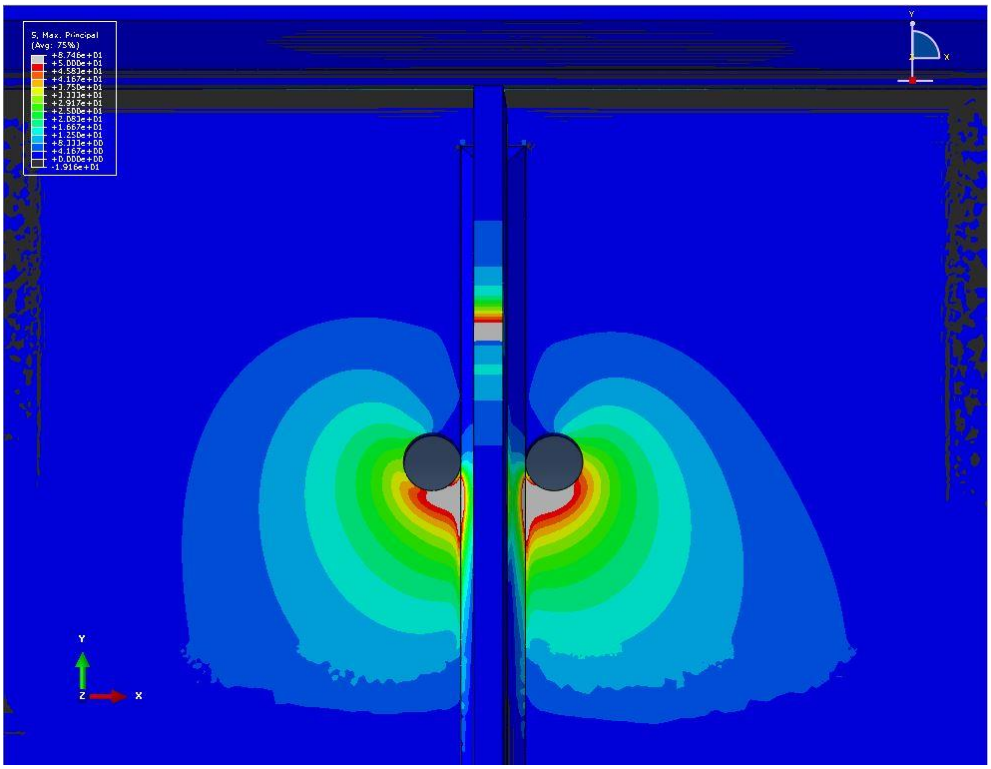

CHSS-1 = 389 Mpa [56.4 ksi]

HSS-1 = 414 Mpa [60.1 ksi]

HSS-2 = -0.23 Mpa [-0.033 ksi]

152.4 mm [6 in.] Crack Length & 25.4 mm [1.0 in.] Hole Diameter

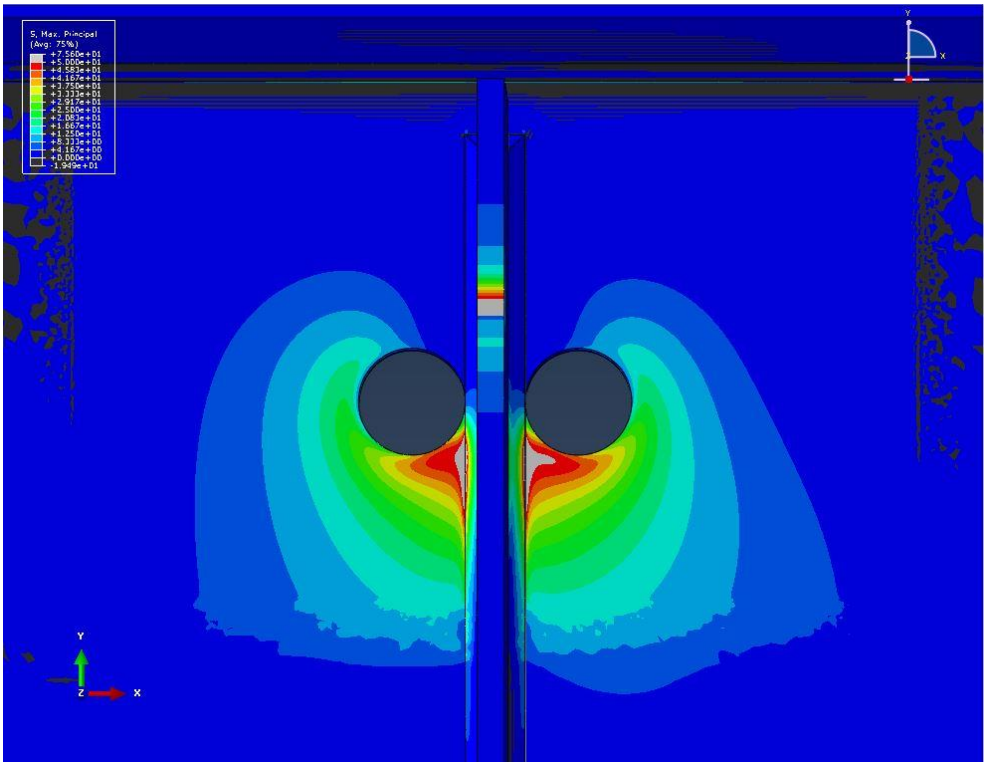

CHSS-1 = 338 Mpa [49.0 ksi]

HSS-1 = 350 Mpa [50.8 ksi]

HSS-2 = -0.20 Mpa [-0.029 ksi]

152.4 mm [6 in.] Crack Length & 50.8 mm [2.0 in.] Hole Diameter

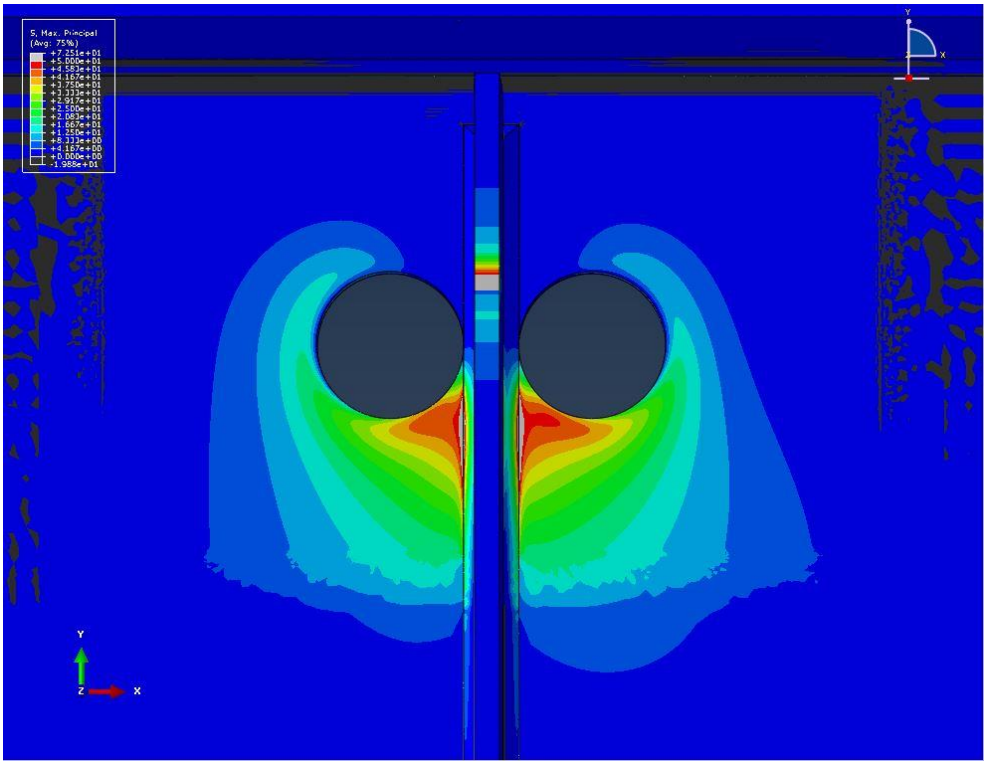

CHSS-1 = 312 Mpa [45.2 ksi]

HSS-1 = 320 Mpa [46.4 ksi]

HSS-2 = -0.24 Mpa [-0.035 ksi]

152.4 mm [6 in.] Crack Length & 76.2 mm [3.0 in.] Hole Diameter

Appendix C: Maximum Principal Stress around Crack-arrest Holes for Horizontal & Horseshoe Crack Type

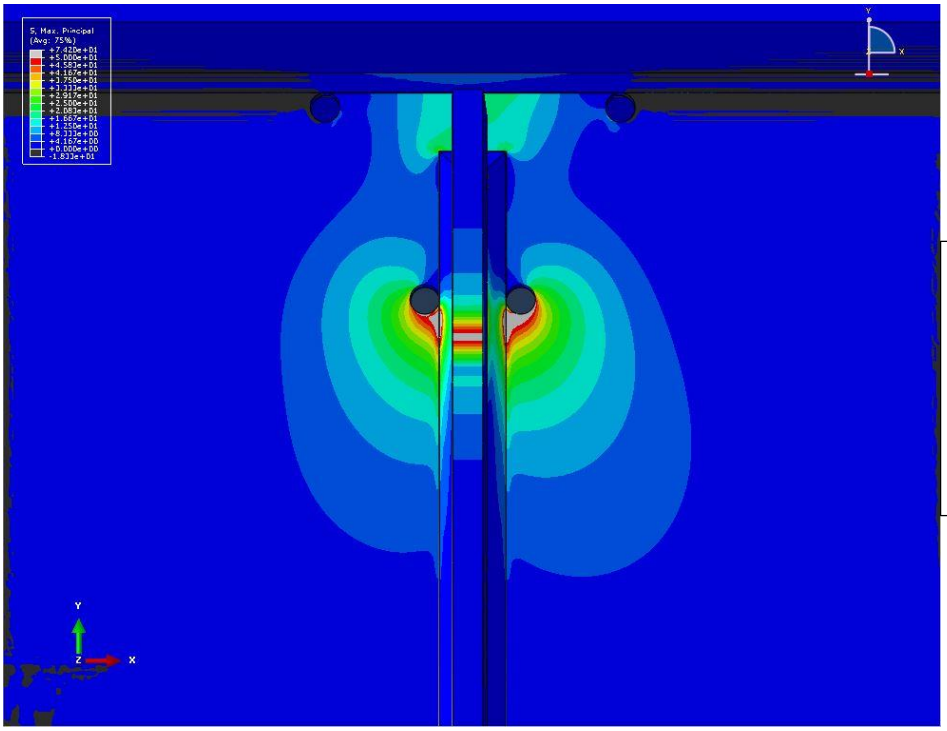

CHSS-1 = 298 Mpa [43.2 ksi]

CHSS-2 = 22.8 Mpa [3.30 ksi]

HSS-1 = 431 Mpa [62.5 ksi]

HSS-2 = 122 Mpa [17.7 ksi]

69.9 mm [2.75 in.] Crack Length & 12.7 mm [0.5 in.] Hole Diameter

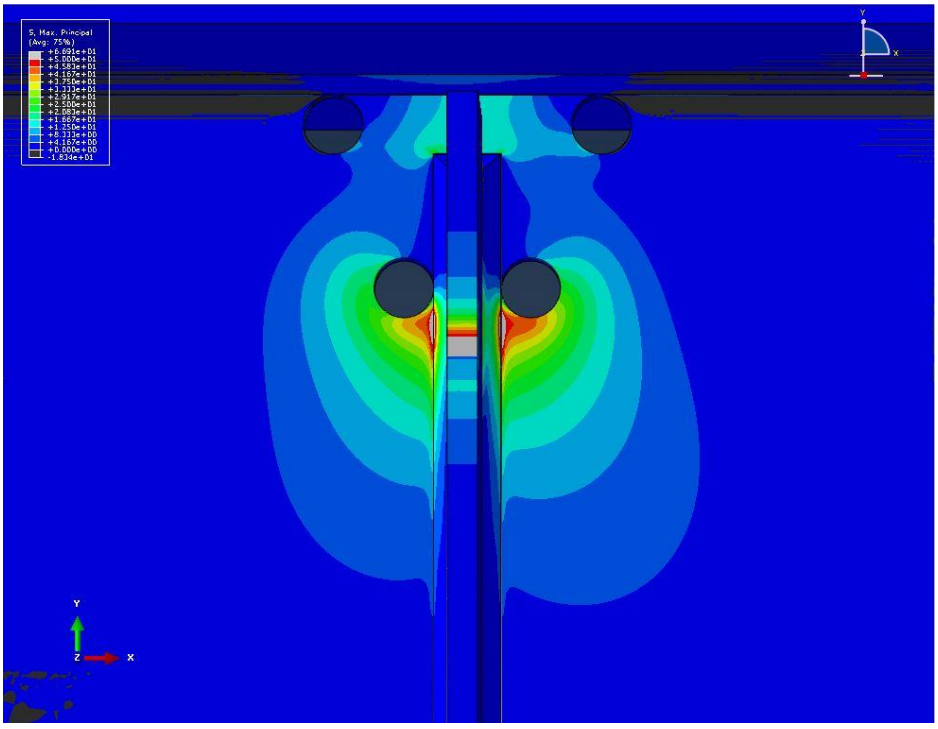

CHSS-1 = 290 Mpa [42.1 ksi]

CHSS-2 = 56.5 Mpa [8.20 ksi]

HSS-1 = 314 Mpa [45.6 ksi]

HSS-2 = 98.6 Mpa [14.3 ksi]

69.9 mm [2.75 in.] Crack Length & 25.4 mm [1.0 in.] Hole Diameter

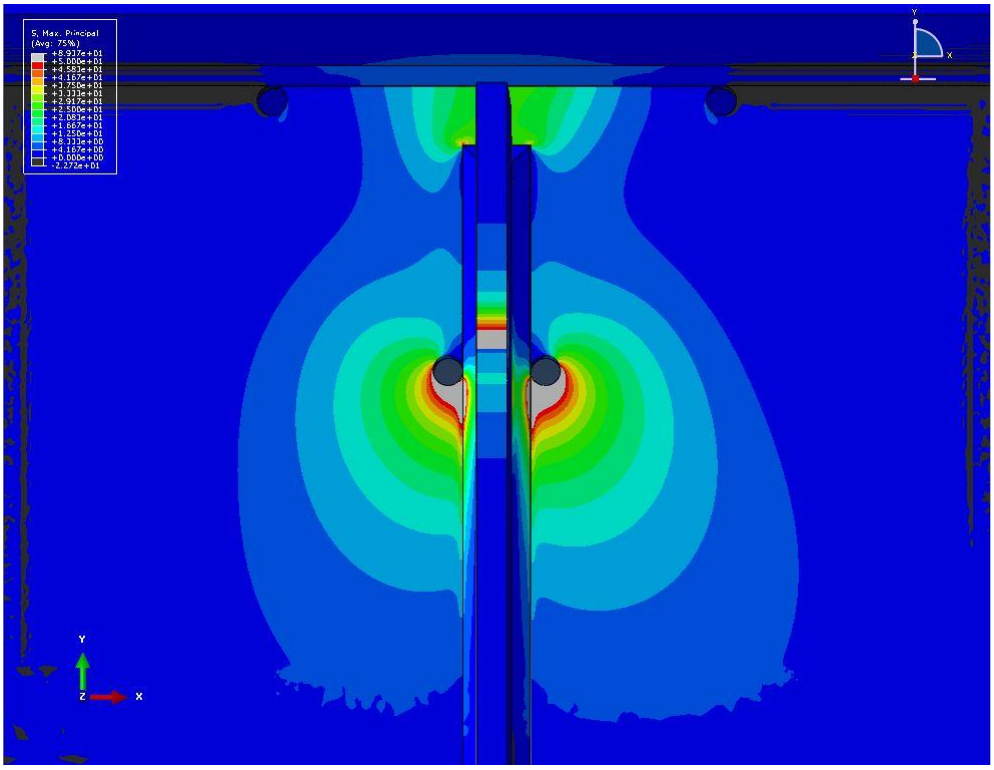

CHSS-1 = 379 Mpa [54.9 ksi]

CHSS-2 = 20.7 Mpa [3.0 ksi]

HSS-1 = 554 Mpa [80.4 ksi]

HSS-2 = 178 Mpa [25.8 ksi]

101.6 mm [4.0 in.] Crack Length & 12.7 mm [0.5 in.] Hole Diameter

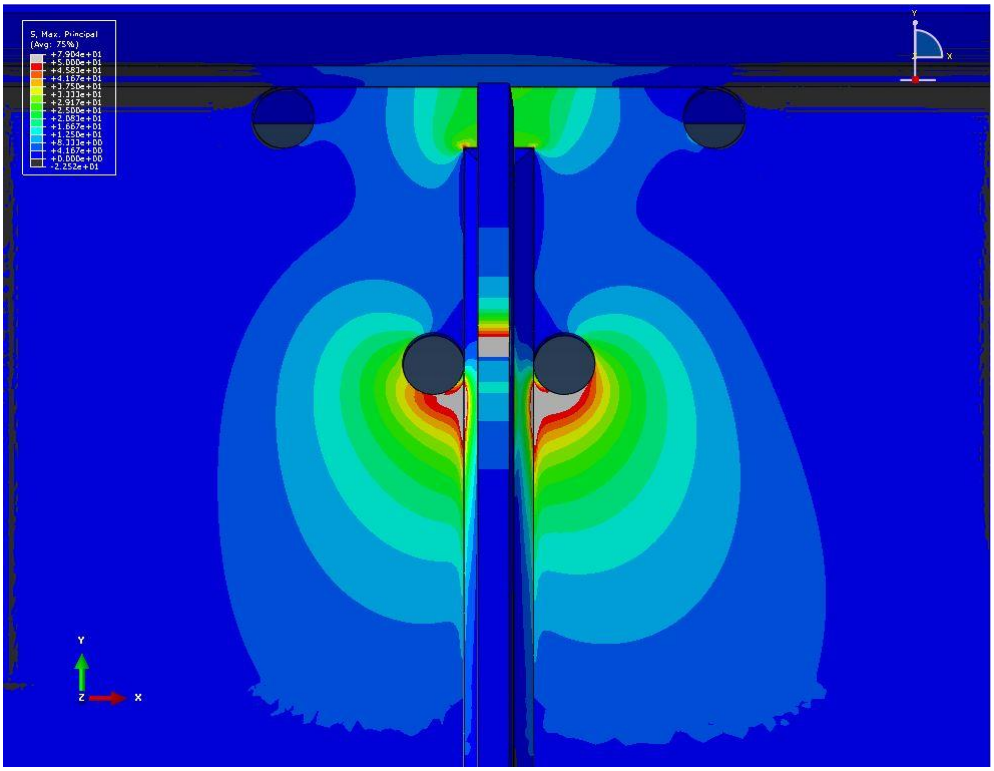

CHSS-1 = 356 Mpa [51.7 ksi]

CHSS-2 = 32.4 Mpa [4.7 ksi]

HSS-1 = 382 Mpa [55.4 ksi]

HSS-2 = 172 Mpa [25.0 ksi]

101.6 mm [4.0 in.] Crack Length & 25.4 mm [1.0 in.] Hole Diameter

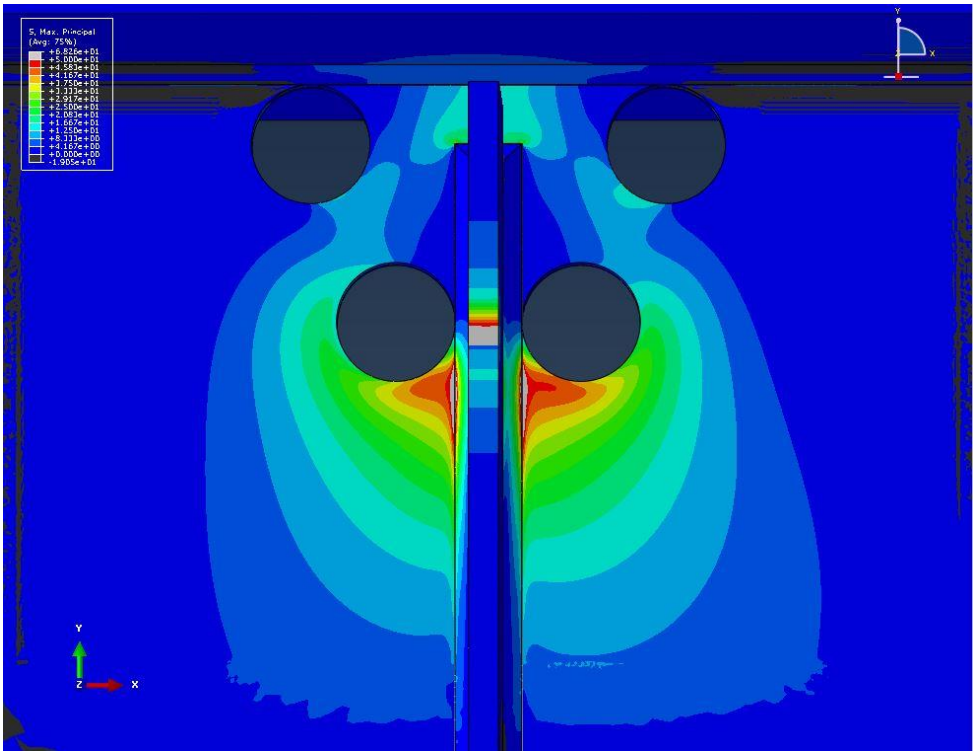

CHSS-1 = 307 Mpa [44.5 ksi]

CHSS-2 = 77.2 Mpa [11.2 ksi]

HSS-1 = 319 Mpa [46.2 ksi]

HSS-2 = 100 Mpa [14.5 ksi]

101.6 mm [4.0 in.] Crack Length & 50.8 mm [2.0 in.] Hole Diameter

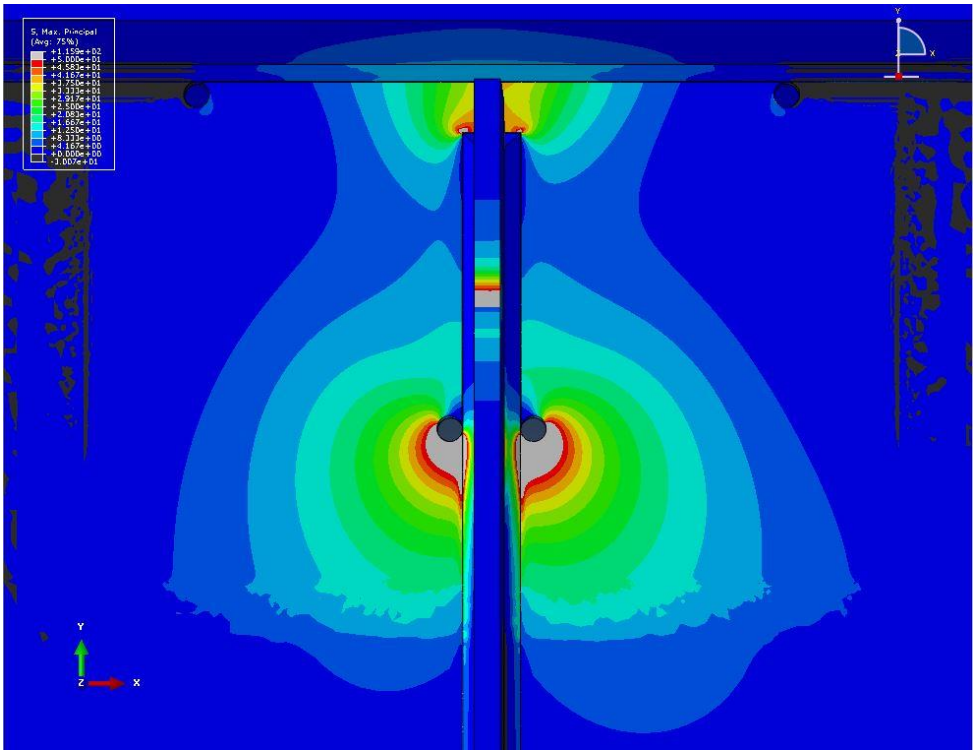

CHSS-1 = 501 Mpa [72.6 ksi]

CHSS-2 = 29.6 Mpa [4.3 ksi]

HSS-1 = 748 Mpa [109 ksi]

HSS-2 = 259 Mpa [37.5 ksi]

152.4 mm [6 in.] Crack Length & 12.7 mm [0.5 in.] Hole Diameter

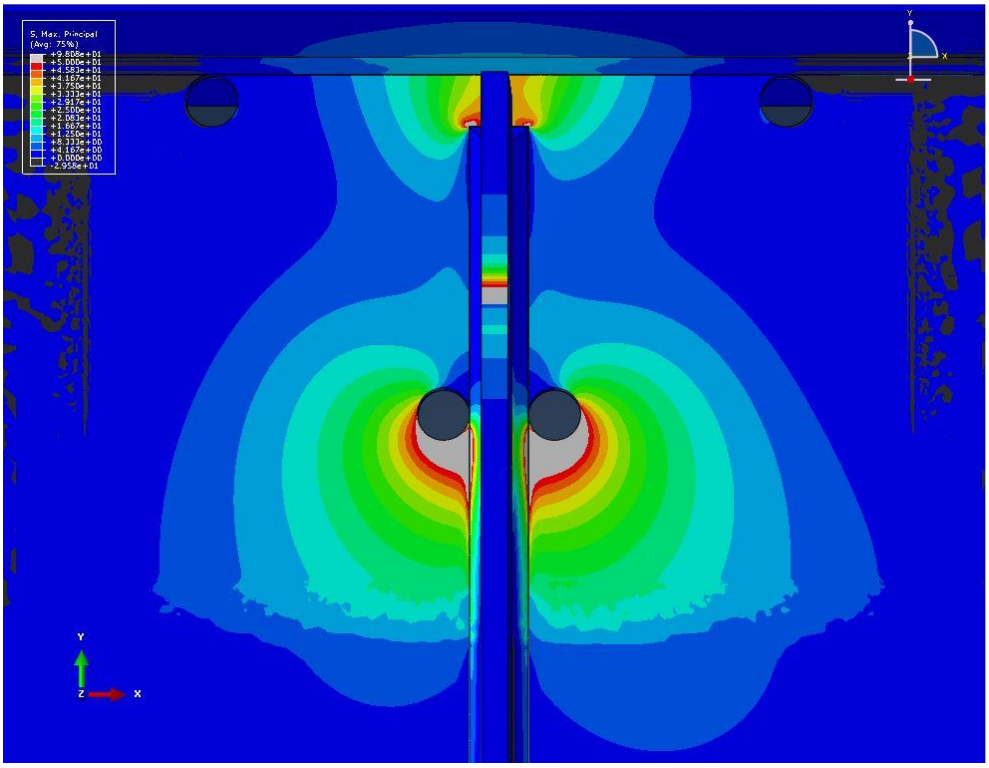

CHSS-1 = 461 Mpa [66.8 ksi]

CHSS-2 = 22.1 Mpa [3.2 ksi]

HSS-1 = 488 Mpa [70.8 ksi]

HSS-2 = 267 Mpa [38.7 ksi]

152.4 mm [6 in.] Crack Length & 25.4 mm [1.0 in.] Hole Diameter

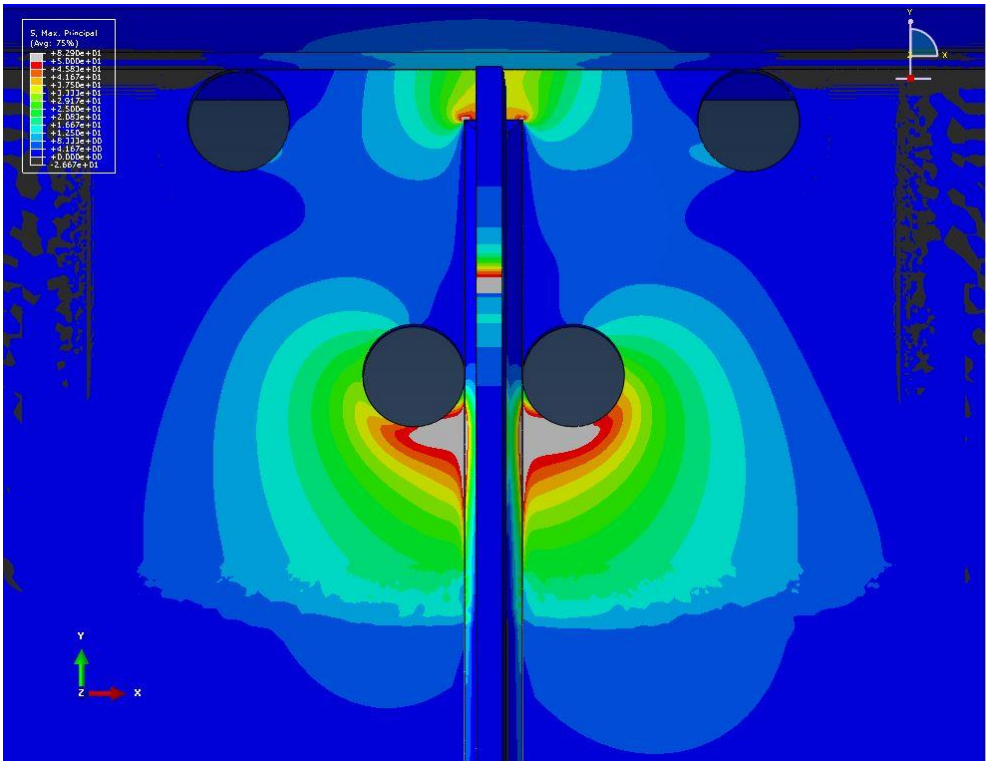

CHSS-1 = 385 Mpa [55.9 ksi]

CHSS-2 = 52.4 Mpa [7.6 ksi]

HSS-1 = 394 Mpa [57.1 ksi]

HSS-2 = 244 Mpa [35.4 ksi]

152.4 mm [6 in.] Crack Length & 50.8 mm [2.0 in.] Hole Diameter

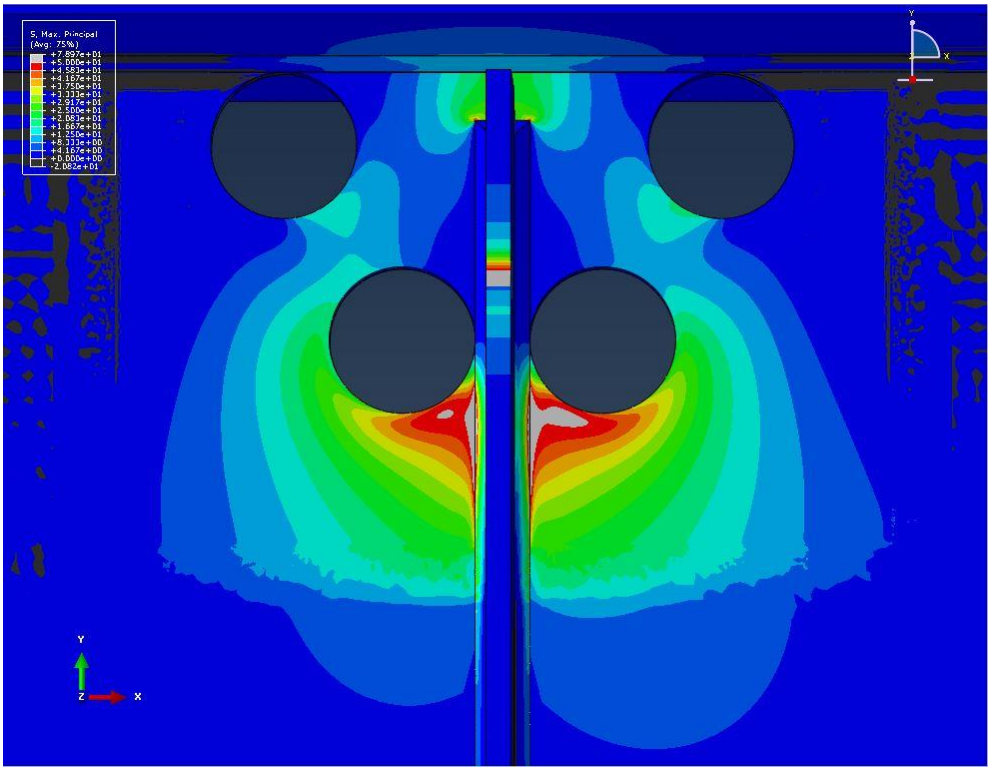

CHSS-1 = 346 Mpa [50.2 ksi]

CHSS-2 = 100 Mpa [14.5 ksi]

HSS-1 = 349 Mpa [50.6 ksi]

HSS-2 = 161 Mpa [23.3 ksi]

152.4 mm [6 in.] Crack Length & 76.2 mm [3.0 in.] Hole Diameter

Appendix D: Maximum Principal Stress around Crack-arrest Holes for Horizontal Crack Type

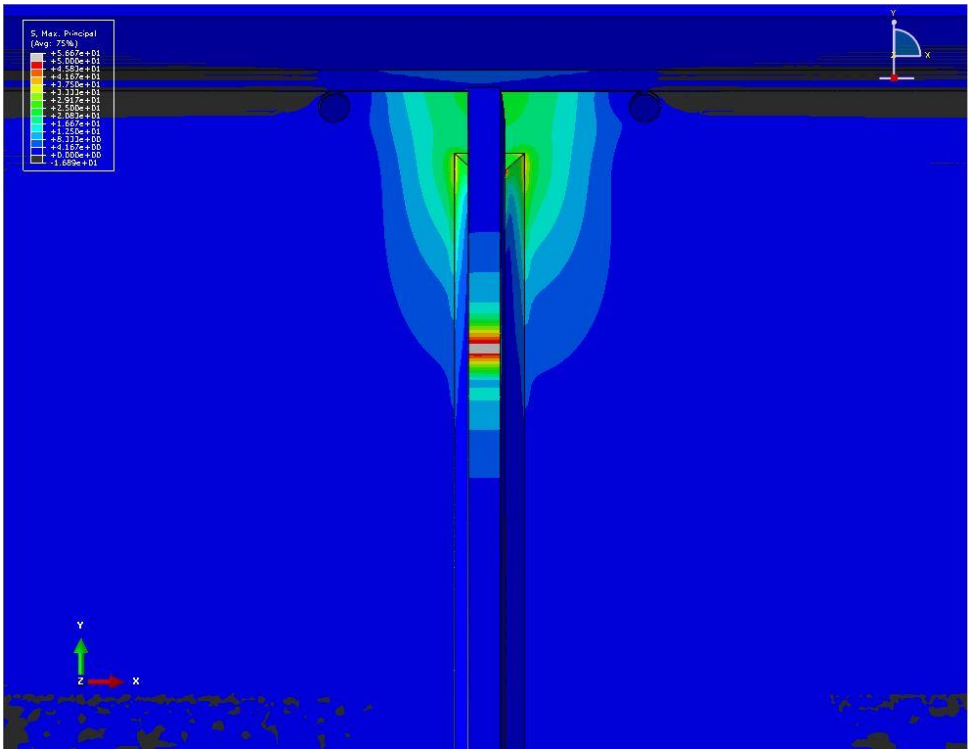

CHSS-1 = 16.2 Mpa [2.35 ksi]

HSS-1 = 141 Mpa [20.4 ksi]

HSS-2 = 154 Mpa [22.3 ksi]

139.7 mm [5.5 in.] Crack Length & 12.7 mm [0.5 in.] Hole Diameter

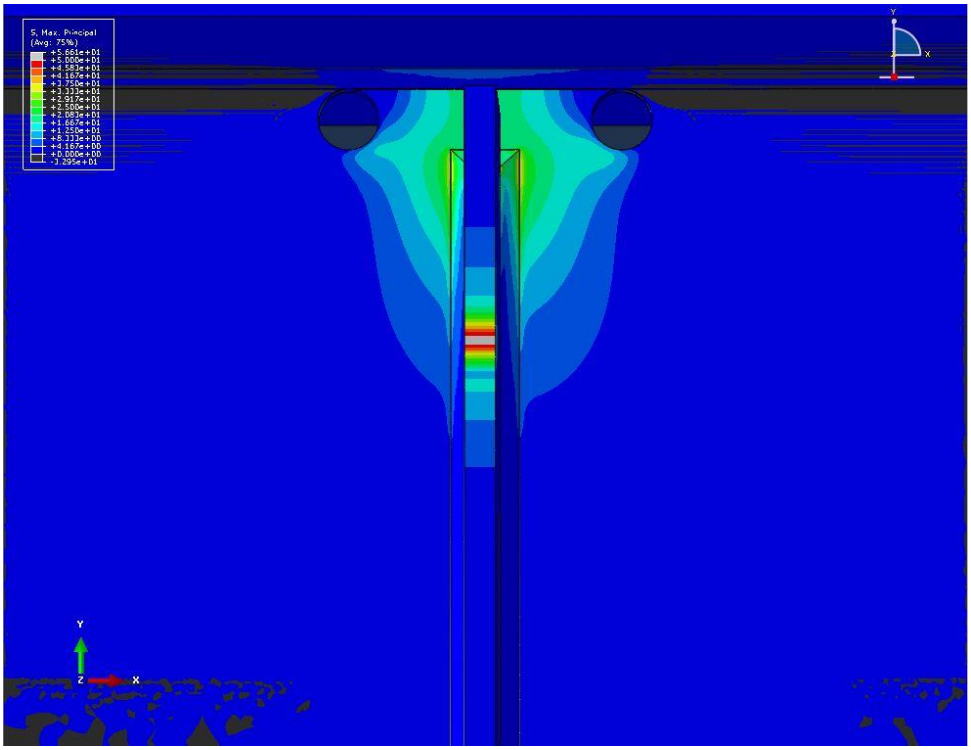

CHSS-1 = 88.1 Mpa [12.78 ksi]

HSS-1 = 147 Mpa [21.3 ksi]

HSS-2 = 129 Mpa [18.7 ksi]

139.7 mm [5.5 in.] Crack Length & 25.4 mm [1.0 in.] Hole Diameter

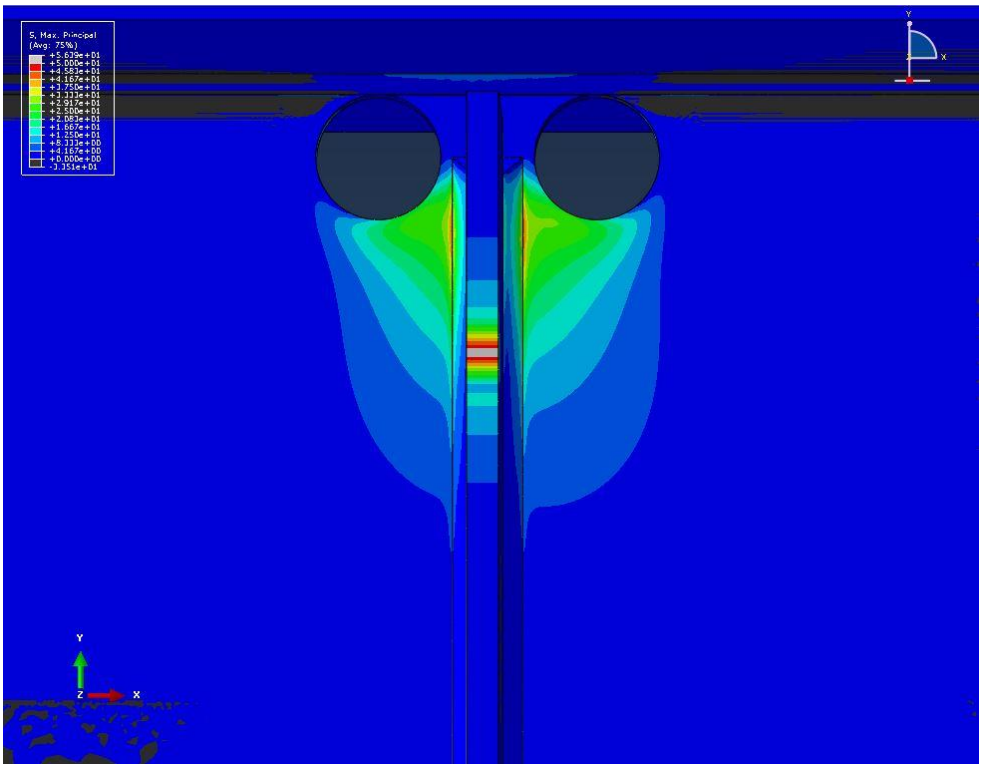

CHSS-1 = 192 Mpa [27.86 ksi]

HSS-1 = 203 Mpa [29.5 ksi]

HSS-2 = 7.58 Mpa [1.10 ksi]

139.7 mm [5.5 in.] Crack Length & 50.8 mm [2.0 in.] Hole Diameter

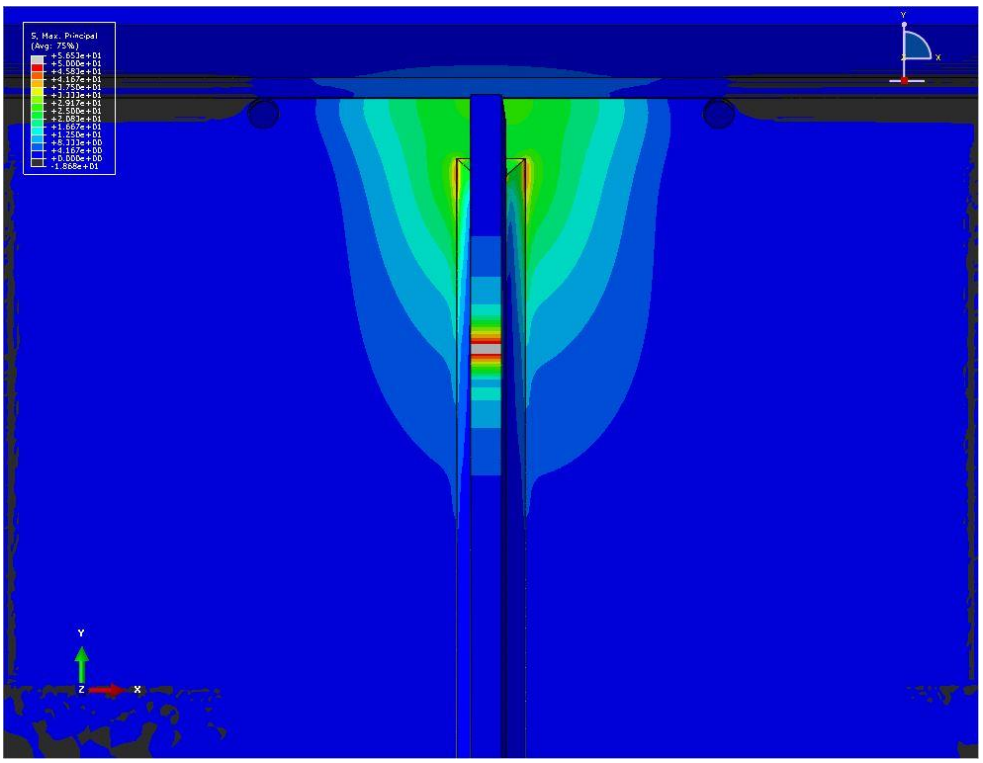

CHSS-1 = 1.72 Mpa [0.25 ksi]

HSS-1 = 179 Mpa [26.0 ksi]

HSS-2 = 179 Mpa [25.9 ksi]

203.2 mm [8 in.] Crack Length & 12.7 mm [0.5 in.] Hole Diameter

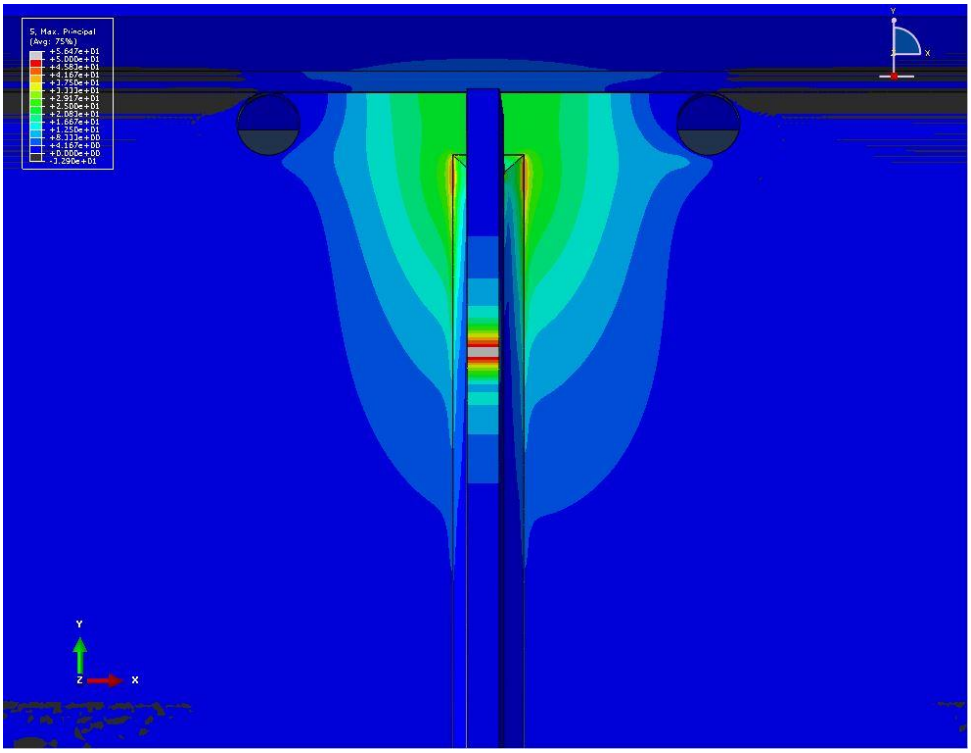

CHSS-1 = 41.4 Mpa [6.0 ksi]

HSS-1 = 180 Mpa [26.1 ksi]

HSS-2 = 168 Mpa [24.4 ksi]

203.2 mm [8 in.] Crack Length & 25.4 mm [1.0 in.] Hole Diameter

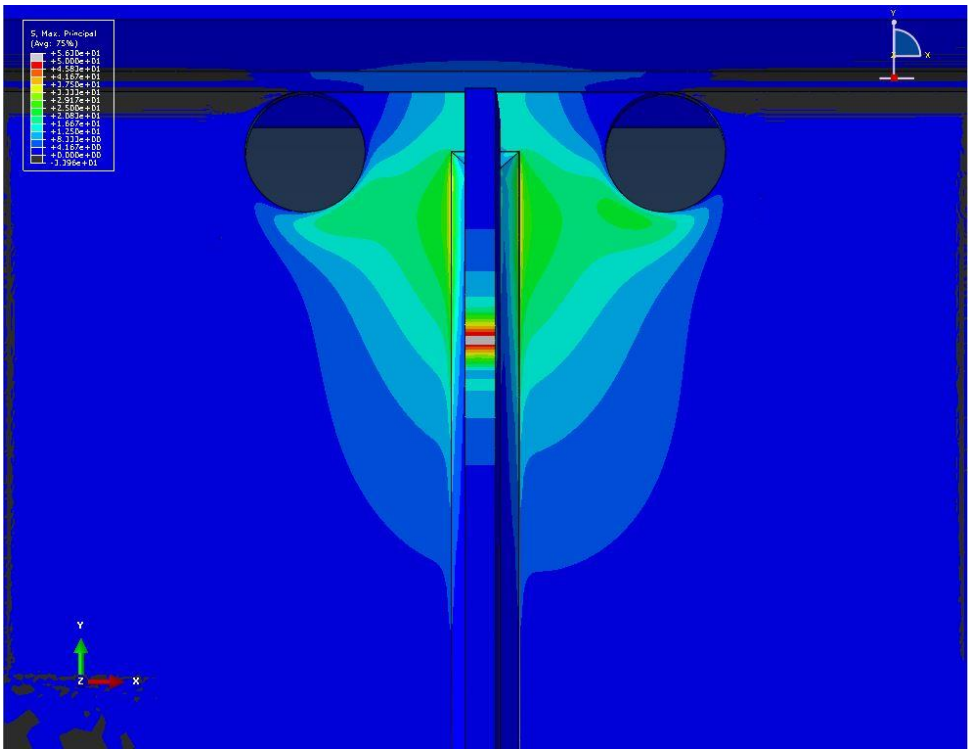

CHSS-1 = 141 Mpa [20.48 ksi]

HSS-1 = 169 Mpa [24.5 ksi]

HSS-2 = 93.1 Mpa [13.5 ksi]

203.2 mm [8 in.] Crack Length & 50.8 mm [2.0 in.] Hole Diameter

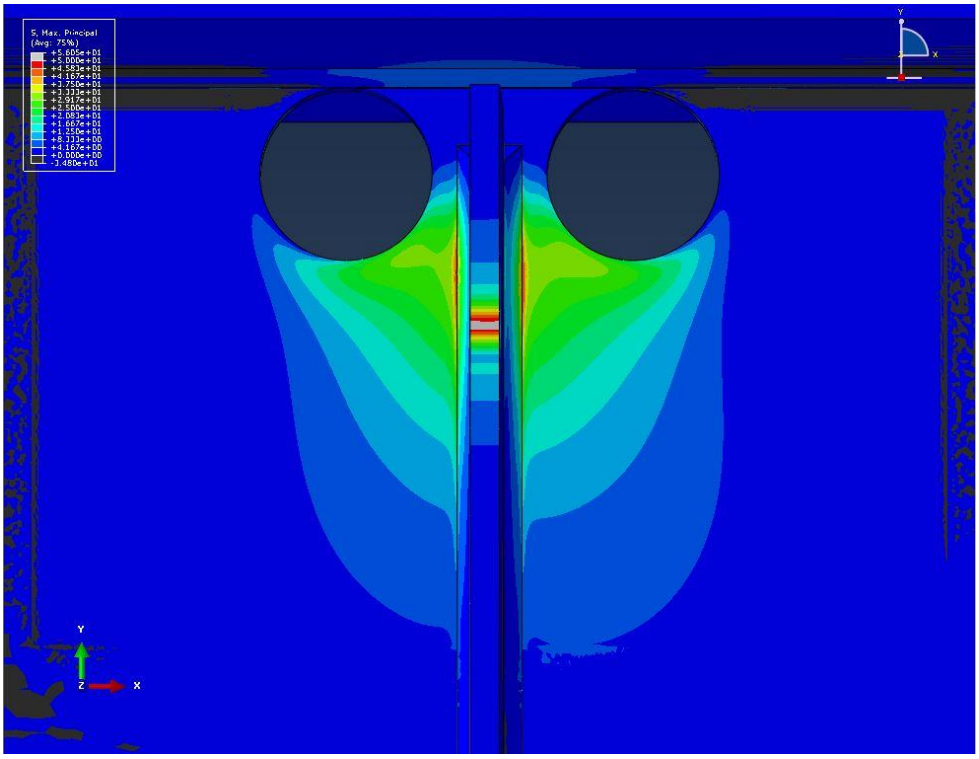

CHSS-1 = 205 Mpa [29.67 ksi]

HSS-1 = 212 Mpa [30.8 ksi]

HSS-2 = 4.48 Mpa [0.65 ksi]

203.2 mm [8 in.] Crack Length & 76.2 mm [3.0 in.] Hole Diameter

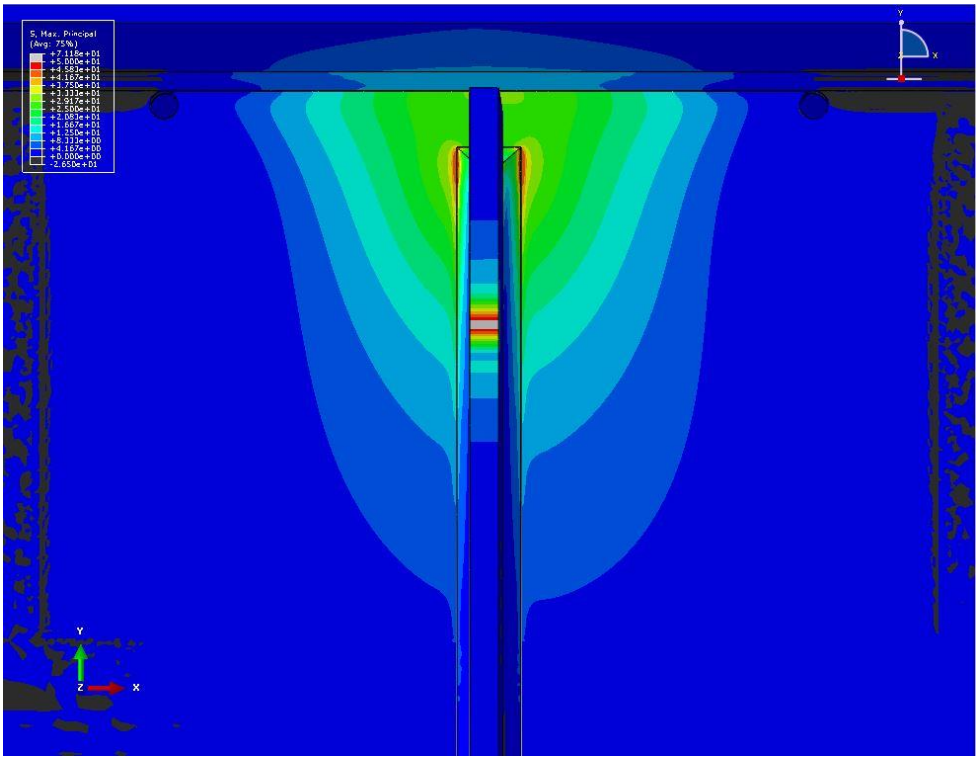

CHSS-1 = 2.21 Mpa [0.32 ksi]

HSS-1 = 219 Mpa [31.8 ksi]

HSS-2 = 201 Mpa [29.13 ksi]

304.8 mm [12 in.] Crack Length & 12.7 mm [0.5 in.] Hole Diameter

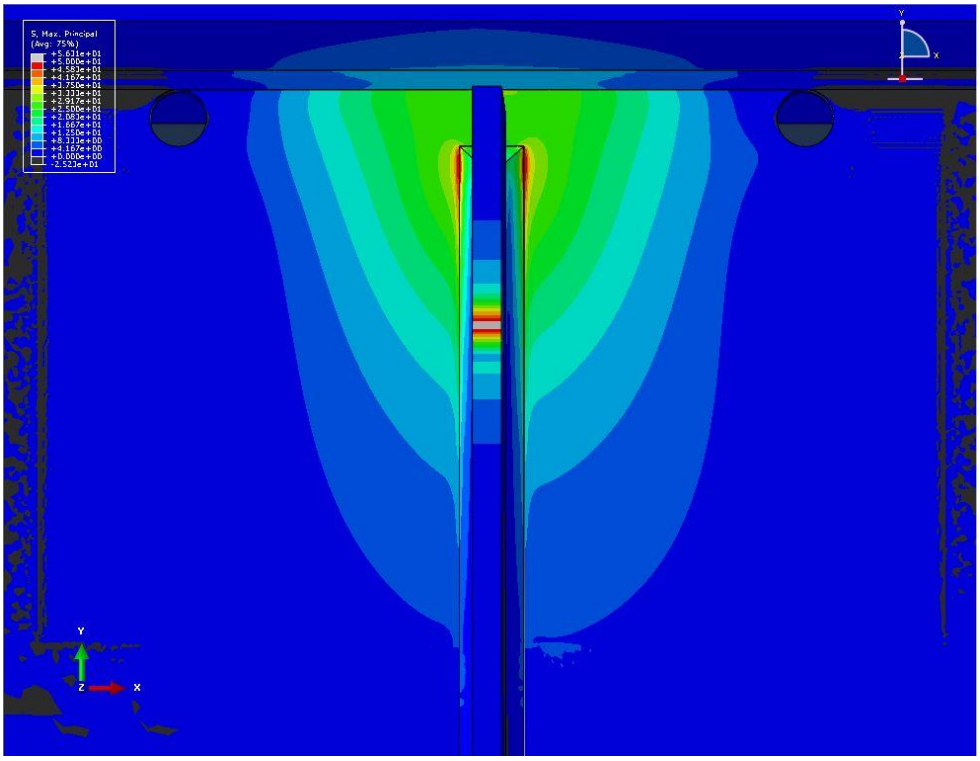

CHSS-1 = 4.34 Mpa [0.63 ksi]

HSS-1 = 220 Mpa [31.9 ksi]

HSS-2 = 199 Mpa [28.83 ksi]

304.8 mm [12 in.] Crack Length & 25.4 mm [1.0 in.] Hole Diameter

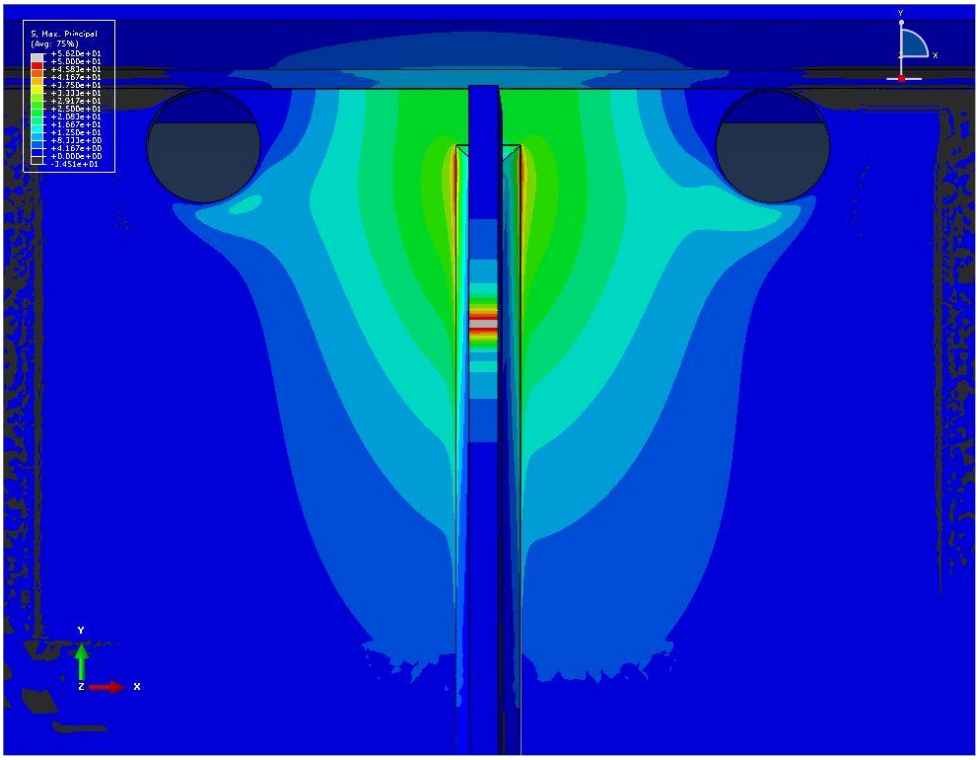

CHSS-1 = 88 Mpa [12.76 ksi]

HSS-1 = 205 Mpa [29.7 ksi]

HSS-2 = 167 Mpa [24.16 ksi]

304.8 mm [12 in.] Crack Length & 50.8 mm [2.0 in.] Hole Diameter

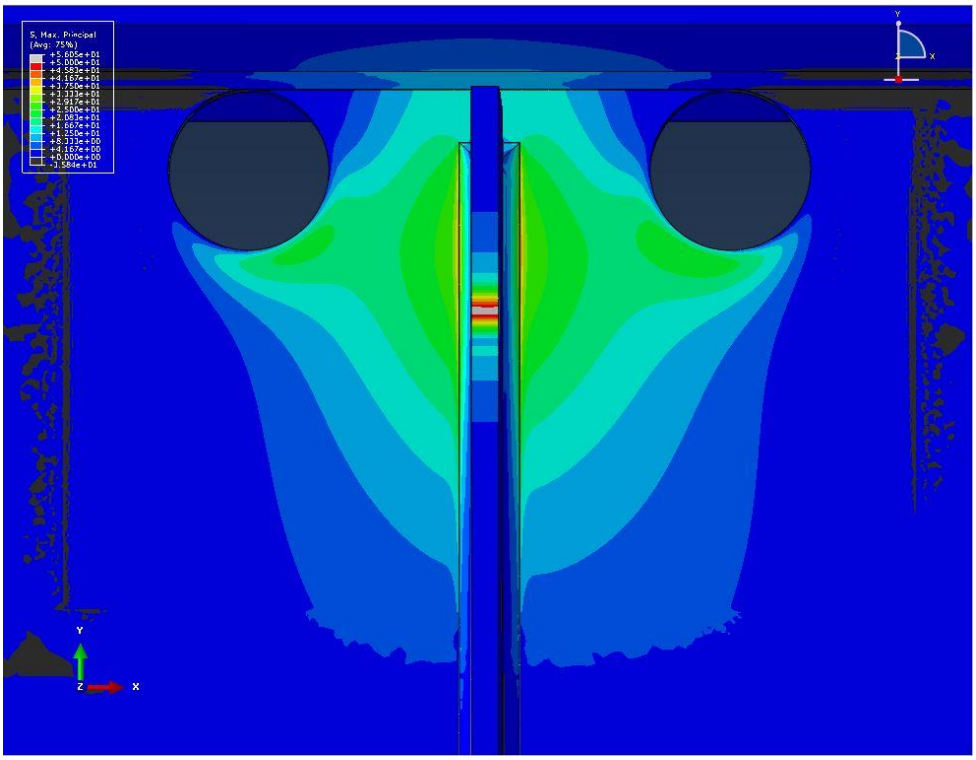

CHSS-1 = 151 Mpa [21.91 ksi]

HSS-1 = 188 Mpa [27.3 ksi]

HSS-2 = 102 Mpa [14.79 ksi]

304.8 mm [12 in.] Crack Length & 76.2 mm [3.0 in.] Hole Diameter

Appendix E: Maximum Principal Stress around Crack-arrest Holes for Large-hole Retrofit

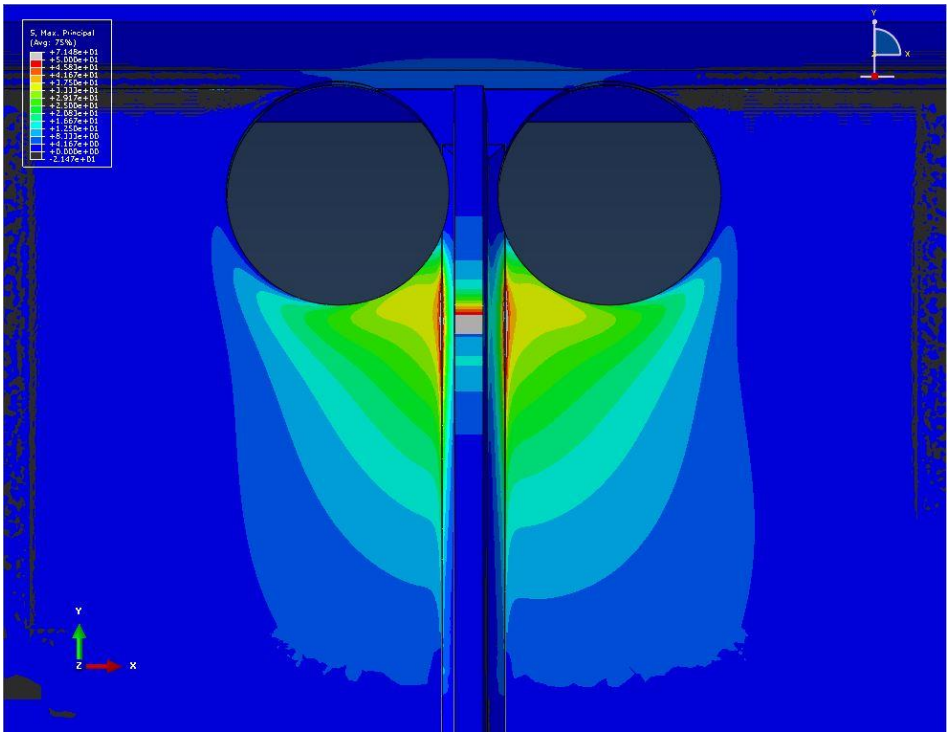

CHSS = 245 Mpa [35.6 ksi]

HSS-1 = 256 Mpa [37.1 ksi]

HSS-2 = 0.717 Mpa [0.10 ksi]

Horizontal Crack with 101.6 mm [4.0 in.] Hole Diameter

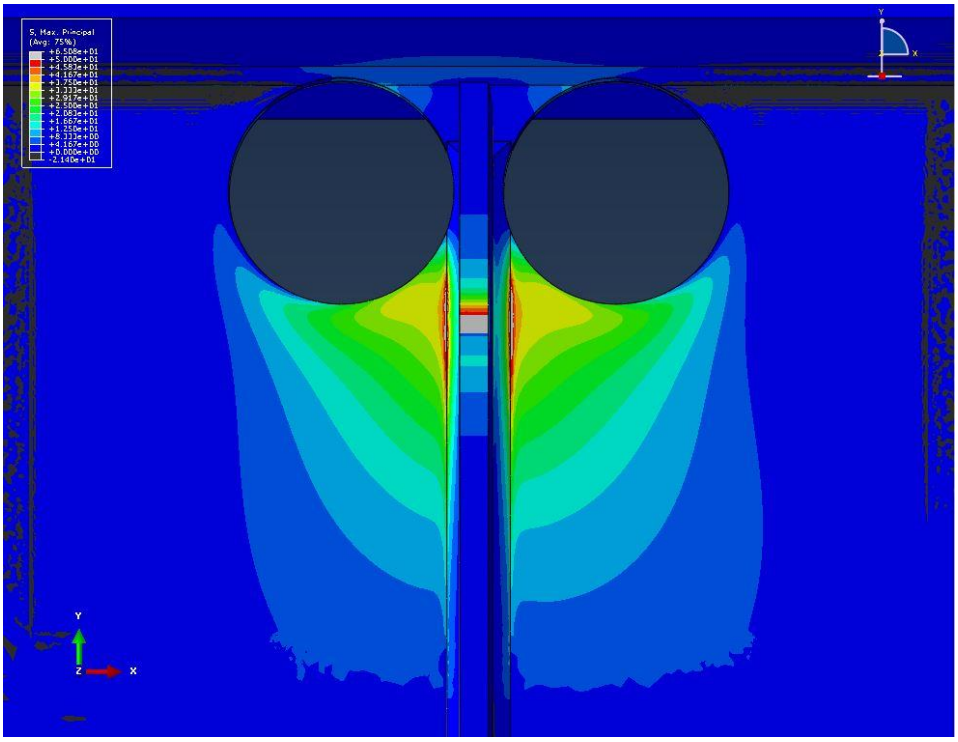

CHSS = 245 Mpa [35.6 ksi]

HSS-1 = 255 Mpa [37.0 ksi]

HSS-2 = 50.7 Mpa [7.35 ksi]

Horseshoe Crack with 101.6 mm [4.0 in.] Hole Diameter

Appendix F: Lab Notes Recorded During Testing Crack-arrest Holes

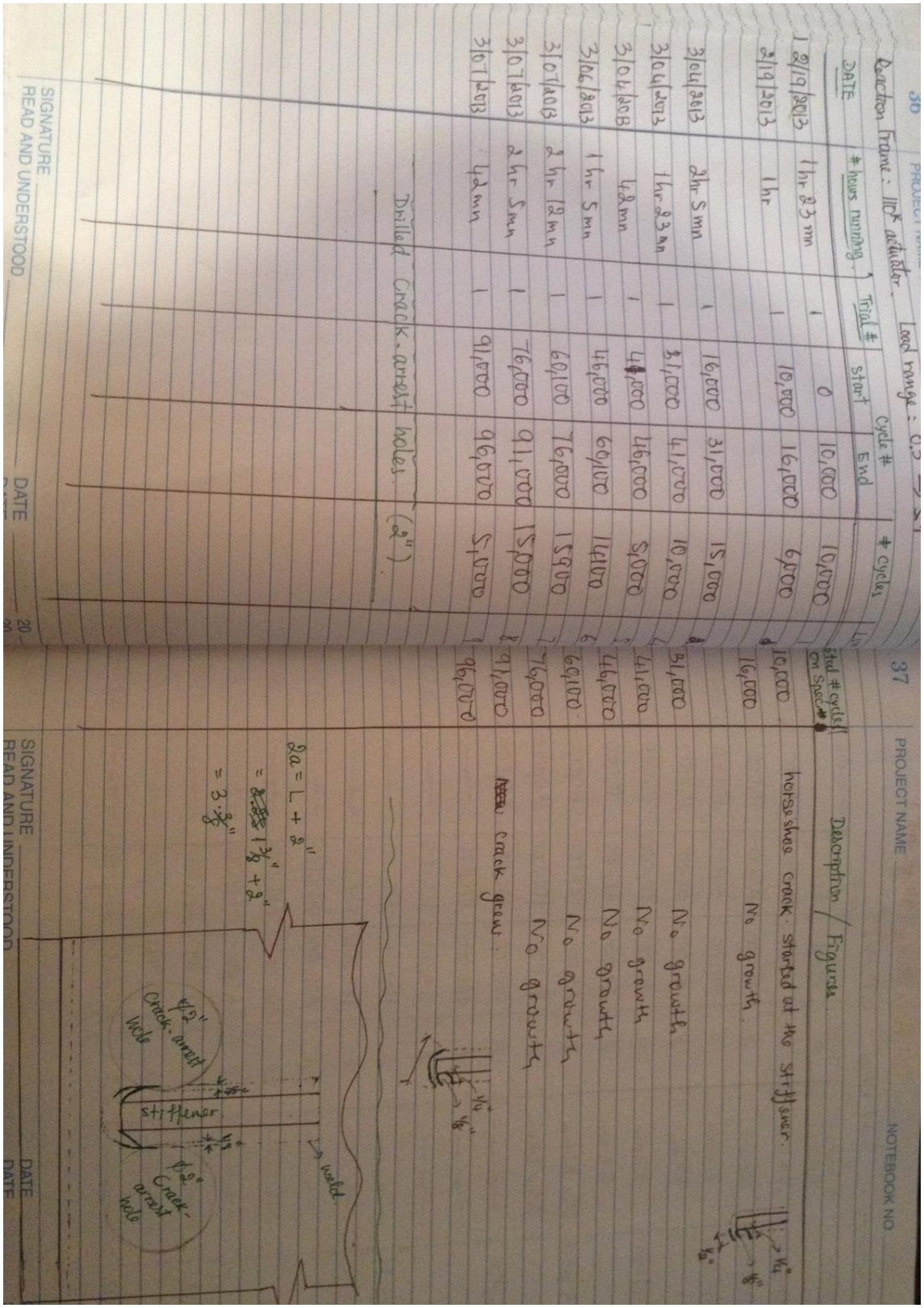

Reaction frame: HCK actuator. Load range: 0.5 – 21

DATE	# hours running	Trial #	Cycle # Start	Cycle # End	# cycles
2/19/2013	1hr 23 mn	1	0	10,000	10,000
2/19/2013	1hr	1	10,000	16,000	6,000
3/04/2013	2hr 5 mn	1	16,000	31,000	15,000
3/04/2013	1hr 23 mn	1	31,000	41,000	10,000
3/04/2013	48mn	1	41,000	46,000	5,000
3/06/2013	1hr 5 mn	1	46,000	60,100	14,100
3/07/2013	2 hr 18 mn	1	60,100	76,000	15,900
3/07/2013	2hr 5mn	1	76,000	91,000	15,000
3/07/2013	42mn	1	91,000	96,000	5,000

Drilled crack-arrest holes (2").

Stnd # cycles @ Spec #	Description / Figures
10,000	horseshoe crack started at the stiffener.
16,000	No growth.
31,000	No growth
41,000	No growth
46,000	No growth
60,100	No growth
76,000	No growth
91,000	Now crack grew.
96,000	

$\delta a = L + 2''$

$= 1\frac{3}{8}'' + 2''$

$= 3.\frac{3}{8}''$

weld

stiffener

½" Crack-arrest hole

½" Crack-arrest hole

SIGNATURE READ AND UNDERSTOOD DATE

38 PROJECT NAME Hot Fuse

Continued Load range : 0.7K -> 5.3K

DATE	# hours testing	Trial #	Cycle # Start	Cycle # End	# cycles	total cycles on spec.
1 4/05/2013	83mn	8	97,467	107,467	10,000	107,467
4/05/2013	83mn	2	10,000	20,000	10,000	117,467
4/11/2013	83mn	2	20,000	30,000	10,000	127,467
	83mn	2	30,000	40,000	10,000	137,467
4/12/2013	83mn	2	40,000	50,000	10,000	147,467
	83mn	2	50,000	60,000	10,000	157,467
4/15/2013	2hr 46mn	2	60,000	80,000	20,000	177,467
	2 hr 46mn	2	80,000	100,000	20,000	197,467
4/16/2013	—	2	100,000	120,000	20,000	217,467
	—	2	120,000	140,000	—	237,467
	—	2	140,000	160,000	—	257,467
4/17/2013	—	2	160,000	180,000	—	277,467
	—	2	180,000	200,000	—	297,467
	—	2	200,000	220,000	—	317,467
4/18/2013	—	2	220,000	240,000	—	337,467
	—	2	240,000	260,000	—	357,467
4/19/2013	—	2	260,000	280,000	—	377,467
	—	2	280,000	300,000	—	397,467
4/23/2013	—	2	300,000	320,000	—	417,467

SIGNATURE _____ DATE _____
READ AND UNDERSTOOD

39 PROJECT NAME _____ NOTEBOOK NO _____

Description / Figures.

No growth.

SIGNATURE _____ DATE _____
READ AND UNDERSTOOD _____ DATE _____

PROJECT NAME Fuel Tank Study (4th spec #5) NOTEBOOK NO.

Continued

DATE	# hrs testing	Trial #	Cycle # Start	Cycle # End	# cycles	Cum Tot #	Total cycles on spec
4/25/2013	4 hr 10 mn	1	330,000	350,000	20,000	20	447,467
4/25/2013	4 hr 10 mn	2	350,000	380,000	30,000	21	477,467
4/26/2013	8 h 16 mn	2	380,000	400,000	20,000	22	497,467
	24 h 46 mn	2	400,000	420,000	20,000	23	517,467
4/29/2013	24 h 46 mn	2	420,000	440,000	20,000	24	537,467
	〃	2	440,000	460,000	20,000	25	557,467
4/30/2013	〃	2	460,000	480,000	20,000	26	577,467
	24 hr 50 mn	2	480,000	515,000	35,000	27	612,467

SIGNATURE _____ DATE _____ 20 _____
DATE _____ 20 _____

41

Description / Figures

New crack appeared!

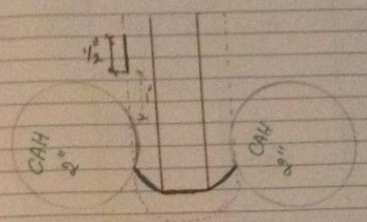

No growth.
the crack above grew to 7/8"
No growth

the crack grew to 1 1/8" downwards.
and a new crack on the right stiffener appeared.

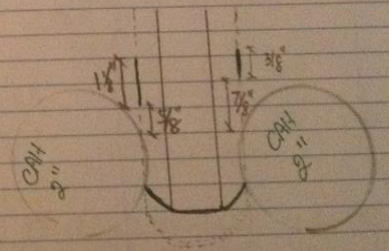

SIGNATURE _____ DATE _____ 20 _____
READ AND UNDERSTOOD _____ DATE _____ 20 _____

42 PROJECT NAME Pool Fund Study (SH- Spec #5) NOTEBOOK NO.

Continued....

DATE	# hrs Testing	Trial #	Cycles Start	Cycles End	# cycles	Total Cycles on spec.
5/01/2013	2hr 46mn	2	515,000	535,000	20,000	28
	2hr 46mn	2	535,000	555,000	20,000	29
5/02/2013	2hr 46mn	2	555,000	575,000	20,000	30
5/02/2013	2hr 46mn	2	575,000	595,000	20,000	31
5/03/2013	2hr 46mn	2	595,000	615,000	20,000	32
5/06/2013	2hr 46mn	2	615,000	635,000	20,000	33
5/06/2013	4h 10mn	2	635,000	665,000	30,000	34
5/07/2013	2hr 46mn	2	665,000	685,000	20,000	35
5/08/2013	〃	2	685,000	705,000	〃	36
	〃	2	705,000	725,000	〃	37
	〃	2	725,000	745,000	〃	38

SIGNATURE DATE 20

DATE 20

43 PROJECT NAME NOTEBOOK NO.

Description / Figures

No growth

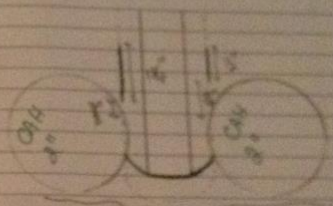

The crack on the right of the viewer grew to 9/16"

The left crack grew to 1 7/8", the right crack grew to 9/16" downwards

The left crack grew to 1 7/8"

The left is 1 3/16" which is 7/8" from CH

The right is 3/16" which is 7/8" above CH

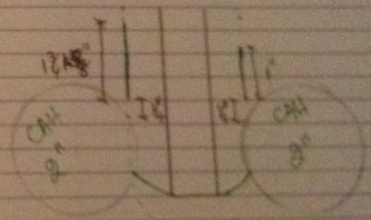

No additional growth

~~Some~~ grew! see figure on next

SIGNATURE DATE 20

READ AND UNDERSTOOD DATE 20

44

PROJECT NAME Fatigue Fluid Study

DATE	# hrs testing	Trial #	cycle Start	cycle End	# cycles	Lvm File #
5/09/2013	2h 46mn + ~~1h~~ 2h 46mn	2	745,000	785,000	40,000	39
/10/2013	2h 46mn	2	785,000	805000	20,000	40

Total cycles on pure

Description / Figures

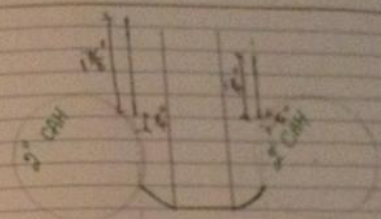

left grew to 2" (1/8" gap above the CSH)
right grew to 1 7/16" (1/16" gap above the CSH)

No growth

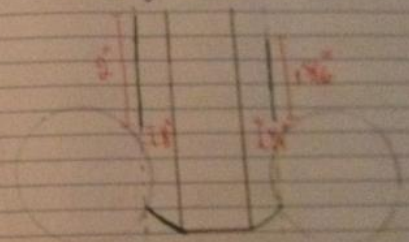

Drilling another ~~set of~~ crack-stop holes

SIGNATURE

DATE

DATE

48

PROJECT NAME Pool Fund Study (9ft - spec #5) NOTEBOOK NO.

Date	Trial #	cycle start	cycle End	# cycles	Lion file
6/16/2013	3	190,000	210,000	20,000	(15)
6/17/2013	3	210,000	230,000	〃	
6/18/2013	3	230,000	250,000	〃	
6/19/2013	3	250,000	270,000	〃	
6/20/2013	3	270,000	300,000	30,000	
6/21/2013	3	300,000	330,000	30,000	
6/21/2013	3	330,000	360,000	30,000	
6/24/2013	3	360,000	390,000	30,000	
6/26/2013	3	390,000	420,000	〃	

SIGNATURE DATE 20

49

Total cycles on spec

Description / Features

No growth.

Cracks on the fascia side

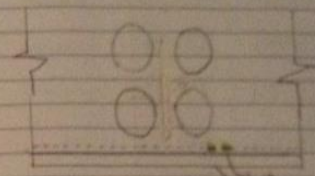

Two horizontal cracks along the weld (Flange-to-web weld) on the right side of fascia side web. The length of the cracks were 1/16"

No growth.

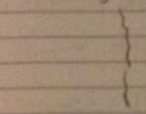

1/16" horizontal crack on left on fascia side about 1/2" from CSH

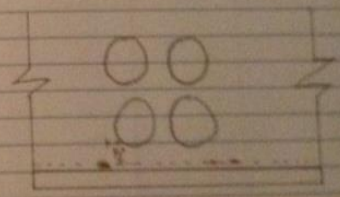

No growth.

Two horizontal cracks on stiffener side 0.45" and 1/16" long with 0.125 apart.

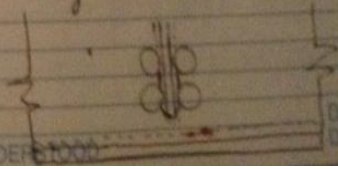

SIGNATURE DATE 20
READ AND UNDERSTOOD DATE 20